UC Irvine
ICS Technical Reports

Title

Simulations of information processing, control, and plasticity effects in the olfactory bulb

Permalink

https://escholarship.org/uc/item/665679bh

Author

Anton, Philip Sean

Publication Date

1991

Peer reviewed

Z
699
C 3
no. 91-63

Simulations of Information Processing, Control, and Plasticity Effects in the Olfactory Bulb

DISSERTATION

Philip Sean Antón

Department of Information and Computer Science
University of California
Irvine, California 92717

Technical Report No. 91-63

This dissertation was submitted in partial satisfaction
of the requirements for the degree of

DOCTOR OF PHILOSOPHY

in Information and Computer Science

Dissertation Committee:

Professor Richard Granger, Chair

Professor Michael Leon

Professor Gary Lynch

1991

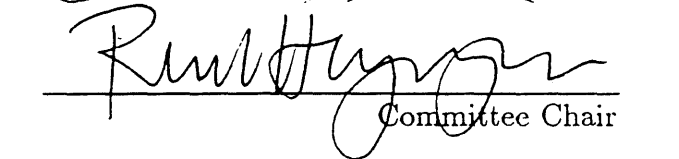The dissertation of Philip Sean Antón is approved,

and is acceptable in quality and form

for publication on microfilm:

Committee Chair

University of California, Irvine

1991

To my wife

Claire Elizabeth Antón

for all of her love and support throughout my doctoral studies,

and to my mother

Tochtli Juliette Mottet-Ugalde-Antón

in appreciation for all of her sacrifices and encouragement throughout the years.

Contents

List of Figures

List of Tables

Acknowledgements

Curriculum Vitae

Philip Sean Antón

Education

Doctor of Philosophy in Information and Computer Science
Artificial Intelligence - Computational Neuroscience
University of California at Irvine
August 1991

Masters of Science in Information and Computer Science
Artificial Intelligence - Computational Neuroscience
University of California at Irvine
June 1988

Bachelor of Science in Engineering
Computer Engineering
University of California at Los Angeles
March 1985

Fields of Study
Computational Neuroscience
Professor Richard Granger
Department of Information and Computer Science
University of California, Irvine.

Academic Positions

Research Assistant. Richard Granger, Department of Information and Computer Science, University of California, Irvine. 6/89 - present.

Lecturer. University of California, Irvine. Introduction to Computer Science Hardware (ICS 151). Summer 1987.

Lecturer. University of California, Irvine. Introduction to Computer Science Hardware (ICS 151). Summer 1988.

Research Assistant. Lubomir Bic, Department of Information and Computer Science, University of California, Irvine. Comparative studies of programming languages for Artificial Intelligence. 3/87-6/87.

Teaching Assistant. University of California, Irvine. Introduction to Computer Science Hardware (ICS 151). Fall 1987.

Publications

1 Granger, R., Ambros-Ingerson, J., Whitson, J., Antón, P. S., and Lynch, G. (1989). Empirical and analytical studies of a brain network. In: L. H. Canter (Ed.), *Proceedings of the Third Annual Parallel Processing Symposium*, Vol. 2. Los Alamitos: IEEE Computer Society, 549-563.

2 Granger, R., Ambros-Ingerson, J., Antón, P.S., Whitson, J., and Lynch, G. (1990). Computational action and interaction of brain networks. In: S. F. Zornetzer, J. L. Davis, and C. Lau (Eds.), *An Introduction to Neural and Electronic Networks.* San Diego: Academic Press, 25-41.

3 Granger, R., Ambros-Ingerson, J., Antón, P., and Lynch, G. (1990). Unsupervised perceptual learning: a paleocortical model. In: S. J. Hanson and C. R. Olson (Eds.), *Connectionist Modeling and Brain Function: The Developing Interface.* Cambridge: MIT Press, 105-131.

4 Antón, P. S., Granger, R., and Lynch, G. (1991). Temporal information processing in synapses, cells, and circuits. To appear in: T. McKenna, J. Davis, and S. Zornetzer (Eds.), *Single Neuron Computation.* New York: Academic Press.

5 Antón, P. S. (1991). Simulations of Information Processing, Control, and Plasticity Effects in the Olfactory Bulb. Ph.D. Dissertation, University of California, Irvine.

7 Antón, P. S., Lynch, G., and Granger, R. (1991). Computation of frequency-to-spatial transform by olfactory bulb glomeruli. To appear in *Biol. Cybern.*

6 Antón, P. S., Granger, R., and Lynch, G. (Submitted). A physiological model of cellular potentials with membrane time-constant and driving-force effects.

8 Antón, P. S., Granger, R., and Lynch, G. (Submitted). Simulated dendritic spines influence reciprocal synaptic strengths and lateral inhibition in the olfactory bulb.

Awards
President's Dissertation Year Fellowship — UC Irvine, 1990–91
Student Fellowship, Neural Networks Course — Boston University, 1990
Ford Foundation Predoctoral Fellowship — UC Irvine, 1987–90
Regents Fellowship — UC Irvine, 1986–87
Bachelor's Degree Cum Laude UCLA, 1985
Tau Beta Pi — California Epsilon Chapter, UCLA
Golden Key — UCLA Charter Member
Dean's Honor Lists — UCLA, UC Riverside

Activities

Memberships
American Association for the Advancement of Science (AAAS)
International Neural Network Society (INNS)
International Student Society for Neural Networks (ISSNNet)
Association for Computing Machinery (ACM)
Computing Professionals for Social Responsibility (CPSR)
Institute for Electrical and Electronic Engineers (IEEE)

Service
Polling Inspector, LA County Registrar of Voters, 12/90–present.
Guide Dog Puppy Raiser, International Guiding Eyes, 12/88–11/90.
Member, North Long Beach Neighborhood Association / Neighborhood Watch
Graduate Student Recruiter — UC Irvine, 1990.
Panel Member: CS graduate experience panel, UC Irvine 1988.
Recording Secretary, Tau Beta Pi, California Epsilon, UCLA, 1983–84.

Citizenship
U.S.A.

Abstract of the Dissertation

Simulations of Information Processing, Control,
and Plasticity Effects in the Olfactory Bulb

by

Philip Sean Antón

Doctor of Philosophy in Information and Computer Science
University of California, Irvine, 1991
Professor Richard Granger, Chair

The olfactory system processes complex and varied information in its detection, recognition, and memory of odors. The exact functions that the olfactory bulb plays in this processing is still largely unknown. Studies were performed to help reveal bulb functionality in the olfactory system while contributing to the set of computer methods available for the study of neural systems.

One interesting property of bulbar neurons is an increase in primary cell firing thresholds with depth. Since increased odor concentrations generally result in higher frequency inputs to the bulb and thus higher summation levels of primary cell membrane potentials, this threshold gradation transforms the frequency-encoded concentration data into a spatial representation in the number of primary cells responding in a single olfactory bulb glomerular region.

Since this transformation relies on temporal summation of post-synaptic potentials (PSPs) to reflect concentration levels, direct physiological modeling of the transformation was possible while providing the added efficiency to permit the simulation of large numbers of cells and synaptic interactions. A novel physiological modeling methodology was developed for these tests that extends the extant physiological models to include time-constant and driving-force interactive effects between post-synaptic inputs. This novel method is derived using linear superposition of inputs to a lumped-circuit cell representation, resulting in a difference-of-exponentials PSP function that is more realistic and flexible than the common empirically-chosen alpha function.

Also, the effects that interneuronal dendritic spines have on bulbar inhibitions were tested using biophysical computer simulations of primary-to-granule dendro-dendritic reciprocal interactions. The graded strength properties of these synapses showed that reciprocal inhibitions to primary mitral cells are facilitated by the spine

structures without the need of a high gain gradation while reducing lateral inhibition to other mitral cells. Furthermore, increases in the neck axial resistance of the synapsed spine further strengthen the reciprocal response and reduce the lateral inhibition; such resistance changes could therefore result in dendrodendritic synaptic plasticities and olfactory memory operations.

General Introduction

In striving to understand the basis of intelligence, different academic disciplines have developed various methods and techniques in an attempt to understand existing intelligent agents and to propose novel or hybrid systems that mimic desired behaviors. While some of the high-level, top-down investigations in intelligent behavior have produced interesting and useful results, a complete understanding of even simple agents has not yet been achieved, especially when it comes to understanding peripheral input/output operations. As a result, many researchers believe that a combined top-down and bottom-up study of existing intelligent structures such as human and animal nervous systems can shed light on how such information processing may be carried out.

Various techniques are employed by computational neuroscientists in their studies of biological neural networks. In the arena of sub-cellular, cellular, and multi-cellular modeling, these techniques range from low- level equivalent circuit models through mid-level physiological models to high-level abstractions such as coarsely temporal automata, oscillator, and analytical models. Chapter 1 surveys these modeling techniques, stratifying the variations employed by researchers along such variables as architectural detail, cell functioning details, cell output forms, and abstraction from the biology.

A simple and computationally-efficient model of neuronal post-synaptic potentials (PSPs) is then derived in Chapter 2. This model includes membrane time-constant and driving-force effects of multiple synaptic inputs overlapping in time. This model provides realistic temporal voltage information similar to biophysical compartmental models and actual biological data. Its advantages include computational efficiency due to the simplicity of its iterative expressions for membrane voltage over time. Starting from a lumped-circuit representation of a cell, equations for membrane voltage transients are derived that permit curve fitting of actual PSPs with varying membrane and synaptic conductance decay constants while maintaining the interactive effects of changing membrane conductances and synaptic driving forces.

By using this model, large neuronal structures can be simulated, yielding more detailed data than higher-level approaches such as those in artificial neural networks while avoiding the complexities of the lower-level biophysical approaches that may not be relevant to the computations under study. Furthermore, even if these interactive effects are deemed negligible to the system under study, a difference-of-exponentials function that includes a current injection parameter is proposed as a much more flexible and realistic candidate for linear PSP summation than the

1

empirical alpha function commonly in use. Derivations of different conductance functions based on probabilistic channel behavior are also presented.

Chapter 3 describes the use of the physiological model developed in Chapter 2 — together with the integrate-and-fire paradigm and realistic activation curves and synaptic delays — to study processing of concentration data by the olfactory bulb. This simulation incorporated 2.5% of the input and inhibitory neurons and 25% of the primary mitral/tufted cells in a single mammalian olfactory bulb glomerulus. The presence of graded increases by depth in the firing thresholds of the primary (mitral/tufted) cells in the olfactory bulb (Schneider and Scott, 1983; Mori, 1987) lead to the hypothesis that the bulb may transform the frequency-encoded data received from the receptors into a spatial excitation of the primary cells. In the simulation, temporal integration of receptor axon firings resulted in a positive relationship between the incoming firing frequency of afferent axons in the olfactory nerve and the general level of excitation in the mitral/tufted cells. Combined with the threshold gradations, the frequency-related excitation levels caused a gradation of primary-cell response based on depth. As a result, low-frequency inputs resulted in a response from superficially located cells alone, while higher-frequency inputs resulted in both superficial and deep primary cells to fire. Although the frequency of mitral/tufted cell firing in bulb was approximately independent of input frequency, the number of cells active in the simulated glomerulus was a roughly linear function of input frequency to the glomerulus, indicating the mechanism's ability to function as a frequency-to-spatial encoder. The simulation also revealed that refractory periods for granule-cell inhibition of mitral/tufted cell activity could lead to relatively fixed-frequency rhythmic activity in the glomerulus, independent of the input frequency from the olfactory nerve.

In the course of physiologically simulating the olfactory bulb, questions arose concerning the function of dendritic spines on the reciprocal dendrodendritic synapses in the bulb. While many theories have been proposed for the function of dendritic spines in axodendritic processing, little attention has been focused on the specific influence of spines on reciprocal dendrodendritic processing. Chapter 4 describes simulations of granule cell dendritic spines in the olfactory bulb and the influence these spines have on synaptic and lateral inhibitions and plasticities in the bulb. Mitral cells in the bulb synapse on granule cell spines (gemmules) which are in turn presynaptic to reciprocal inhibitory synapses back onto the same mitral cells. The postulate that these synapses respond with synaptic strengths graded by presynaptic depolarization resulted in a sensitivity of the reciprocal response to the local depolarization in the spine head. Biophysical computer simulations were performed to study these effects and the effect of changing the spine neck diameter and cytoplasmic resistance on the reciprocal and lateral inhibitory responses. Since spine head local potentials are larger than similar inputs on dendritic shafts, the spines facilitated the graded reciprocal response even for low levels of activity. The synapsing on spine heads also reduce the synaptic current, lowering the contribution to the

rest of the granule dendritic tree and thus reducing lateral inhibition. In addition, an increase in the effective spine neck axial resistance further increased the reciprocal synaptic response and decreased the lateral inhibitory response. Short-term, reversible, and long-term methods of implementing this resistance-based dendro-dendritic plasticity are discussed as well as the partial dependence of the reciprocal increase/lateral decrease effect on a broad synaptic gradation. Candidate memory operations by the bulb are also discussed, including a possible recognition memory pass/block function.

Chapter 1

Methodologies in Computational Neuroscience

1.1 Introduction

Computational neuroscientists employ mathematical and computer models of biological "hardware" to test their hypotheses about the functionality of neuronal structures and to gain additional insight into the structures' behavior and capabilities. These models are useful in that they allow the measurement of cellular parameters that can be difficult or impossible to obtain from biological tissue. Also, the models can often yield results much faster than laboratory experiments, allowing rapid modification of experimental parameters. Furthermore, the modeling results can provide anatomical, physiological, or functional predictions of the structures under study.

The modeling techniques employed by computational neuroscientists emphasize different functional aspects of cell behavior in the hope that the behaviors relevant to the computation under study are included while other behaviors not included for efficiency and other reasons are not relevant to the computation. The models described below employ quite different boundaries between included and excluded cellular properties, resulting in useful models that range from low-level equivalent circuit models that emphasize the electrical properties of the cellular membranes, through mid-level physiological models that reflect actual observed physiological changes in membrane potential due to cellular interactions rather than theoretical circuit effects, and finally to high-level abstract models that emphasize pure analytical descriptions of cells and their interactions, the oscillatory behavior of single or multiple cells, or coarsely temporal automata abstractions that emphasize spatial anatomical architectural properties over the time course of cellular potentials and conductances (see Table 1.1).

While the models take quite different approaches and emphasize different neurobiological properties of the systems under study, they are not in competition with each other. Together the models provide a collection of complementary tools to the computational neuroscientist. These tools should provide different points of view into the problem under study to facilitate a non-biased and multi-level approach. For example, if one believes that a certain architecture's principle function can be found in the discrete action potentials of individual cells, one should not completely disregard the predictions of oscillatory models based on field potential measurements such as electroencephalograms (EEGs); such oscillatory information could prove useful in the selection of anatomical, biophysical, or physiological properties

for inclusion in the more discrete simulations by providing global behaviors that should be demonstrated at these discrete lower levels.

These tools can also directly complement each other. Lower-level models can be used to test higher-level assumptions or provide more detailed data while the high-level assumptions can provide broad-scope data that the lower-level models cannot test due to computational complexity or lack of low-level explanations for certain cellular phenomena.

Thus, an understanding of the various modeling techniques employed in computational neuroscience, an appreciation of the powers and limits of each technique, and an understanding of the usefulness of employing multiple techniques in the assault of a problem can greatly aid an investigator by providing a foundation for his/her techniques and by providing the widest range of viewpoints in the attack of the problem in the hope of gaining long-lasting insights into the functionality of a neural architecture.

Artificial Neural Network Models. One should note that there is a difference between the abstract models described in this chapter and the more abstract models used in the field of artificial neural networks and connectionist systems. Connectionists try to discover useful algorithms that provide intelligent solutions to problems in engineering, artificial intelligence, and cognitive science without restricting themselves to biologically faithful solutions. They may borrow different ideas from the biology, but their approach is often so abstract as to not yield models of biological systems in any real sense. Excellent reviews of artificial neural networks and connectionist systems can be found in (Hinton, 1987; Carpenter, 1989).

1.2 Biophysical Models

To a certain extent, neurons are electrical devices. The classical description of cellular output is by way of an action potential (a.k.a., spike or firing) on the cell's axon that is a sudden change in the axon's membrane potential due to a rapid flux of ions through the axonal membrane. Also, the straightforward electrical influence one cell's action potential can have on another cell is to (temporarily) change the membrane potential of a target cell (PSP) through a synaptic action that either directly changes the target cell's membrane potential (electrical synapse) or changes the target cell's membrane conductance to one or more ionic species, causing a change in the target cell's membrane potential (chemical synapse). In addition, the membrane potential of a cell at the axon hillock determines whether the cell will fire or not. Furthermore, the resting potential of a neuron's membrane depends on a number of electrical properties of the membrane and the electrical driving forces of the major ionic species in and around the cell (Koester, 1985a,b,c,d; Kandel and Siegelbaum, 1985; Kandel, 1985).

Models	Method	Extent	Cell Output
Rall 1964, 1967	Biophysical: Cables / Multi-compartmental	Cell Components	* ----
Jack, Noble, & Tsien 1975	Biophysical	Varied	Varied
	Physiological	Varied	Varied
Segev & Parnas 1983	Biophysical: Multi-compartmental	Cell Components	* ----
Rall & Shepherd 1968	Biophysical: Multi-compartmental	Few Cells	* ----
Wehmeier et al. 1989	Biophysical: Uni-compartmental	Many Cells	Spike (Threshold)
Wilson & Bower 1989	Biophysical: Uni- & Multi-compartmental	Many Cells	Spike (Threshold)
Koch & Poggio 1987	Biophysical	Varied	Spike
Getting 1989	Biophysical	Few Cells	Spike (Threshold)
Antón 1991a	Physiological	Many Cells, Structures	Spike (Threshold)
Shamma 1989	Physiological	Many Cells	Firing Frequency
Perkel 1964	Physiological	Cell Components	Spike (Threshold)
Granger, Ambros-Ingerson, & Lynch 1988	Abstract: Event-based	Many Cells	Spike (Threshold)
Granger, Ambros-Ingerson, Staubli, Lynch 1989	Abstract: Event-based	Many Structures	Spike (Threshold)
Schild 1986	Abstract: Analytical	Few Cells	* ----
Kleinfeld & Sompolinsky 1989	Abstract: Amplifiers - Analytical	Few Cells	Firing Frequency
Li & Hopfield 1989a,b	Abstract: Amplifiers - Analytical	Few Cells	Potential Oscillation
Eisenberg, Freeman, & Burke 1989	Abstract: Amplifiers - Hardware	Many Cells	Firing Frequency

* Intracellular measurements only

Table 1.1: Categorization of selected models in Computational Neuroscience.

Since these and other major neuronal functions are dependent on the electrical properties of a neuron and its environment, neurobiologists have been successful in modeling the electrical behavior of neurons by modeling their properties in equivalent electrical circuits and differential equations for cellular voltages and conductances. These low-level models incorporate cellular electrical properties to varying levels of detail, employing techniques such as equivalent circuits of passive and active membrane patches, linear cable theory equations describing the spread of membrane currents and potentials through different parts of a cell, and compartmental models of cellular components.

Note that while neurons do have electrical behaviors, their electrical properties are based in the physical structures and chemical interactions of a cell. Thus these equivalent circuit models are theoretical approximations to the interactions in a neuron just as conventional electrical circuits based in non-organic materials are in general designed and analyzed in an abstract and theoretical manner. As with conventional circuits, the hope is that the abstractions will adequately describe the behavior of the circuit in its environment and in the modes under study. While these assumptions are not valid in all cases, many insights into the performance of neural components and architectures have been gained by taking the equivalent circuit approach and incorporating more detailed chemical effects whenever necessary. Since computationalists in neuroscience are presently more concerned with multi-cellular functions as a whole, direct chemical models will not be covered in this chapter (if interested, see (MacGregor, 1987: Ch. 4) for more on chemical modeling).

1.2.1   Equivalent Circuit Models of Membrane Patches

The passive and active properties of membrane patches can be modeled using electrical circuits that incorporate the different properties of cellular membranes (see Figure 1.1). The membrane itself is composed of a bi-lipid layer that acts as a thin layer blocking the flow of fluid in and out of the cell. The cellular fluid contains Na^+, Cl^-, and K^+ ions as well as larger protein anions that impart an electrical property to the fluid. As a result, the movement of ions is an electrical current in much the same was as the movement of electrons is an electrical current. Since the bi-lipid layer is very thin, electrical charge can build up on opposite sides of the membrane, resulting in a capacitance C_m across the membrane. Despite the insulation property of the bi-lipid layer, the membrane also contains paths through which Na^+, Cl^-, and K^+ ions may pass. These narrow channels are selective for particular ions and have a resistance to ionic flow represented by R_{Na}, R_{Cl}, and R_K. Furthermore, the concentration and effective charge of these ions inside and outside the cell are unbalanced, resulting in a potential force on each ion for movement into or out of the cell during the resting condition (Koester, 1985a). This driving force is represented by a voltage source E for each ion in series with its associated channel resistance. The net membrane potential, then, can be calculated by determining
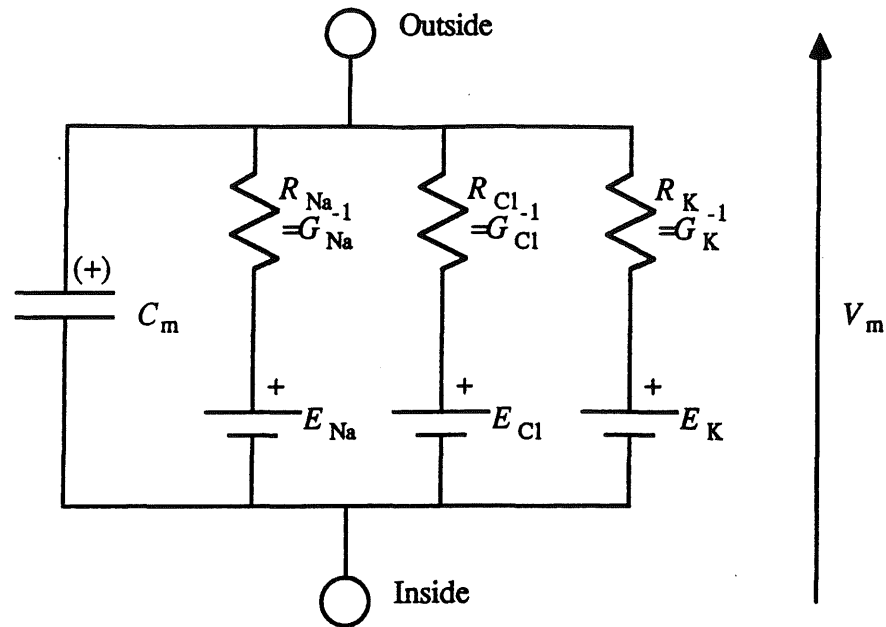
Figure 1.1: Equivalent electrical circuit of the membrane properties of a cell patch. V_m is the membrane potential, C_m is the membrane capacitance, and the R_i's and G_i's are the ionic channel resistances and conductances, respectively. The plus sign (+) on the capacitance indicates the resting charge polarity that can change during transitory periods. Typical values for E_{Na}, E_{Cl}, and E_K are +55mV, -69mV, and -75mV respectively (Rall, 1964, 1989; Koester, 1985b; Shepherd, 1979).

the potential difference between the inside and outside of the cell (i.e., the voltage drop across any path from the inside to the outside of the cell in the equivalent circuit).

Passive Membranes. Many parts of the cell, particularly the soma and most parts of the dendritic tree, have membranes that behave passively since they do not amplify signals. In terms of the equivalent circuit, this means that the ionic conductances are independent of time and voltage. While a passive membrane can be excited by a synaptic transmitter or current injection (see the section below on cellular excitation), the membrane merely conveys the synaptic effects rather than amplifying them. Thus, one can model a passive membrane by determining the values of the electrical circuit components either experimentally or theoretically and incorporating these values in one's computations or simulations.

The membrane potential V_m is controlled by the relative balance of Na^+, Cl^-, and K^+ ions inside and outside the cell. Changes in these concentrations resulting

from ionic current through the membrane transiently change the membrane potential from its resting nominal value. To facilitate synaptic influences and action potentials, neurons are built so that these concentrations are out of balance, resulting in chemical and electrical driving forces that try to move these ions through the membrane. The driving force of an ion can be calculated using the theoretical Nernst equation. For example, the driving force for Na^+ is given by:

$$E_{Na} = \frac{RT}{ZF} \ln \frac{[Na^+]_o}{[Na^+]_i}$$

where $[Na^+]_o$ and $[Na^+]_i$ are the ionic concentrations outside and inside the cell respectively, R is the gas constant, T is the temperature in degrees Kelvin, and Z is the ionic valence (Koester, 1985a). This equation allows modelers to approximate the driving force of an ionic species from concentration measurements in addition to direct measurements of this force through measurement of reversal potential. One assumption commonly made in the use of the Nernst equation is that the ionic concentrations inside and outside the cells remain relatively constant (neglecting local effects), so this driving force E is modeled as an ideal voltage source (see Figure1.1). The ionic resistances and membrane capacitance of the circuit can be measured directly from tissue samples; typical values can be found in (Koester, 1985b).

Active (Excitable) Membranes. Axonal and possibly some dendritic membranes have active properties and can generate ionic current through the cell by opening gates based on their membrane potentials. These voltage-gated channels for K^+ and Na^+ can be modeled directly by expressing their ionic conductances using the equations developed by Hodgkin and Huxley (1952) and cited in the forms given by (Kuffler et al., 1984):

$$g_K(V, T) = g_{K_{max}} n^4$$

and

$$g_{Na}(V, T) = g_{Na_{max}} m^3 h$$

where the functions n, m, and h are given by

$$n = 1 - e^{-t/\tau_n},$$

$$m = 1 - e^{-t/\tau_m},$$

$$h = e^{-t/\tau_h},$$

and $g_{K_{max}}$, $g_{Na_{max}}$, τ_n, τ_m, and τ_h are all voltage dependent (see Kuffler et al., 1984 for typical values and ranges).

While modelers can include these Hodgkin-Huxley equations directly into their simulations to obtain the time courses of action potentials, the equations can demand much computational time. Many modelers, therefore, have turned to polynomial approximations to the time courses of action potentials which result in reasonable fits to actual data and reduced computational loads, combining their biophysical simulation of the dendritic interactions and voltage spread with physiological modeling of cellular spikes.

1.2.2 Linear Cable Theory

Since a small section of membrane can be represented by the equivalent circuit in Figure 1.1, it was observed that long sections of membrane could be represented by repeating this circuit in parallel, thus forming a typical electrical cable made up of resistors, batteries and capacitors (see Figure 1.2). The study of such cables has since lead to an understanding of the general behavior of parts of cells, methods for combining the effects of dendritic trees into equivalent cylinders, normalized lengths and time constants of membrane cylinders providing easy comparison of effective lengths for different cell types, and the foundation for the compartmental models that followed (Rall, 1964, 1967, 1989). Unfortunately, this field called *Linear Cable Theory* has not been able to obtain closed-form analytical solutions for such questions as cable propagation of signals for complex cellular structures, especially in the transitory effects caused by the membrane capacitance. It is at this point that compartmental methods, covered below, have excelled.

Cable Equation for Membrane Voltage

The general cable equation that expresses the membrane voltage V in space and time is given by the partial differential equation:

$$\frac{\partial^2 V}{\partial X^2} = \frac{\partial V}{\partial T} + V,$$

where the dimensionless space and time variables are given by

$$X = \frac{x}{\lambda}$$

and

$$T = \frac{t}{\tau_m}.$$

X is often called the *electrotonic length* while λ is the *characteristic length* that expresses the efficiency of the cable for transmitting information and thus is used in the comparison of different cell membranes. The characteristic length and time constant are given by

$$\lambda = \sqrt{\frac{r_m}{r_i}} = \sqrt{\frac{R_m d}{4 R_i}}$$
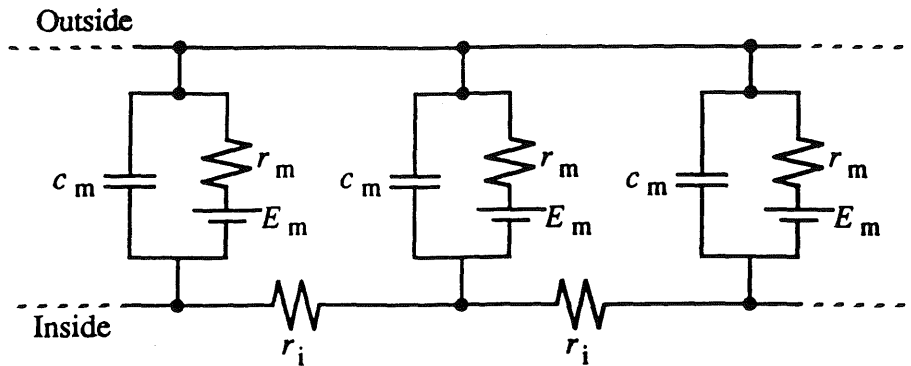
Figure 1.2: Cable representation of a length of cell membrane. E_m is the combined driving force for all ionic species, r_i is the intracellular resistance to current flow in the axial direction, r_m is the equivalent membrane resistance to all the ions that cross the membrane, and c_m is the membrane capacitance (after Rall, 1989). This particular model assumes that the resistance to axial flow outside the cell is negligible, although this resistance can readily be included if necessary.

and

$$\tau_m = r_m c_m = R_m C_m$$

respectively (Jack, 1979). In these equations, x is the distance along the cylinder under study, d is the diameter of the cylinder, t denotes time, r_i is the intracellular resistance to current flow in the axial direction, R_i is the specific resistance of the intracellular flow, r_m is the equivalent membrane resistance to all the ions that cross the membrane, and c_m is the membrane capacitance. For an excellent derivation of the cable equation see (Jack et al., 1975; Jack, 1979).

Electrical Geometry of a Cell: The Rall Model

In order to solve the cable equations for the cell under study, boundary conditions must be specified. The geometry of the cell under study and the format of the inputs are the major sources for boundary conditions. The standard assumptions made for the cables are given in the Rall Model which specifies the representation of the cell soma, the type of termination at the end of the processes, and the changes in cylinder diameters at branch points (Jack, 1979). Inputs to the cells will be covered in the next section.

Cell Soma. Although the soma often contains many branch points to dendritic and axonal processes, the soma is represented in the Rall model as a single resistor

and capacitor in parallel. This results in a uniform membrane potential over the whole soma in the model.

Termination. Although Rall has calculated the effects of many boundary conditions on long and short cables (Rall, 1989), the most appropriate condition for cell processes has been determined to be an open circuit termination where the resistance is infinite, the axial current becomes zero, and $\partial V/\partial X = 0$ at the terminal.

Branching. While dendritic trees contain much branching, Rall has determined that some typical types of branching occur in such a way that the descendant branches can be considered an equivalent single branch with the same properties as the parent segment for the purposes of calculating current spread through the tree. This consolidation of the cylinders is possible when the diameters d of the parent and children branches obey the relationship

$$d_{\text{parent}}^{3/2} = d_{\text{child}_1}^{3/2} + d_{\text{child}_2}^{3/2},$$

which holds for a large number of dendritic trees (Rall, 1989; Jack et al., 1975; Jack, 1979).

Nature Of Cellular Excitation: Post-Synaptic Potentials

Experimentally. In laboratory experiments, membranes are typically excited by current injection into the cell or by the placement of electrodes on either side of the membrane and forcing the membrane potential to a clamped value, thus forcing current to flow across the membranes in accordance with Ohm's Law.

Physiologically. An axon carrying an action potential can change the membrane potential of other cells directly through a communication structure called a synapse. Electrical and chemical synapses can cause this post-synaptic potential (PSP) change either directly or indirectly, respectively. The electrical synapses inject ionic current from the presynaptic axon directly into the post-synaptic membrane; this current injection will upset the potential balance in the post-synaptic membrane, causing a transient fluctuation in cellular potential. Chemical synapses, on the other hand, release chemical agents called *transmitters* that transiently changes the conductance of the membrane to different ionic species; this large conductance change behaves like the opening of a gate, allowing a rush of ions across the membrane and thus upsetting the membrane potential balance. Note, however, that in the case of the chemical synapse, a direct change in membrane potential will only occur if the present value of the membrane potential is different from the driving (reversal) potential for the ion(s) for which their conductance is changed. By examining the equivalent circuit (Figure 1.1), one will note that no current will flow

through an ionic segment if the ionic battery exactly matches the membrane voltage V_m since such a current flow across the ionic resistance will cause an additional voltage drop, violating Kirchhoff's voltage law.

The biophysical models can easily incorporate these synaptic influences since the equivalent circuits directly represent ionic flow as electrical current and membrane conductance by way of current resistors. Thus, the effects of electrical synapses can be modeled as a temporary current injection into the circuit by gating in a current source during the time of current injection. Also, chemical synapses that form transient conductive channels for an ionic species when activated can be modeled as a transient change in the resistance in series with that ion's driving force battery (see Figure 1.1). This change measured in actual cells is rather abrupt — much like a square pulse. As a result, modelers often use step functions for the change in resistance. If, however, a continuous function is desired for mathematical reasons, an alpha function or a difference-of-exponentials function may be used in approximating the time course of the resistance change (Rall, 1967; Jack et al., 1975; Antón et al., 1991a).

Solving The Cable Equation

Now that the equations have been set up and the boundary conditions have been determined, we must consider whether closed-form solutions exist for the steady-state and transient propagation behavior of membrane cables.

Steady-State During steady excitation we can neglect the membrane capacitance, so the cable equation reduces to a second-order ordinary differential equation since $\partial V/\partial T = 0$. Thus, we get the general solution

$$V(X) = Ae^{-X} + Be^{-X},$$

where $X = x/\lambda$ is the length of the cable normalized by the characteristic length λ to adjust for different diameters. A particularly useful solution can be obtained by considering a very long cable in which the change in voltage becomes negligible, i.e.,

$$\lim_{X \to \infty} V(X) = 0,$$

so $B = 0$. In this case the cable equation becomes

$$V(X) = V_0 e^{-X},$$

where $V_0 = V(0)$ (Jack, 1979). As with electrical resistive cables of infinite length, therefore, the signal in very long (relative to λ) cellular processes decreases exponentially (Mead, 1989).

Transient Solutions   Unlike the steady-state solutions, transient solutions to the general cable equation that meet the boundary and initial conditions in cells are much more difficult to obtain. The three techniques currently employed to solve this problem involve the use of the Laplace transform, general solutions to the equation, and numerical methods such as compartmental models (Jack, 1979).

Laplace Transformation.   The first analytical method involves the use of Laplace transforms. In this approach, the cable equation is taken into the complex domain in which the equation becomes an ordinary rather than a partial differential equation. The boundary and initial conditions can then be used to determine a complex solution which is then brought into the real domain using an inverse Laplace transform (Jack et al., 1975; Jack, 1979). This method is limited by the absence of appropriate inverse transforms for many problems (Jack, 1979).

General Solutions.   Two general solutions are currently used to solve the cable equation under circumstances when the constants in the solutions can be obtained.

One general solution involves the use of the *fundamental solution* or *Green's function*

$$V(X,T) = C_0(\pi T)^{-1/2} e^{-(T+X^2/4T)},$$

where C_0 is a constant given by

$$C_0 = \frac{Q_0}{\lambda c_m}$$

for semi-infinite cables. Here Q_0 is the amount of instantaneous point charge at $X = 0$ when $T = 0$ and λc_m is the membrane capacitance for a segment of length λ (Rall, 1989).

Another general solution to the cable equation is given by

$$V(X,T) = [A\sin(\alpha X) + B\cos(\alpha X)]^{-(1+\alpha^2)T},$$

where A and B are constants and α^2 is called the separation constant (Jack et al., 1975; Jack, 1979; Rall, 1989). One then uses boundary conditions and experimental data to solve for these constants. Unfortunately, it turns out that solving for A and B is quite difficult (Jack, 1979).

Compartmental Method.   The most productive method for solving the cable equation, especially in the case of complex geometries, involves numerical methods, especially the compartmental method (Rall, 1964; Jack, 1979). Since compartmental methods involve a conceptually different approach and do not lead to closed-form equations for signal propagation through a cable, they will be treated as a separate methodology altogether (see Section 1.2.3 below).

1.2.3 Compartmental Method

As noted above, the solution of the cable equation in the transient state is very difficult, especially as the geometry of the cell under study becomes complex. This difficulty in obtaining a closed-form analytical equation describing the signal propagation led Rall (1964) to develop the compartmental model which treats the sections of the cell under study as compartments of membranes represented by isopotential equivalent circuits. The compartments can be connected in the same way as the actual cellular processes to be modeled while the number of compartments determines the resolution of the model. Thus, a very finely detailed model can be constructed by breaking the cellular cables into a large number of segments, each being represented by a single compartment.

Advantages Over Linear Cable Theory. The advantages of this compartmental approach over linear cable theory are twofold. First, the use of the simple local equivalent circuit reduces the complexity of the cable equation from a second-order partial differential equation to a first-order ordinary differential equation describing the current flows in the circuit that can easily be solved along with the boundary and initial conditions. These compartmental calculations involve the determination of the membrane and outgoing axial currents given the incoming axial current from adjacent compartments. The membrane current determines the membrane potential for the compartment via Ohm's Law while the outgoing axial current through the axial resistance specifies the signal propagation to other adjacent compartments of the cell.

Second, each compartment does not have to contain the same parameters, so different types of connected membranes can easily be modeled by putting the appropriate equivalent circuits for these membranes and their associated parameters together in the model. For example, dendritic trees with small section of excitable membrane among the mostly passive tree can be modeled by including compartments that contain the excitable functions in the compartment tree (Rall, 1964; Segev et al., 1989).

Mathematical Description. During the calculations for the jth compartment, Kirchhoff's Current Law specifies that the membrane current i_{m_j} must be the difference between the incoming and outgoing axial currents

$$i_{m_j}(t) = i_{in_j}(t) - i_{out_j}(t)$$

since this membrane flow is the only remaining current path. Also, the membrane current will be split between the net flow through the ionic channels i_{ion_j}, the transient flow across the membrane capacitance c_{m_j}, and the stimulus input current i_{stim_j} at this compartment (if any):

$$i_{m_j}(t) = c_{m_j} \frac{dV_j}{dt} + i_{ion_j}(t) + i_{stim_j}(t).$$

As a result, the current equation for the jth compartment is given by

$$c_{m_j} \frac{dV_j}{dt} + i_{\text{ion}_j}(t) + i_{\text{stim}_j}(t) = \frac{V_{j-1} - V_j}{r_{j-1,j}} - \frac{V_j - V_{j+1}}{r_{j,j+1}}$$

where $r_{j-1,j}$ is the axial resistance between the $j-1^{\text{st}}$ and j^{th} compartments (Segev et al., 1989).

Implementations. Computationally, modelers either custom-build programs to solve the compartment equations or use general-purpose equation or circuit solving programs such as SPICE and SABER (Segev et al., 1989). The advantages of custom systems are speed and flexibility while general-purpose systems available "off-the-shelf" can provide rapid prototyping and computer access without programming. (Segev et al., 1989) also provides an extensive list of compartmental models used by many researchers in modeling neuronal systems.

1.3 Physiological Models

Models at a physiological level of description have also been used to simulate neural systems when the computations under study are believed to arise from temporal combinations of membrane potential transients or patterns of input combined with rigid or plastic synaptic weights (Perkel, 1964; Walløe et al., 1969; Jack et al., 1975; Shamma, 1989; Antón et al., 1991a,d). These physiological-level models are motivated by the simple linear summation of membrane transients observable in cells at low levels of input (Shepherd, 1979). Their efficiency permits large studies of the temporal interplay of excitatory and inhibitory post-synaptic potentials (EPSPs and IPSPs) as well as investigations into the maps between cellular inputs and responses by way of spiking thresholds or firing-rate functions.

If the biophysics underlying all cellular potentials were well understood and sufficient computational power was available, then biophysical models would be preferable to physiological models on the grounds of precision. However, in many situations cellular potentials are well characterized in terms of their shape and amplitude, whereas the precise mechanisms and sources underlying these responses remain uncertain. In such cases, physiological models can attempt to model cellular behavior by combining copies of PSP measurements juxtaposed in time. Unfortunately, the simplest physiological models do not accurately reflect the non-linearities due to time-constant and driving-force interactions between multiple PSPs. In addition, the functions typically employed for the representation of PSPs often do not contain enough parameters to allow accurate curve-fitting of actual PSPs measured from neurons. These shortcomings can become extremely relevant if, for instance, the size of PSPs begins to be reduced as a result of nonlinear interactions that change the effective membrane time constant and synaptic driving force. Also, particular
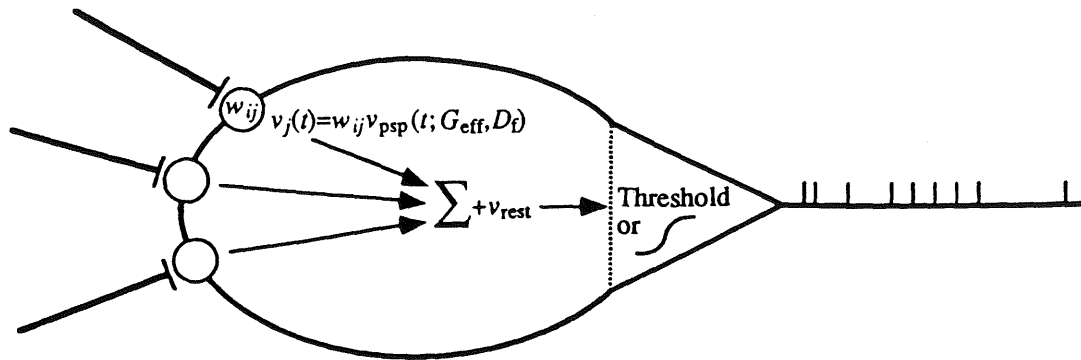
Figure 1.3: Components in a typical physiological model of a cell. Synaptic strength variables w_{ij} (or G_{syn_0}) are multiplied by the PSP shape function v_{psp} to yield the synaptic potential contribution. These contributions are then summed linearly with the resting potential v_{rest} to obtain the membrane potential for the cell. This potential is then compared to a firing threshold or firing-rate function to determine cell output. (From Antón et al., 1991c, with permission).

shapes of PSPs cannot be modeled using intuitively-realistic alpha functions, yet precise PSP shapes may be crucial for studies involving patterns of input including temporal overlap. In addition, silent inhibition cannot be modeled in the simplest physiological representations since their inhibitory effects are due to changes in the effective membrane time constant rather than an IPSP summed with membrane potential.

A set of novel PSP functions, however, are available that do accurately model these interactive effects and fit precise physiological PSP data (Antón et al., 1991a). These functions are presented below and derived from single lumped-circuit cell representations in Chapter 2. These new PSP functions provide computationally efficient, closed-form iterative solutions to the lumped circuits, permitting iterative maintenance of interactive effects in an efficient manner during simulation while retaining the simplicity of physiological modeling approach. These new findings partially bridge the gap between biophysical and physiological models without greatly increasing the computational complexity of the physiological simulations.

1.3.1 PSP Functions

The PSP temporal aspects included in a physiological simulation are modeled by way of PSP functions. Let us represent PSP transients by a weight variable w_{ij}

between the ith afferent cell and the jth cell multiplied by the shape function v_{psp}:

$$v_j = w_{ij}v_{psp}. \tag{1.1}$$

Of course, if weights are not an issue, the we can set $w_{ij} = 1$ so the PSP will be represented by v_{psp} alone.

Commonly used functions and the properties they model include

- delta functions $v_j = w_{ij}\delta(t - t_0)$
  (modeling a simple time-delayed synaptic weight),

- step functions $v_j = w_{ij}s(t_1, t_2)$
  (modeling a non-instantaneous synaptic weight),

- decaying exponentials $v_j = w_{ij}e^{-at}$
  (modeling a decaying temporal value),

- alpha functions $v_j = ew_{ij}\alpha t e^{-\alpha t}$
  (modeling non-zero rise and fall times),

- simple difference-of-exponentials functions
  $v_j = \left(e^{-b_j t} - e^{-G_m t/C_m}\right) D_{f_j}(0)G_{syn0_j}/\left(G_m - b_j C_m\right)$
  derived in Chapter 2 (modeling realistic rise and fall times), and

- interactive difference-of-exponentials functions (Equation 2.12) derived in Chapter 2 (modeling time-constant and driving-force effects as well as realistic rise and fall times)

(see Figure 1.4). While alpha and the difference-of-exponentials functions are visually similar to a typical PSP transient, quantitative measurements of the rise and fall times of actual PSPs often yield shapes that a single-parameter alpha function cannot match. Thus, the difference-of-exponentials functions — derived below and similar to the cable theory solution by Rall for a current step pulse (Rall, 1962, 1969, 1989) — are the most complex yet also the most realistic.

As pointed out by Shamma, the use of simple delta functions will concentrate the simulator's emphasis on the synaptic weights rather than the temporal properties of the PSPs, thus allowing clear study of the importance of these weights on the network computation without interference from temporal effects (Shamma, 1989). On the other hand, difference-of-exponentials have enough parameters to allow curve fitting of actual PSP measurements from the soma; these curves implicitly reflect the electrotonic changes imposed by the cell's dendritic structure on a PSP when traveling from the dendritic input site to the soma since most intracellular physiological data presently involves somatic measurements. Curve fitting can therefore allow the physiological simulation to reflect some of the influences imposed by the spatial geometry that is not directly simulated. This benefit is most relevant in simulations where the primary output is axonal since cell firing is determined by somatic membrane potential relative to the firing threshold.

1.3.2 Summation

Once the voltage contributions have been determined by the PSP function, simple linear summation of these contributions together with the resting potential of the cell determines the simulated cell potential. Even the more sophisticated PSP functions can be summed linearly due to the use of the linear superposition theorem in their derivation. The cell membrane potential is then given by

$$v_{\mathrm{m}}(t) = v_{\mathrm{rest}} + \sum_j v_j(t) \qquad (1.2)$$

for the PSP functions $v_j(t)$. Note that any long-term inputs that may elevate all the resting potentials of the cells under study can be modeled and studied by merely changing the resting potential summed together with the transient PSP inputs.

1.3.3 Output Determination

After the inputs to the cell have been combined into a resultant potential value, the model must somehow make the decision whether to fire or not. Common approaches in physiological models include a firing threshold technique, an instantaneous firing-rate function, or a direct implementation of the Hodgkin-Huxley or polynomial equations for voltage-dependent activations.

The most straightforward yet least efficient approach is to model directly the non-linear dynamics of the excitable membrane of the axon using Hodgkin-Huxley or polynomial equations. Here the simulation would merely input the summed voltage into the desired non-linear equations to produce continuous action potential voltages (Jack et al., 1975; Bunow et al., 1985; Segev et al., 1989; Rinzel and Ermentrout, 1989).

The action potential waveforms could, however, be represented by a simplified instantaneous spike or linear approximations together with an output determination

---

Figure 1.4: **Plots of various PSP functions.**
(a) Unit delta function $\delta(t - t_0)$.
(b) Unit step function. $s(t_1, t_2)$.
(c) Unit exponential decay e^{-at}. $a = 10, 20, 50$, and 100.
(d) Unit alpha functions $eate^{-\alpha t}$. $\alpha = 10, 20, 50$, and 100.
(e) Difference-of-exponentials $\left(e^{-b_j t} - e^{-G_{\mathrm{m}} t / C_{\mathrm{m}}}\right) D_{\mathrm{f}_j}(0) G_{\mathrm{syn}0_j} / (G_{\mathrm{m}} - b_j C_{\mathrm{m}})$.
$C_{\mathrm{m}} = 270\mathrm{pF}$ and $b = 100$ while $G_{\mathrm{m}} = 15\mathrm{nS}, 30\mathrm{nS}, 54\mathrm{nS}, 100\mathrm{nS}, 200\mathrm{nS}$, and $500\mathrm{nS}$.
(f) Same function as in (e) but with $G_{\mathrm{m}} = 54\mathrm{nS}$, $b = 45$, and $C_{\mathrm{m}} = 9\mathrm{pF}, 270\mathrm{pF}, 800\mathrm{pF}, 1600\mathrm{pF}, 3000\mathrm{pF}$, and $7000\mathrm{pF}$. (From Antón et al., 1991c, with permission).

(a) — graph with vertical axis from 0 to 1, dashed vertical line at t_0 on time axis.

(b) — graph with vertical axis from 0 to 1, pulse between t_1 and t_2.

(c) — graph, vertical axis 0 to 1, horizontal axis 0 to 140 (msec), curves labeled $a=10$.

(d) — graph, vertical axis 0 to 1, horizontal axis 0 to 140 (msec), curves labeled $\alpha=10$.

(e) — graph, vertical axis (μv) 0 to 200, horizontal axis 0 to 140 (msec), curves labeled $Gm=15nS$.

(f) — graph, vertical axis (μv) 0 to 200, horizontal axis 0 to 140 (msec), curves labeled $Cm=9pF$ and $Cm=7nF$.

function. This simplified approach is especially appropriate if the primary function of the action potentials in the simulation is merely to activate efferent synapses or if the simulation time steps are of the same order as action potential dynamics.

One such approach simplifies the voltage dependence of axonal activation to a comparison of total membrane potential with an abstract firing threshold (Perkel, 1964; Walløe et al., 1969; Jack et al., 1975; Getting, 1989; Antón et al., 1991a). In this integrate-and-fire method, an axonal output is generated when the membrane potential crosses an activation threshold. This threshold may be fixed or variable in order to reflect absolute and relative refractory periods of the cell. Absolute refraction is modeled by an infinite threshold while relative refraction is modeled by some type of elevated threshold behavior after firing. Hyperexcitability can even be included by following the relative refractory period with a period containing a lower-than-normal firing threshold.

A second approach is to use an instantaneous firing-rate function to transform the cell activity level into an output firing frequency (Shamma, 1989). This approach simplifies the threshold and refractory period behavior into a simple transformation that models the peak firing frequency (reflecting the absolute refractory period), scaling of firing frequency (reflecting a decaying relative-refractory period), and minimum activity level for output (reflecting the minimum firing threshold). Sigmoidal functions such as

$$z(t) = \frac{z_{\max}}{1 + e^{a(v_b - v)}} \tag{1.3}$$

(Shamma, 1989) are useful for this purpose since they suppress low-level inputs, have a nearly linear mid-range, and a decaying peak to maximum (see sketch in Figure 1.3). Here $z(v_b) = z_{\max}/2$ and the slope of $z(t)$ at v_b is $a/4$.

1.4 Abstract Models

Beyond the simplifications employed in the physiological models over the biophysical models, many more abstract modelling approaches have been used in order to emphasize particular anatomical or physiological features of the structures under study, to provide quick and rough prototypes to help in the selection of the biological feature to model, or to allow simulation of much larger numbers of cells and structures through the reduction in computational complexity of the algorithms employed. While an exhaustive survey of abstract models is beyond the scope of this chapter, a restricted view of some of the abstraction possibilities helps to put the biophysical and physiological models into perspective.

1.4.1 Event-Based/Asynchronous Models

In the olfactory models by Granger et al., the modelers have built simulations that assume certain performance operations and perform asynchronously to simulate the

consequences of the behavioral events that are assumed (Granger et al., 1989, 1990a, 1990b). For example, the input to the piriform cortex is assumed to be in one of two forms (Granger et al., 1990b): bursts of a few spikes every 200ms (Macrides et al., 1982) or single spikes every 25ms based on global EEG observations of the lateral olfactory track (Freeman and Schneider, 1982). As a result, the decision was made to simulate only the performance of the olfactory system at these events in time rather than at a more detailed time steps. Since the time between events is long compared to the time courses of most PSPs, the simulations neglect the temporal aspects of cellular potentiation and merely perform abstract calculations of the maximum membrane potential for the events and use this abstract potential for spike determination. These events can even represent the summation of many PSPs caused by bursting on the input axons, so even the resolution of individual PSPs may be lost. While many of the temporal components of cellular potentials are neglected, Granger's model does allow for the incorporation of large amounts of spatial anatomical detail in addition to realistic physiological behaviors such as premises for synaptic potentiation.

1.4.2   Amplifier Models: Analytical

Another abstract approach to neuronal modeling takes advantage of the measured oscillatory behavior of individual cells, groups of interconnecting cells, and large field readings from cellular structures. Kleinfeld and Sompolinsky, for example, employ abstract synaptic weights for PSPs, non-linear gain amplifiers for firing thresholds, and instantaneous firing rates for the cell output (Kleinfeld and Sompolinsky, 1989). Li and Hopfield take the abstraction one step further and model the oscillatory field behavior of the olfactory bulb using a collection of non-linear oscillators (Li and Hopfield, 1989a,b). The Li model proposes that the global oscillatory behavior itself provides information on the function that the bulb performs, neglecting realistic PSPs and the behavior of single cells.

1.4.3   Amplifier Models: Hardware

One of the obvious advantages of amplifier models is that they can be simulated directly in hardware to obtain rapid solutions. Eisenberg et al. (1989), for example, have a model of the olfactory bulb that employs an analog computer to recreate the oscillatory behavior of the extracellular field potentials in the bulb as measured in EEGs. The use of an analog computer rather than discrete components allows for easy modification of the system parameters as well as direct, rapid, and continuous solution of the differential equations involved in their oscillatory model.

1.5 Discussion

Advantage and Disadvantages of Each Approach

Each modeling approach discussed above has advantages and disadvantages result-
ing from the level of abstraction from the biology, the precision desired, the number
of cells and/or structures modeled, and the approach taken.

Biophysical models are able to model directly the electrical behavior of cells by
modeling their electrical properties such as resistances, capacitances, and voltage
sources. Since these models include low-level components, they can reveal unex-
pected behaviors caused by electrical component arrangements that may not be
known already. Such unexpected behaviors might be missed in physiological mod-
els since the phenomena would not have been conscientiously included in the model.
Biophysical models, however, do make assumptions about the biochemical behav-
iors of cells and will therefore not reveal processing based on chemical interactions
that are not accounted for.

The more efficient physiological models can easily incorporate observed phenom-
ena for which the underlying biophysical or biochemical causes are not understood
(e.g., what ionic species causes a PSP) and can then be used to study system ef-
fects that are based on the properties that are included, such as timing effects,
spatial effects, and anatomical influences. This slightly higher-level approach as the
advantage of retaining the temporal and spatial membrane potential changes while
greatly reducing the computational requirement of the model, permitting simulation
of larger neural structures. Also, there is a wealth of physiological data on which
to base the modeled forms. In addition, this approach has the advantage of being
able to incorporate physiological phenomena directly whether or not the underlying
biophysical and biochemical causes are understood. Thus, if a new phenomenon is
discovered by physiologists, the influence of this discovery on the membrane poten-
tial in space and time can be easily approximated.

Various PSP functions can be selected in the physiological models, depending on
the emphasis of the simulation on synaptic weights, temporal summation, or interac-
tive effects between synaptic inputs. The parameters of these functions — whether
abstract or biophysical — adjust the approximation of PSP amplitudes, rise-times,
fall-times, and channel dynamics, depending on the function chosen. Interactive
effects can impose shape and amplitude modulation that may be important to the
computations under study. Shape modulation, for example, may be important when
testing the differences between simultaneous and slightly offset arrival times of ac-
tivation and inhibitory inputs to a cell. Amplitude modulation may be important
when incoming signal strength is critical to the cellular operation or when testing
the difference between one large input and several smaller simultaneous inputs.

Abstract models allow simulation of the properties that might lead to a better
understanding of cellular functions while neglecting the properties that seem to
be irrelevant. While the abstract approach has the pitfall of possibly omitting of

properties critical to the computation under study, it also has the advantage of greater computational efficiency, allowing the study of large, global functions of neuronal structures.

Interdependence Between Modeling Approaches

As mentioned above, the modeling approaches are not in competition with each other but provide a host of tools to the computational neuroscientists to study systems at varying levels of detail. The insights gained at one level may help a researcher in the selection of parameters and functions for a simulation at another level. The compartmental studies of the effects of shunting on voltage propagation in a dendrite (Rall, 1964, 1989; Segev et al., 1989), for example, aid the physiological modeler in deciding whether shunting makes an important contribution to the system under study, and if so, in the selection of functions and approaches to take in modeling a shunting effect. Also, the models by Wilson and Bower of the piriform cortex combined the results of multi-compartmental simulation to get membrane potentials at different points in the cell, together with single-compartment cells for simulating large numbers of cells, to gain global as well as local information on cellular behavior (Wilson and Bower, 1989). In addition, many modelers have combined their biophysical models of synaptic and dendritic interactions and summations with physiological models of action potential time courses by using polynomial approximations to these action potentials rather than incorporating the Hodgkin-Huxley equations into their model directly (Segev et al., 1989).

Chapter 2

A Physiological Model of Cellular PSPs with Membrane Time-Constant and Driving-Force Effects

2.1 Introduction

The spatial and temporal patterns of neuronal action potentials are believed to underlie information processing in the brain. Cell spiking is the result of all-or-none threshold decisions based on the membrane potential at the axon hillock which itself is determined by responses to dendritic activation by afferent cells. Thus, one method of modeling the behavior and function of neuronal structures is to model the physiological interplay between excitatory and inhibitory post-synaptic potentials (PSPs) in dendrites while eliminating as much of the device physics of a cell as possible. Such a physiological model attempts to simplify cellular operation in order to allow the modeling of more extensive neuronal structures than would be possible using more detailed biophysical simulations that require much more computational power.

A number of dendritic models using linear summation of functions representing PSP transients have been described (Jack et al., 1975; Shamma, 1989; see Chapter 1). These models use linear summation of independent functions representing PSP transients. Unfortunately, interactive non-linearities begin to take effect as the number of inputs to a cell increases. Increased synaptic conductances increase the overall effective membrane conductance (G_{eff}) of the cell, thus speeding the membrane decay constant $G_{\text{eff}}/C_{\text{m}}$ due to faster discharging of the membrane capacitance (C_{m}) (Rall, 1962). Such time-constant changes will therefore change the amplitude as well as the rise and fall times of PSPs. Changes in membrane potential also cause changes in subsequent synaptic currents since the driving forces at the synapses are different from the resting driving forces. Furthermore, the PSP functions commonly employed in physiological models — delta functions, exponentials, and alpha functions — cannot usually be adjusted to match actual PSP shapes. Alpha functions, the most realistic of the three, contain only one parameter and often cannot match both the rise and fall times of the PSPs under study.

The physiological model presented below approximates these membrane property and driving-force effects via the interactions of simple PSP functions in order to simulate more realistic behaviors. The simplicity of these equations maintains the computational efficiency of physiological models that allow for easy modeling of

large numbers of cells and structures.

2.2 Theoretical Development

Closed-form solutions for the membrane potential as a function of time for multiple inputs into a cable are often quite complex or difficult to obtain. As a result, biophysical modelers of multiple interacting cells have turned to numerical solutions of compartmental approximations of dendritic components (Rall, 1964). Thus, simple physiological functions to model cellular PSPs have not risen out of the more detailed biophysical models.

The approach developed here uses superposition to derive from the Lapicque lumped-circuit model of a cell (Rall, 1962; Jack et al., 1975; Tuckwell, 1988) the linear contribution of an active synapse to the membrane potential, compensating both for driving-force effects and for changes in effective membrane conductance due to channel openings of other active synapses. The general PSP function yields iterative contributions in time steps. These contributions are then summed together in a step-wise linear fashion to yield the resultant time course of the membrane potential.

2.2.1 The Lumped Model of a Cell

Let us represent the electrical properties of a cell's passive dendritic tree and soma by a simple resistor/capacitor (RC) circuit. Such a linear representation has been useful in modeling cellular voltage behavior (Rall, 1962; Jack et al., 1975; Tuckwell, 1988). Figure 2.1a shows an RC circuit with two parallel branches representing two synapses on the cell. Here each of two synapses is represented by a time-varying synaptic conductance $G_{\text{syn}_j}(t)$ representing the combined channel openings of an active synapse. This conductance $G_{\text{syn}_j}(t)$ is in series with the reversal potential E_{syn_j} (a constant electromotive force) for the ionic species that passes through the synaptic channels. More active synapses can be added by including their conductance/battery branches in parallel with the other synaptic branches.

Since the synaptic current injected into the RC circuit causes the membrane-potential transient response, the shape of the current function affects the shape of the resulting PSP equation. The combined effect of many randomly-closing channels at an end-plate can be approximated by a simple exponential-decay function for the overall current (Colquhoun, 1981). For single synapses that have nearly constant driving forces, this implies an exponential conductance transient for the synapse.

Mathematically, if the probability of a channel remaining open during a unit of time was q, then the probability of the channel remaining open as a function of time is q^t (an exponential). Thus, if all of the channels opened at the same time, a reasonable simplification of the combined conductance at a synapse activated at
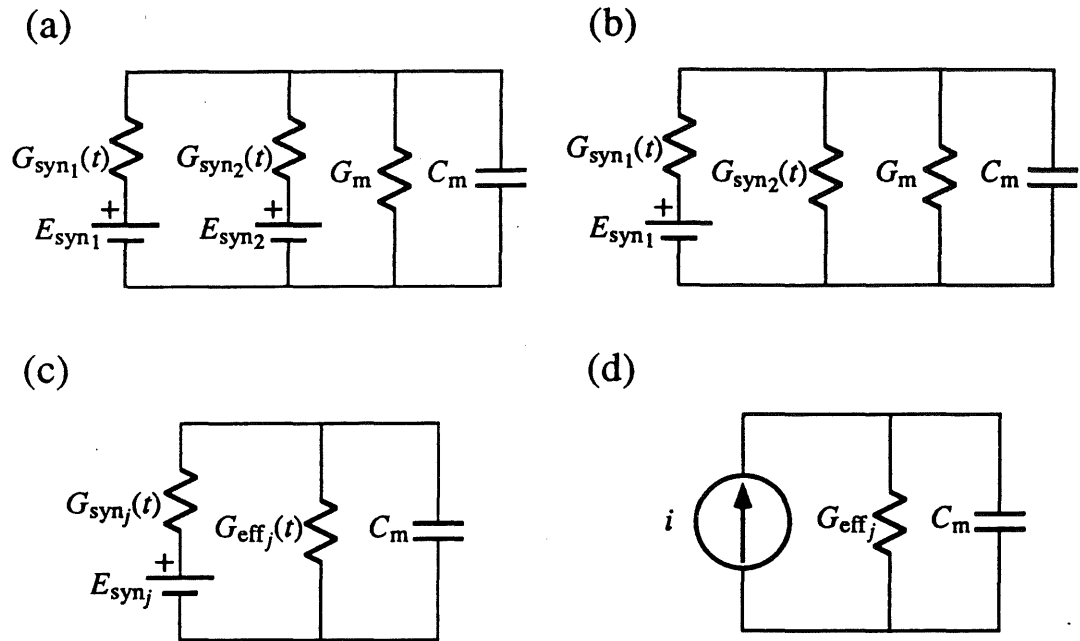
Figure 2.1: Development of RC circuit used for PSP transient equation. (a) Typical lumped-circuit model of a cell's passive dendritic tree and soma with two parallel paths representing two synapses (Rall, 1962; Tuckwell, 1988). (b) Circuit representing the linear response of E_{syn_1} using superposition. (c) Circuit for response of E_{syn_j} that combines all other synaptic conductances with the membrane conductance. (d) Small time-step replacement of synaptic path with an exponential source i.

time $t = 0$ would be the function

$$G_{\text{syn}}(t) = G_{\text{syn0}}e^{-bt} \qquad (2.1)$$

for $t \geq 0$, where G_{syn0} is the peak synaptic conductance at $t = 0$ and b is a constant such that $b > 0$. Note that in actuality all the channels do not open at the same time, but this approximation of discontinuity is often reasonable (Colquhoun, 1981), especially if the time resolution used in a simulation is low compared to the rise time of the conductance.

If, however, the conductance rise time does become important for some reason, more general conductance functions can be used. Let $n(t)$ be the number of synaptic channels open at time t. Let us make the simple assumption that the number of new channel openings is 0 for $t < 0$ and a decaying exponential Ne^{-at} for $t \geq 0$ with N being the initial rate of channel openings at time $t = 0$ and constant a. Let us also assume that each channel closes independently with probability p (Colquhoun, 1981). The differential equation for open channel rate is then given by

$$\frac{dn}{dt} = Ne^{-at} - pn. \qquad (2.2)$$

If $n(0) = 0$, then the solution for $n(t)$ can easily be shown to be

$$n(t) = \frac{N}{p - a}\left[e^{-at} - e^{-pt}\right] \qquad (2.3)$$

for the general case $a \neq p$, or an alpha function

$$n(t) = Nte^{-at} \qquad (2.4)$$

for the special case $a = p$. Thus, a more general conductance function would be a difference-of-exponentials function. Also, a more specific alpha function can be employed and has been used by Rall (1967, 1989) for synaptic conductances. As will be shown below, however, realistic and useful PSP functions can be derived using the simpler exponential conductance function of Equation 2.1.

2.2.2 Superposition of Individual Synaptic Potentials.

Since the circuit in Figure 2.1a is linear, we can use the superposition theorem to determine the voltage contribution that each single synapse gives to the total membrane potential.

Superposition asserts that the response of any linear network due to multiple, independent sources is equal to the sum of the responses when each source is considered independently and all other sources are set to zero (Desoer and Kuh, 1969). Thus, the voltage contribution to the combined membrane potential of one synaptic battery is given by the circuit response when all other synaptic batteries are short

circuited. For example, in the two-synapse case, the circuit in Figure 2.1b will give the contribution of E_{syn_1} to the membrane potential. Note that if one short circuits the reversal-potential battery of a synapse, then this leaves the synaptic conductance in parallel with the membrane conductance constant G_{m}. Since conductances in parallel add, the effective membrane conductance as seen by a single synapse is therefore the sum of all other synaptic conductance transients with the normal membrane conductance:

$$G_{\text{eff}_j}(t) = G_{\text{m}} + \sum_{k \neq j} G_{\text{syn}_k}(t). \tag{2.5}$$

Once we calculate this effective membrane conductance we can determine the voltage contribution of the single synapse by solving the effective circuit represented in Figure 2.1c. Unfortunately, this solution involves a differential equation with time-varying coefficients. We can, however, consider the conductance coefficients as constants by breaking time into short steps relative to the speed of the conductance swings, approximating the conductances with one of the values they obtain during each time step and solving the differential equation representing each time step. This approach is especially appropriate for computer simulations of interacting PSPs that operate in such small time steps.

For each time step and PSP, then, let us replace the synaptic conductance and battery with a current source:

$$i_j(t) = \left(E_{\text{syn}_j} - v_{\text{m}_j}(t)\right) G_{\text{syn0}_j} e^{-b_j t}, \tag{2.6}$$

where E_{syn_j} is the synaptic reversal potential, $v_{\text{m}_j}(t) = v_j(t) + v_{\text{rest}}$ is the membrane potential due to the single synapse j, and v_{rest} is the resting membrane potential. If $v_{\text{m}_j}(t)$ undergoes only small changes during a single time step Δt, then the synaptic driving force $(E_{\text{syn}_j} - v_{\text{m}_j}(t))$ is relatively constant during the interval $t \in (T, T + \Delta t]$. Thus, the only effective change during the interval is from the synaptic conductance decay $e^{-b_j t}$. We then have a simple exponential current injection

$$i_j(t) = I_j e^{-b_j t} \tag{2.7}$$

for $t \in (T, T + \Delta t]$, where $I_j = (E_{\text{syn}_j} - v_{\text{m}_j}(T)) G_{\text{syn0}_j}$ is the synaptic current at the start of the time interval. Also, if we select time steps that are very short relative to the length of the conductance transients, we can approximately consider G_{eff_j} as a constant during the time step.

For each time step and each synaptic battery, then, the solution for the circuit in Figure 2.1c is given by the solution of Figure 2.1d. The differential equation for the voltage transients $v_j(t)$ at time step t in the circuit in Figure 2.1d is

$$i_j(t) = I_j e^{-b_j t} = C_{\text{m}} \frac{dv_j}{dt} + G_{\text{eff}_j} v_j \tag{2.8}$$

32

(Desoer and Kuh, 1969). Taking the Laplace transform we get

$$\frac{I_j}{s + b_j} = C_{\mathrm{m}} s V_j(s) - C_{\mathrm{m}} v_j(0) + G_{\mathrm{eff}_j} V_j(s).$$

Solving for $V_j(s)$ yields

$$V_j(s) = \frac{I_j / C_{\mathrm{m}}}{(s + b_j)\left(s + G_{\mathrm{eff}_j}/C_{\mathrm{m}}\right)} + \frac{v_j(0)}{\left(s + G_{\mathrm{eff}_j}/C_{\mathrm{m}}\right)}.$$

Taking the inverse Laplace transform we get the general solution

$$v_j(t) = \frac{I_j}{\left(G_{\mathrm{eff}_j} - b_j C_{\mathrm{m}}\right)} \left[e^{-b_j t} - e^{-G_{\mathrm{eff}_j} t/C_{\mathrm{m}}}\right] + v_j(0) e^{-G_{\mathrm{eff}_j} t/C_{\mathrm{m}}} \tag{2.9}$$

for $b_j \neq G_{\mathrm{eff}_j}/C_{\mathrm{m}}$ and the special case alpha function solution

$$v_j(t) = \frac{I_j}{C_{\mathrm{m}}} t e^{-G_{\mathrm{eff}_j} t/C_{\mathrm{m}}} \tag{2.10}$$

for $b_j = G_{\mathrm{eff}_j}/C_{\mathrm{m}}$. Interestingly, alpha functions have been used elsewhere to model synaptic conductance transients (Rall, 1967, 1989) and synaptic currents (Jack et al., 1975) as well as synaptic voltage responses (Shamma, 1989).

We are considering the voltage $v_j(t)$ at a time $t \in (T, T + \Delta t]$ for time steps of length Δt, so the iterative solution then becomes

$$\begin{aligned} v_j(T + \Delta t) &= \frac{\left(E_{\mathrm{syn}_j} - v_{\mathrm{m}_j}(T)\right) G_{\mathrm{syn}0_j} e^{-b_j T}}{G_{\mathrm{eff}_j}(t) - b_j C_{\mathrm{m}}} \left[e^{-b_j \Delta t} - e^{-G_{\mathrm{eff}_j}(t)\Delta t/C_{\mathrm{m}}}\right] \\ &\quad + v_j(T) e^{-G_{\mathrm{eff}_j}(t)\Delta t/C_{\mathrm{m}}} \end{aligned} \tag{2.11}$$

since the synaptic conductance has decayed down to the value $G_{\mathrm{syn}0_j} e^{-b_j T}$ by time T.

We now define variables for the driving force, active component, and passive components of $v_j(t)$. Let

$$\begin{aligned} D_{\mathrm{f}_j}(T) &= \left(E_{\mathrm{syn}_j} - v_{\mathrm{m}_j}(T)\right), \\ A_j(t) &= \frac{D_{\mathrm{f}_j}(0) G_{\mathrm{syn}0_j} e^{-b_j T}}{G_{\mathrm{eff}_j}(t) - b_j C_{\mathrm{m}}} \left[e^{-b_j \Delta t} - e^{-G_{\mathrm{eff}_j}(t)\Delta t/C_{\mathrm{m}}}\right], \text{ and} \\ P_j(t) &= v_j(T) e^{-G_{\mathrm{eff}_j}(t)\Delta t/C_{\mathrm{m}}}. \end{aligned}$$

The voltage transient for synapse j is then given by

$$v_j(t) = A_j(t) \frac{D_{\mathrm{f}_j}(T)}{D_{\mathrm{f}_j}(0)} + P_j(t).$$

This notation confirms our intuition that the active term $A_j(t)D_{f_j}(T)/D_{f_j}(0)$ should remain sensitive to the present driving force $D_{f_j}(T)$ while the passive term $P_j(t)$ just decays along the exponential decay of the dynamic membrane time constant $G_{\text{eff}_j}(t)/C_m$. At this point we may wish to update the driving force from $D_{f_j}(T)$ to $D_{f_j}(t)$ to obtain a better approximation of $v_j(t)$. Thus, the expression for $v_j(t)$ becomes

$$v_j(t) = A_j(t)\frac{D_{f_j}(t)}{D_{f_j}(0)} + P_j(t).$$

Now note that $D_{f_j}(t)$ is a function of $v_j(t)$ rather than the old known value $v_j(T)$. Solving for $v_j(t)$, then, yields the expression

$$v_j(t) = \frac{A_j(t) + P_j(t)}{1 + A_j(t)/D_{f_j}(0)}. \tag{2.12}$$

Physiological PSP data from cells with unknown biophysical parameters can be matched by adjusting the parameters of $v_j(t)$. Figures 2.2a, 2.2b, and 2.2c show the families of unitary EPSPs obtained by adjusting $G_{\text{eff}_j} = G_m$, b, and C_m, respectively, while holding everything else constant in Equation 2.12. Note that changes in G_m and b have similar effects on the EPSPs since multiplication of the numerator and denominator of $A_j(t)$ by -1 reverses the positions of G_{eff_j}/C_m and b_j.

For multiple interacting excitatory and inhibitory PSPs (EPSPs and IPSPs) we merely use superposition to sum linearly the individual voltage transients given by Equation 2.12 for each type of PSP to get the overall voltage transient. Thus, the total membrane potential

$$v_m(t) = v_{\text{rest}} + \sum_j v_j(t) \tag{2.13}$$

is given by:

$$\boxed{v_m(t) = v_{\text{rest}} + \sum_j \frac{A_j(t) + P_j(t)}{1 + A_j(t)/D_{f_j}(0)}.} \tag{2.14}$$

Note that silent inhibition can easily be modeled by cancelling the $D_{f_j}(0)$ term in $A_j(t)$ with the $D_{f_j}(0)$ in the denominator of Equation 2.14 to prevent the division of the null driving force $D_{f_j}(0)$.

This iterative expression for the combined membrane transient has a number of useful properties. First, the (shunting) effects of channel openings on the membrane time constant are included in the effective conductance calculation $G_{\text{eff}_j}(t)$ for each PSP j. Second, the effects of driving-force changes on synaptic current injection are also modeled. Third, the computational complexity of the equation is linear in the number of synapses. Fourth, many of the factors and terms in $A_j(t)$ and $P_j(t)$, such as b_jC_m, $e^{-b_j\Delta t}$, and $G_{\text{syn}0_j}e^{-b_jT}$ (for T as multiples of Δt), can be pre-calculated to reduce the linear factor in the complexity of the equation since many of the
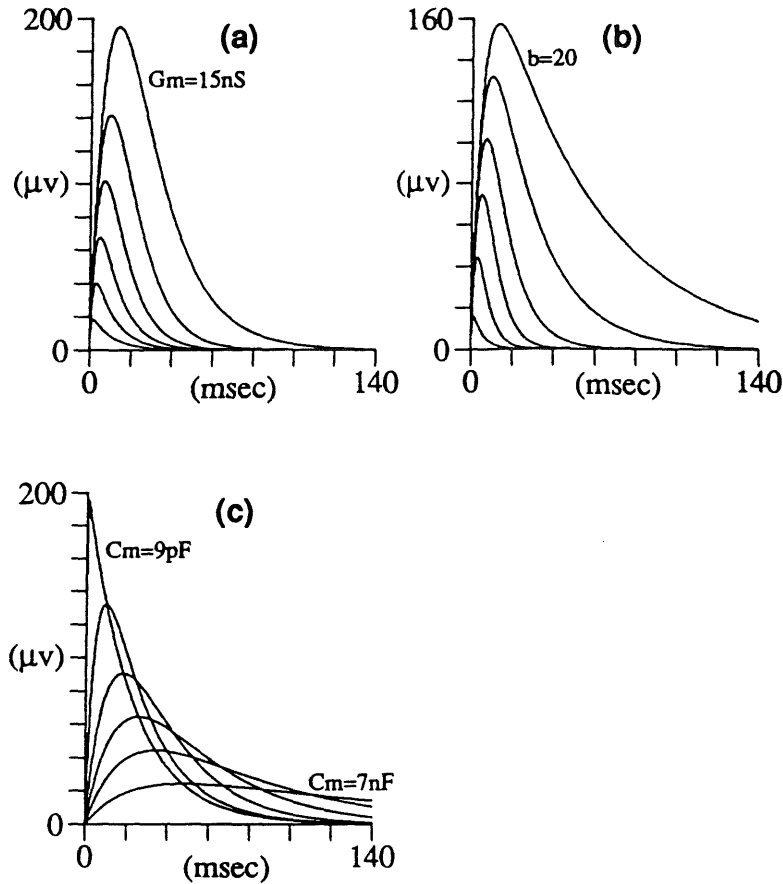
Figure 2.2: Plots of Equation 2.12 for unitary EPSPs. Here the effects of adjusting the lumped-circuit membrane conductance $G_{\text{eff}_j} = G_m$, current injection decay constant b, and the membrane capacitance C_m on the EPSP are shown in parts a, b, and c respectively, holding $D_f(0)$ at 55mV and G_{syn0} at 0.2nS. (a) Conductance G_m modulation. The parameter values were $C_m = 270\text{pF}$, $b = 100$, and $G_m = 15\text{nS}$, 30nS, 54nS, 100nS, 200nS, and 500nS. The curves decreased and shorten with increasing G_m values. (b) Current injection time-constant b modulation. The parameter values were $G_m = 54\text{nS}$, $C_m = 270\text{pF}$, and $b = 20, 45, 100, 201, 500$, and 2000. The curves decreased and shorten with increasing b values. (c) Capacitance C_m modulation. The parameter values were $G_m = 54\text{nS}$, $b = 45$, and $C_m = 9\text{pF}$, 270pF, 800pF, 1600pF, 3000pF, and 7000pF. The curves flatten and lengthen with increasing C_m values.

synapses will share common values for b_j and $G_{\text{syn0}_j}(t)$. Overall, Equation 2.14 is quite simple and yields realistic results as shown below.

In many cases, we can simplify the computation of $v_j(t)$ by using the conductance

$$G_{\text{total}}(t) = G_{\text{m}} + \sum_k G_{\text{syn}_k}(t)$$

rather than $G_{\text{eff}_k}(t)$ in Equation 2.11. Such a conductance change is negligible since unitary PSPs are so small and $G_{\text{syn}_j}(t) \ll G_{\text{eff}_j}(t)$ in cases of large numbers of overlapping PSPs. This use of $G_{\text{total}}(t)$ will then make $v_j(t) = v_k(t)$ for all j, k, and t in similar PSP types. In simulations involving simultaneous PSPs, therefore, a single $v_j(t)$ can be calculated for each PSP type starting at the same time step to increase the simulation speed while retaining shunting and driving-force effects.

Furthermore, if we find that the changes in effective conductance (shunting) due to channel openings have negligible effects on the computations under study, then G_{eff_j} can be approximated by G_m. In this case we can pre-calculate each $A_j(t)$ for each T as well as each $e^{-G_{\text{eff}_j}\Delta t/C_{\text{m}}}$ used in $P_j(t)$, thus eliminating the run-time calculation of exponentials for each $v_j(t)$ and yielding a significant saving in the computational complexity of the model.

Also, if the changes in driving force are also negligible or approximately so (e.g., if only small numbers of synapses are active at the same time or if the peak amplitude of a unitary PSP remains much smaller than the driving force for the PSP), then we can neglect the driving force and pre-calculate the entire PSP voltage for each simulation time step by

$$v_j(t) = \frac{D_{f_j}(0)G_{\text{syn0}_j}}{(G_{\text{m}} - b_j C_{\text{m}})} \left[e^{-b_j t} - e^{-G_{\text{m}}t/C_{\text{m}}} \right] \qquad (2.15)$$

and use linear summation of these unitary PSPs to obtain the total membrane potential transient. Each active synapse would then only require a simple addition during run time. This difference-of-exponentials function provides a more realistic and flexible PSP function that the alpha, single-exponential, and time-delay functions used previously (Shamma, 1989).

Figure 2.3 illustrates the differences between the non-linear effects of Equation 2.14 and the linear summation approximation of Equation 2.15 for the case of n simultaneous EPSPs. Note that the amplitudes of the resultant transient are very similar for the low activity case of $n = 100$, but the transients diverge as n increases. As the magnitude of the voltage transient approaches the magnitude of the reversal potential E_{rev}, Equation 2.14 is able to compensate for the conductive and driving-force effects that lower the amplitude contribution from each EPSP. Equation 2.15, however, has no such compensation and thus unrealistically overshoots the reversal potential.
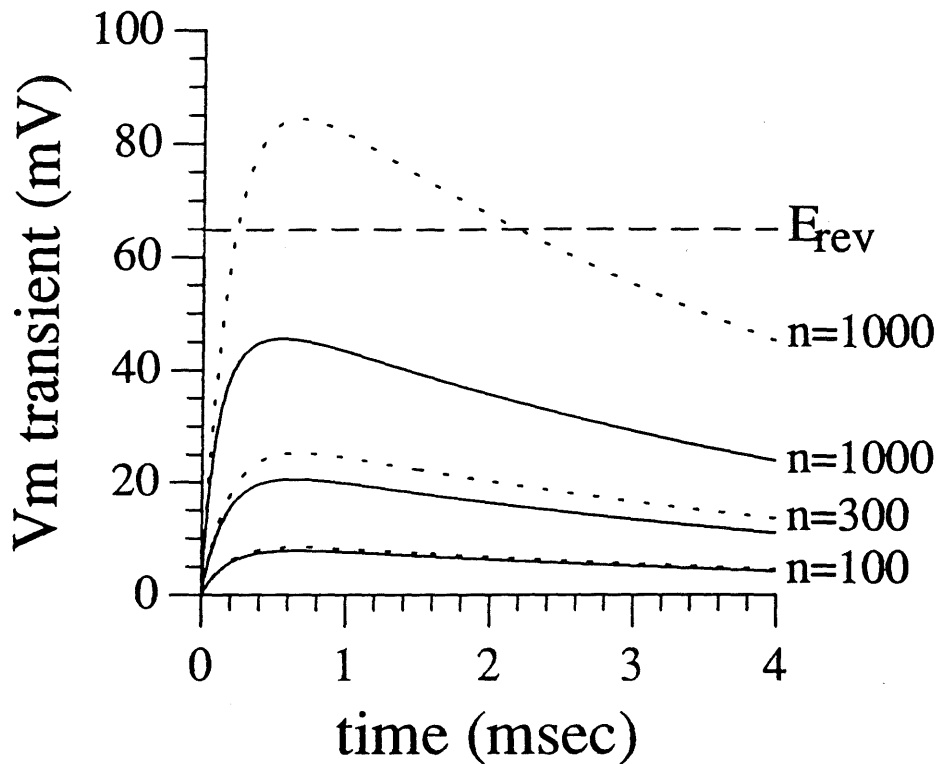
Figure 2.3: Comparison of combined membrane potential for multiple EPSPs with (solid lines) and without (dashed lines) the effective membrane contuctance (G_m) and driving-force (D_f) effects (Equations 2.12 and 2.15) for increased cellular activity. Notice that one can neglect the time-constant effects for low levels of activity, but the simple linear summation of PSPs without time-constant compensation causes the membrane potential to jump unrealistically beyond the reversal potential for the PSP if the level of activity is high. The parameters for the unitary EPSPs were $G_m = 54nS$, $C_m = 270pF$, $D_f(0) = 65mV$, $G_{syn0} = 2nS$, and $b = 5000$. The numbers of simultaneous EPSPs n were 100, 300, and 1000.

2.3 Simulation Results

A comparison was made between the time-constant and driving-force effects on integrated PSPs in a multi-compartmental biophysical model and in the integration method of Equation 2.14. Monosynaptic EPSP, IPSP, and combined EPSP/IPSP transients were generated by SPICE simulations using the thirteen-compartment representation of a cell soma and dendritic tree given by Segev et al. (1989) (see Figure 2.4a). The parameters of Equation 2.11 were then adjusted to produce PSPs that matched the individual EPSP and IPSP from the SPICE runs (see Figure 2.4b — top and bottom curves). Finally, the integration method of Equation 2.14 was employed to combine these two curve-fit PSPs, resulting in the middle trace in Figure 2.4b. Note that the PSPs combine in the same non-linear fashion in both approaches, demonstrating that the simple Equation 2.14 can simulate the time-constant and driving-force effects observed at the soma when compared to a detailed multi-compartment simulation.

Since the physiological model presented above provides an analytical closed-form algorithm for simulated membrane potentials, the model performs much more efficiently than numerical simulators such as SPICE. The data for the multi-compartmental SPICE simulation shown in Figure 2.4a used 25.4 seconds of CPU time on an N1000 NeXT computer. An implementation of the physiological model of Equation 2.14 and Equation 2.11, written in C on the same computer, generated the data for Figure 2.4b in only 0.75 seconds of CPU time (33.9 times faster than SPICE). A single-compartmental SPICE simulation (not shown) using the same membrane and synaptic parameter values in Figure 2.4b used 5.5 seconds of CPU time (7.3 times longer than the physiological model).

The physiological approach for dendritic integration described above has also been used in a simulation of 753 cells and inputs (including 6,104 synaptic connections and up to 23,725 simultaneously active PSPs) in a glomerular section of the mammalian olfactory bulb (see Chapter 3; also Antón et al., 1991d). This simulation was constructed to determine the physiological consequences of receptor cell firing frequencies on mitral/tufted primary cell threshold gradations. The integration method was combined with a firing threshold and refractory periods to form an integrate-and-fire paradigm for cellular activity. The interactive effects of the EPSPs and IPSPs were deemed important to the study due to the large numbers of receptor axons afferent on the primary mitral/tufted cells in the bulb. Figure 2.5 shows a sample tufted cell response to a 20Hz olfactory nerve input to the bulb, demonstrating the use of Equation 2.14 together with a firing threshold with absolute and relative refractory periods. Periglomerular and granule cell inhibitory interneurons were activated both directly from the receptor inputs and indirectly via dendrodendritic synapses with the tufted cell.

(a)

(b)
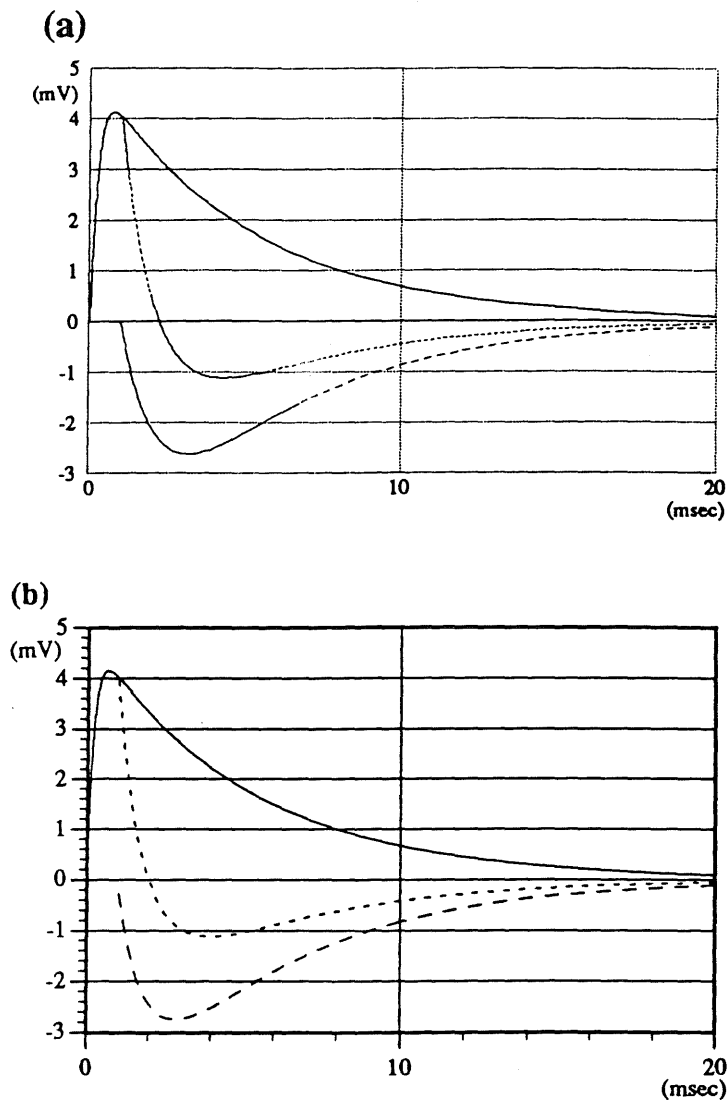
Figure 2.4: (a) SPICE simulation of a single EPSP (solid line) input on a distal dendritic branch and measured at the soma, a single IPSP (long dashed line) on a separate dendritic branch measured at the soma, and the combined membrane transient (dashed line) measured at the soma using the multi-compartmental representation of a dendritic tree given by Segev et al. (1989). The EPSP and IPSP were induced by exponential synaptic conductance transients with peak values of 5.1nS and 14nS at compartment nodes 302 and 216, respectively. (b) Simulation of the same EPSP and IPSP interaction using Equation 2.14. These exponential synaptic conductance transients had peak values of 66nS and 132nS, respectively, while $G_m = 54$nS and $C_m = 270$pF.
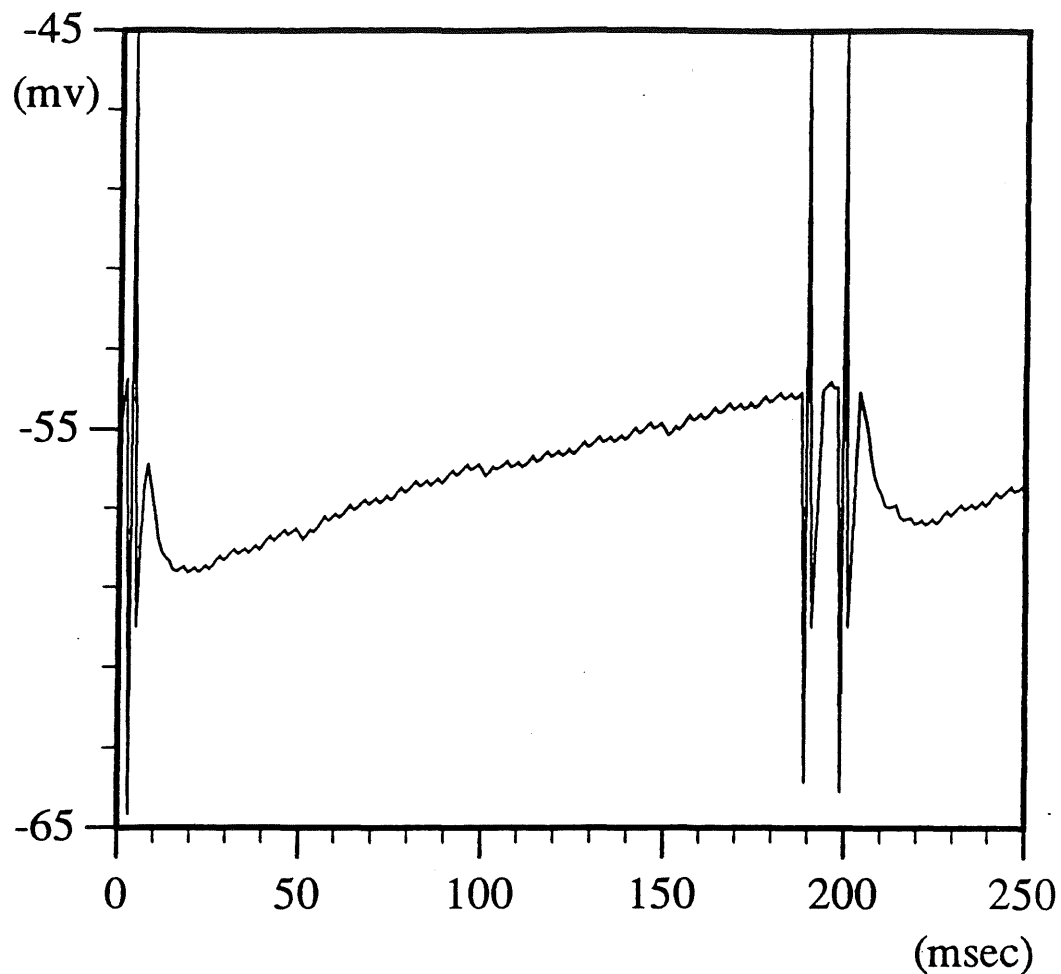
Figure 2.5: Simulated membrane response of a tufted primary cell in a simulation of a glomerular slice of a mammalian olfactory bulb employing the physiological dendritic integration of Equation 2.14 combined with a firing threshold. Each spike is composed of a simple jump-to-peak upon reaching threshold, followed by a jump-to-minimum and a linear rise back to the dendritic integration value. Absolute and relative refractory periods were imposed on the cell firing. The mitral/tufted EPSP parameters were $G_m = 135nS$, $C_m = 270pF$, $D_f(0) = 55mV$, $G_{syn0} = 2nS$, and $b = 550$. The mitral/tufted IPSP parameters were $G_m = 54nS$, $C_m = 270pF$, $D_f(0) = -20mV$, $G_{syn0} = 5nS$, and $b = 8$.

2.4 Discussion

The physiological model described above gives a dendritic integration approach that reflects the membrane time-constant and driving-force interactions between post-synaptic potentials (PSPs). The model gives shape functions for unitary PSPs (with or without channel conductive effects between synapses via the effective membrane conductance in the lumped RC circuit) and integrates these shape functions together in a non-linear manner, adjusting the amplitudes of the unitary PSPs given the dynamic ionic driving force per iteration. Cell firing can be determined by thresholds on the resulting membrane potential with the possible inclusion of absolute and relative refractory periods via a simple threshold manipulation.

Using exponential current injections, the general form of a unitary PSP is a difference of two decaying exponentials (Equation 2.9) which subsumes the special-case alpha function (Equation 2.10) used previously by Shamma (1989). It is interesting to note that this form for $v_j(t)$ is quite similar to the cable theory solution given by Rall (1962, 1969, 1989) for the membrane voltage decay following a simple current step pulse:

$$v(X, T) = \sum_{j=0}^{\infty} C_j e^{-t/\tau_j}$$

if we consider only the first two terms and set $C_j < 0$. Rall has noted that this sum yields realistic PSP transients when the C_j have alternating signs and that synaptic potentials do seem to decay with the membrane time constant τ_0 after the equalizing time constant $\tau_1 < \tau_0$ causes the second decaying exponential to have negligible effect (Rall, 1969).

Beyond simple current pulse decays, the model described here provides a parameter for adjusting PSP length based on the length of the current injection in addition to the effective membrane decay. The inclusion of the current-injection time constant b provides the flexibility of modeling cells that contain both very short and very long PSPs — for example, 15ms EPSPs and 400ms IPSPs in rat olfactory bulb external tufted cells (Schneider and Scott, 1983).

Additional research may provide a way of rationalizing the approximation of electrotonics by addition of a third decaying exponential (i.e., the τ_1 term in the Rall sum) to Equations 2.9 and 2.15 to account for the equalizing of voltage charge along a dendrite. Some electrotonic effects, however, are indirectly included in this model since the difference of exponential expression can be curve fit to known PSPs. Thus, if somatic potential is the primary measurement to be modeled (e.g., if cell firing is the primary concern), then the PSP shapes that are curve fitted have already undergone some electrotonic degradation.

Further extensions of this model are possible by using different expressions for the current injected at a synapse (see Equations 2.3 and 2.4). Tuckwell (1988, eqn. 3.21) has derived the response of the Lapicque model to the special-case alpha conductance function (Equation 2.4); his expression for a unitary PSP is slightly more

complicated than a simple difference-of-exponentials function but can easily be used in place of Equation 2.9. Additionally generalized PSP functions could be derived by using the general difference-of-exponentials conductance function (Equation 2.3) which contains a parameter for the rate of channel openings in addition to the rate of channel closings of Equation 2.1.

Note that the model presented can simulate short and long-term synaptic modifications. Changes in synaptic strength can be incorporated by changing the peak synaptic conductance G_{syn0_j} in Equation 2.6. Other changes in the effectiveness of receptor activation or transmitter removal rates can be reflected through changes in the synaptic time constant b_j (Equation 2.6). Still other changes in resting membrane potential can be incorporated directly into the summation expression (Equation 2.14). These modifications can easily be incorporated into a simulation via supervisory modulations of the above parameters while incurring negligible computational costs. Static weights are useful when studying temporal input patterns or during the performance operation of the system. Dynamic weights are useful in testing the effect of various learning rules on the system under study or to investigate the structure as a possible memory site.

While the equations derived above are simple lumped-circuit approximations of cellular membrane potentials that reflect conductance interactions and driving-force effects, they do provide a physiological model that is of considerable value for testing the significance of effects of such detailed physiological variables on the computations performed by neuronal aggregates. The efficiency of this new approach allows very large numbers of interacting cells to be modeled, thus permitting the testing of theories about the function of these structures if they are indeed based merely on PSP area summation over time with shape modulation due to channel openings and amplitude modulation due to driving-force effects. Shape modulation, for example, may be important when testing the differences between simultaneous and slightly offset arrival times of activation and inhibitory inputs to a cell. Amplitude modulation may be important when incoming signal strength is critical to the cellular operation or when testing the difference between one large input and several smaller simultaneous inputs.

The model presented above is more efficient than cable and compartmental models (Rall, 1962, 1964, 1989; Jack et al., 1975; Segev et al., 1989) and the membrane voltage expressions of Koch et al. (1982) since simple, closed-form, non-recursive analytical solutions are obtained for each individual PSP expression and for the subsequent linear summation of these membrane transients. Cable theory provides many analytical expressions for voltage transients in abstract situations that unfortunately contain extremely complex expressions and functions that preclude their use in the simulation of large numbers of neurons. Also, compartmental methods and SPICE simulations are quite useful in representing complex dendritic trees, cable effects, and active membranes but require more computational overhead. If these added capabilities are deemed irrelevant to the interactions or computations under

study then the more efficient physiological approach may be used. Furthermore, the membrane voltage expressions of Koch et al. (1982) involve either convolution integrals for voltage transients or multiplicative Volterra expressions for steady-state membrane potentials. While the steady-state equations are simple enough, they are limited to the steady-state. The more general transient-case expressions involve greater run-time computational overhead in calculating local responses than does the physiological model while excelling when cable effects are studied.

In addition to the speed benefits of this approach, actual PSPs can be modeled to reasonably reflect biophysical interactions without knowing the actual electrical properties of the cells in question. While multi-compartmental simulations may more accurately model the interactions of PSPs since they model the spatial dynamics of a cell, the electrical properties of a cell's dendritic tree and soma must unfortunately be investigated in great detail. If approximations of the actual cell properties are used through curve fitting of physiological data, then much of the foundation for the accuracy of the multi-compartmental approach is undermined; observed phenomena would then be based on approximations and would thus have similar validity to the physiological approach. Investigations of computations not requiring spatial input properties can then be investigated physiologically with lower overhead while maintaining time-constant and driving-force effects.

This physiological model, then, provides a tool for modeling structures of neuronal cells at a level of detail between the biophysical cable theory and compartmental models on one hand and more abstract physiological models on the other. While it therefore shares in some of the limitations of both approaches, it also shares in some of the benefits in aiding our understanding of the function of neuronal systems.

Chapter 3

Frequency-to-Spatial Transformation in the Olfactory Bulb

3.1   Introduction

The olfactory system is able to detect odor molecules over a very wide range of concentrations: from 10^{-13}M to 10^{-4}M (Vodyanoy, 1988); as little as one odor molecule can activate a nasal receptor (deVries and Stuiver, 1961). For concentration levels higher than these detection thresholds, the system is also capable of discriminating between very similar odors (Castellucci, 1985). Anatomically, the olfactory cortex receives information that has passed through only two synaptic connections and is thus very close to the environment; this allows easier investigations into cortical functions since the information received has not been processed much.

The olfactory bulb is the gateway for sensory information from the nasal receptors to higher parts of the brain (Allison, 1953; Shepherd, 1972; Mori, 1987). Since no other olfactory structures receive information directly from the receptors, an understanding of the processing performed by the bulb is crucial to understanding how odors are perceived.

Extant computational models of the bulb typically involve high-level modeling of mitral and granule cells simplified to non-linear oscillatory interactions (Freeman, 1987; Eisenberg et al., 1989; Li and Hopfield, 1989a,b). These extant models predict that such architectures have the capability of classifying odors via the pattern of oscillatory behavior of the mitral cells, proposing that the bulb manipulates receptor inputs but the output is still based on spatial patterns of frequency responses; mixed-odor inputs are transformed into the selection of an odor or odor combination represented by a spatial pattern of oscillators.

The new model described below proposes that the input may be transformed into a spatial representation of odor concentration in addition to odor type (Granger et al., 1990b). The pattern of glomeruli that respond may indicate the odor type while the number of primary cells responding in the glomeruli may indicate the concentration of the odor. As a result, this model does not preclude the spatial pattern for representation of odor type detected since different glomeruli may respond depending on the odor type, but does suggest that the concentration may be transformed into a spatial response within the responding glomeruli rather than an amplitude or phase component of the responding cells.

3.1.1 Bulb Anatomy and Physiology

The main olfactory bulb receives massively-convergent yet roughly-topographic inputs from approximately 50 million peripheral olfactory receptors (in rabbit) onto about 175,000 primary excitatory (mitral/tufted) cells in bulb (Allison, 1953; Shepherd, 1972). Olfactory receptor inputs (via the olfactory nerve) contact mitral/tufted and periglomerular cells in 1900 synaptic bundles, termed glomeruli. Each mitral/tufted cell in higher animals typically sends a dendrite to only a single glomerulus, so the primary bulbar cells can be divided into groups of 92 cells based on their glomerular membership. About 600 periglomerular interneurons ring each glomerular region, each receiving inputs from olfactory nerve axons and mitral/tufted dendrites. Mitral/tufted cells also send out long laterally-directed dendrites generating cross-glomerular dendrodendritic interactions with the inhibitory granule cells which total about 3 to 7 million. (Allison, 1953; Shepherd, 1972; Mori, 1987; Vodyanoy, 1988). The dendrodendritic contacts are two-way synapses that transmit direct excitation of the interneurons by primary cells and subsequent inhibition of primary cells by the interneurons in a graded (continuous) fashion (Rall et al., 1966; Shepherd, 1979). This operation is in contrast to the discrete action (excitatory and inhibitory) afforded by more typical axodendritic synapses in which the axon is activated in an all-or-none manner to transmit quanta of information to the dendrite it contacts. Figure 3.1 illustrates the glomerular anatomy simulated in the set of studies reported here.

Epithelial receptors fire with generally increased frequencies as the odor concentration in the epithelium increases (Getchell and Shepherd, 1978). Thus, there appears to be some type of temporal coding of odor concentration in the firing frequencies input to the bulb. Furthermore, the primary mitral/tufted cells of the bulb are less excitable with increasing depth (Onoda and Mori, 1980; Mori, 1987). This reduced excitability correlates with increased firing thresholds by depth (Schneider and Scott, 1983) while their secondary dendrites that synapse with inhibitory granule cells are also longer by depth (Macrides and Schneider, 1982; Mori et al., 1983; Orona et al., 1984; Mori, 1987).

Simulations were made to determine the effect of this excitability gradation on the frequency-related inputs to the bulb. Temporal summation of excitatory postsynaptic potentials (EPSPs) should lead to a positive relationship between input receptor firing frequency and the combined membrane potentials in the primary cells. The excitability gradations in these cells should then cause the number of mitral/tufted cells responding to reflect in some way the input frequency (see Figure 3.2).
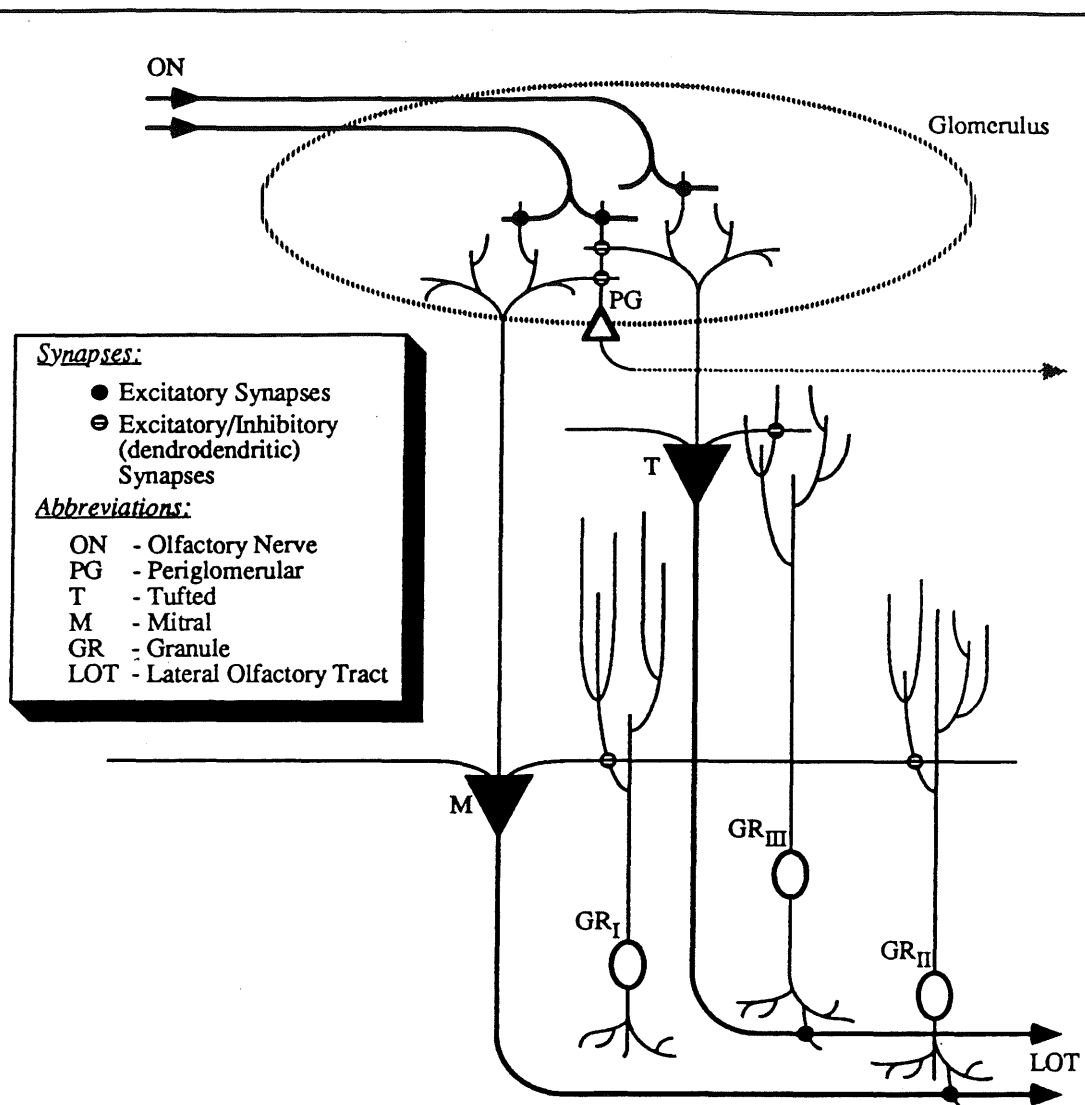
Figure 3.1: Schematic diagram of the simulated anatomy of an olfactory bulb glomerulus. The height achieved by the different types of granule cells (I, II, and III) reflects the approximate connectivity with the mitral/tufted cells at various depths, resulting in some restriction of the lateral inhibition between primary cells at various depths (Mori, 1987). The periglomerular axons (arrow at right) synapse with cells in adjacent glomeruli (not simulated). Mitral/tufted cell axons (bottom lines in figure) generate the lateral olfactory tract (LOT), the primary output from bulb and input to layer I olfactory cortex. (Allison, 1953; Shepherd, 1972; Mori, 1987).

3.2 Methods

The simulations used the integrate-and-fire paradigm with functions representing PSPs curve fit to actual physiological traces reported by (Mori and Takagi, 1978a; Kuffler et al., 1984; Schneider and Scott, 1983; Mori, 1987). The PSP function and integration method used was that described in Chapter 2 (Antón et al., 1991a), including the time constant and driving-force interactive effects.

The resting potentials $v_{m_j}(0) = v_{rest}$ for each cell were -55mV. The reversal potentials E_{syn_j} for the excitatory and inhibitory synapses were 0mV and -75mV, respectively. G_{syn0_j} was normally 2nS. The PSP function parameters were selected to yield realistic PSP shapes and time courses while remaining within reasonable bounds. The membrane conductances G_m for the mitral cells and the interneurons were 135nS and 54nS, respectively. The membrane capacitances C_m were all 270pF. The synaptic decay constants b_j were 550, 8, and 45 for the mitral EPSPs, mitral IPSPs, and interneuron EPSPs, respectively.

The 1ms simulation time step Δt was short enough to provide the temporal integration of PSPs deemed necessary for transforming incoming frequencies to membrane potential levels. Saturation and non-linear summation were considered particularly important since each primary cell synapses onto 5-25% of the 26,000 afferent receptor axons in each glomerulus (Mori, 1987). This physiological model, based on the lumped- circuit biophysical model (Rall, 1962; Jack et al., 1975; Tuckwell, 1988), provided lower computational overhead than the biophysical models that also exhibit these effects. It also allowed for representation of the very differing lengths of the PSPs found in the bulb — 13ms EPSPs and 400ms IPSPs in mammalian mitral/tufted cells (Schneider and Scott, 1983; Mori, 1987) — as well as incorporation of electrotonic modulation of the PSP shapes as seen by the cell soma without direct incorporation of electrotonic parameters.

Cell firing was determined by a firing threshold that entered absolute and relative refractory periods after firing. The absolute refractory period was set to reflect the desired minimum PSP spacing (see below). During the 10ms relative refractory period, the firing thresholds were increased by a constant 5mV. Since the simulation

Figure 3.2: Schematic of the frequency-to-spatial transformation based on threshold gradations. **(a)** The olfactory nerve (ON) input frequency results in a temporal summation in the primary cells that causes the two most superficial tufted cells to cross their firing thresholds and respons to the input. **(b)** A higher ON input frequency than in (a) results in a temporal summation in the primary cells that pushes all but the two deepest mitral cell membrane potentials across their firing thresholds, resulting in a greater number of cell responses in the glomerulus.

(a)

ON input firings

θ_M

Firing
Thresholds

θ_{eF}

Membrane
Voltage

Time

M

eT

Tufted | Mitral

(b)

ON input firings

θ_M

θ_{eT}

Membrane
Voltage

Time

M

eT

Tufted | Mitral
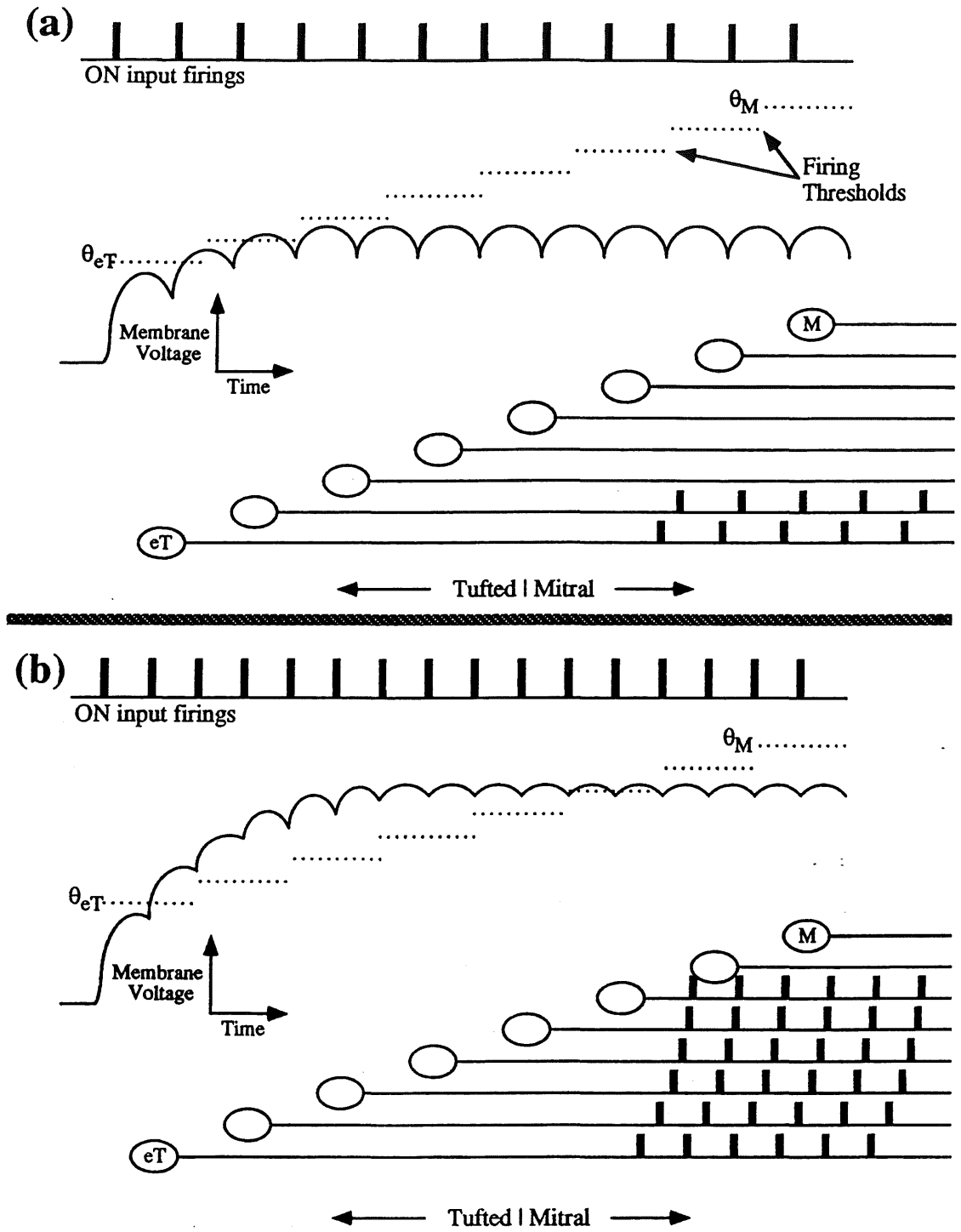
time step was on order the same length of an action potential, cell spiking was represented as a simple jump to peak (10mV), followed by a drop to minimum (-60mV), followed by a 10ms linear decay back to the dendritic membrane potential. Efferent axodendritic synaptic activations were all-or-none based on the spiking with realistic synaptic delays of 1–2ms (Mori and Takagi, 1978a). Passive spike propagation back through the primary mitral cells was also approximated with attenuation factors of 0.95 to the soma, 0.8 to the secondary dendrites, and 0.7 to the primary dendrites in the glomerulus.

Figure 3.1 illustrates the anatomical structures incorporated. The simulation included 625 olfactory nerve (ON) axonal inputs, 23 mitral/tufted (M/T) primary excitatory cells, 90 inhibitory granule (GR) interneurons, and 15 periglomerular (PG) interneurons. Therefore, the simulation was composed of 753 cells and inputs. These numbers compose approximately 25% of the primary cells and 2.5% of the cells afferent on these primary cells in a glomerular section. Thus, enough primary cells were modeled to obtain an excitability gradation while maintaining the approximate ratios between excitatory and inhibitory inputs to these primary cells.

The only type of M/T–PG connections simulated were reciprocal excitatory/inhibitory dendrodendritic synapses (Nowycky et al., 1981, fig. 8); restriction of the simulation to a single glomerulus precluded the activation of PG axons from adjacent glomeruli while inconclusive physiological data on the other periglomerular synapses (Mori, 1987) precluded their inclusion in this study.

The synaptic connections in the simulation were made using a pseudo-random selection from the appropriate postsynaptic candidate cells; this random selection process resulted in a realistic deviation in the number of excitatory and inhibitory inputs to each cell while approximately reflecting reported connectivities between bulbar cell types (or reasonable connectivities if actual numbers were not available). The ON axons each randomly synapsed 5 M/T cells and 3 PG cells, resulting in an approximate 20% connectivity from each M/T and PG cell to the axonal inputs in the glomerulus; the reported M/T percentage was 5-25% (Mori, 1987). Each M/T cell dendrodendritically synapsed 20% (3 cells) of the PG population. Each mitral cell dendrodendritically synapsed 15 granule cells (16.7% of the granule cell population) from their secondary dendrites, selecting candidate granule cells according to the M/T cell depth and the extent of each granule cell dendritic tree (see Figure 3.1). The number of the tufted secondary dendrodendritic synapses with granule cells was either set equal to the same number for the mitral cells (15) or to a smaller number (12, 4, or 3) that reflected the approximate length reduction of the secondary dendrites of the primary cells with decreasing depth; length factors were approximately 1.0, 0.8, 0.3, and 0.2 for mitral, internal tufted, middle tufted, and external tufted, respectively, based on Mori et al. (1983), Orona et al. (1984), and Mori (1987). The number of somatic and primary dendrite M/T to granule dendrodendritic synapses was 5 per cell (5.6% of the granule cells).

Each M/T cell axodendritically synapsed 2 granule cells (2.2% of the granule cell population). Thus, the ratio of axodendritic to dendrodendritic mitral to granule connections (2:20) was close to the reported value of 3:32 (Mori, 1987). Note that each dendrodendritic synapse required two connections between the cells: one for each activation direction. The number of synaptic connections, then, totaled 6,104.

The PSP lengths were set to 13ms and 400ms for M/T EPSPs and IPSPs, respectively, (Schneider and Scott, 1983) regardless of depth, 100ms for GR EPSPs (Mori and Takagi, 1978a), and 100ms for the PG EPSPs. The minimum PSP spacings per synapse for the simulator were 16ms (ON outputs), 5ms (M/T dendrodendritic outputs), 4ms (M/T axodendritic outputs), and 25ms (interneuronal dendrodendritic outputs). Since most of these spacings are shorter than the PSP lengths, multiple synaptic activations could overlap in time. Thus, multiple time counters were needed at each synapse to track the progress of each of the overlapping PSPs. For example, 25 time counters were needed for each M/T to GR axodendritic synapse (PSP length/spacing = 100ms/4ms = 25). As a result, up to 23,725 PSPs could be active at the same time if the shortest PSP spacings were used.

The currents reported by Schneider and Scott (1983) for the primary firing thresholds were approximately 205 microamps for the external tufted cells to 436 microamps for the deep mitral cells. M/T firing thresholds were set to be proportional to these values with a linear gradation (lowest threshold was approximately 47% lower than the highest threshold). Thresholds for activation of M/T dendrodendritic synapses were 1mV above the -55mV resting potential with a linear weight factor based on the highest membrane potential achieved during the synaptic event relative to the peak action-potential value of +10mV. The reciprocal inhibitory activations from PG and GR cells were activated in a shorter linear range of 1mV to 4mV over resting (followed by saturation) in order to reflect that the gemmule spine heads of the interneurons cause a much larger local head potential when compared to similar activations on dendritic shafts (Jack et al., 1975; Koch and Poggio, 1987; Antón et al., 1991b), thus causing easier activation of the reciprocal inhibitory response. This approach allowed us to include this local effect into the simulation without having to simulate a larger local EPSP in addition to the somatic EPSP since the somatic depolarization should be relatively unaffected by this local phenomenon (Koch and Poggio, 1987).

The response of the bulb simulation was tested at constant olfactory nerve input frequencies between 1 impulse/sec for background noise and 60 impulses/sec for peak excitatory activity (Getchell, 1986; Vodyanoy, 1988). Such step increases to the testing frequency approximates the rapid jump to a concentrate-graded high-frequency discharge following a short latency period reported by Getchell and Shepherd (1978) for a step pulse of odorant.

3.3   Fixed-frequency bulb response

Fixed-frequency firing has been observed in mammalian olfactory bulbs (Adrian, 1950; Freeman and Schneider, 1982), and fixed-frequency stimulation of a major target of bulb, olfactory cortex, results in both behavioral learning and synapse-specific synaptic modification in freely-moving animals (Roman et al., 1987), suggesting that fixed-frequency firing might be characteristic of naturally-occurring and behaviorally-relevant bulb activity.

Fixed-frequency rhythmic activity in the simulation was generated in two independent ways, corresponding to distinct hypotheses of how such rhythmic firing might arise intrinsically in bulb. Figure 3.3 shows the result of giving dendro-dendritic synapses between M/T cells and the GR and PG interneurons in the simulation an inherent 200ms refractory period for both synaptic directions (M/T-to-interneuron and interneuron-to-M/T); the result was that M/T cells responded regularly at 200ms intervals (5 bursts/sec). This refractory period suppressed interneuronal activity without direct implementation of the 180ms GR IPSP reported by Wellis and Scott (1990). Interestingly, the initial firing of a (relatively small) number of M/T cells was sufficient to elicit lateral inhibition (via dendrodendritic contacts with GRs) that drove other cells to respond at the 5 bursts/sec rhythm; this effect was observed even in low-frequency input runs of the simulation that caused only a few M/T cells to fire (partially since the axodendritic connections between M/T and GR cells were set randomly).

Figure 3.4 illustrates a version of the simulation that eased the GR inhibitory refractory period but which nevertheless exhibited the 5 bursts/sec firing pattern. Here the GR refractory period was reduced from 200ms to 25ms. The PG cells were turned off for this simulation since their direct inputs from the receptor axons would have caused their inhibitions to begin every 25ms, preventing the M/T cells from firing. The M/T to GR dendrodendritic activations were maintained at 200ms intervals during which the strengths of the GR EPSPs were graded by the highest M/T potential achieved; the axodendritic M/T to GR connections, however, could still activate the GR cells once every 4ms which then provided an avenue for GR potential buildup for strong M/T activation. Even though the M/T IPSPs caused by the GR cells were 400ms long, they decayed sufficiently after about 200ms for the M/T membrane potentials to reach their firing thresholds, resulting in the 5 bursts/sec pattern.

Note that the firing pattern shown in Figure 3.3 is very regular since the inhibitory cell populations were all activated at the same time due to the strong initial M/T spikes; this synchronized the beginning of the interneuronal refractions regardless of their levels of excitation, resulting in the synchronous M/T inhibitions. The bursting pattern in Figure 3.4, however, was not synchronous since the rhythmic behavior was due to the M/T potentials reaching firing threshold depending on the relative strengths of the EPSP and IPSP inputs. The random nature of the cell
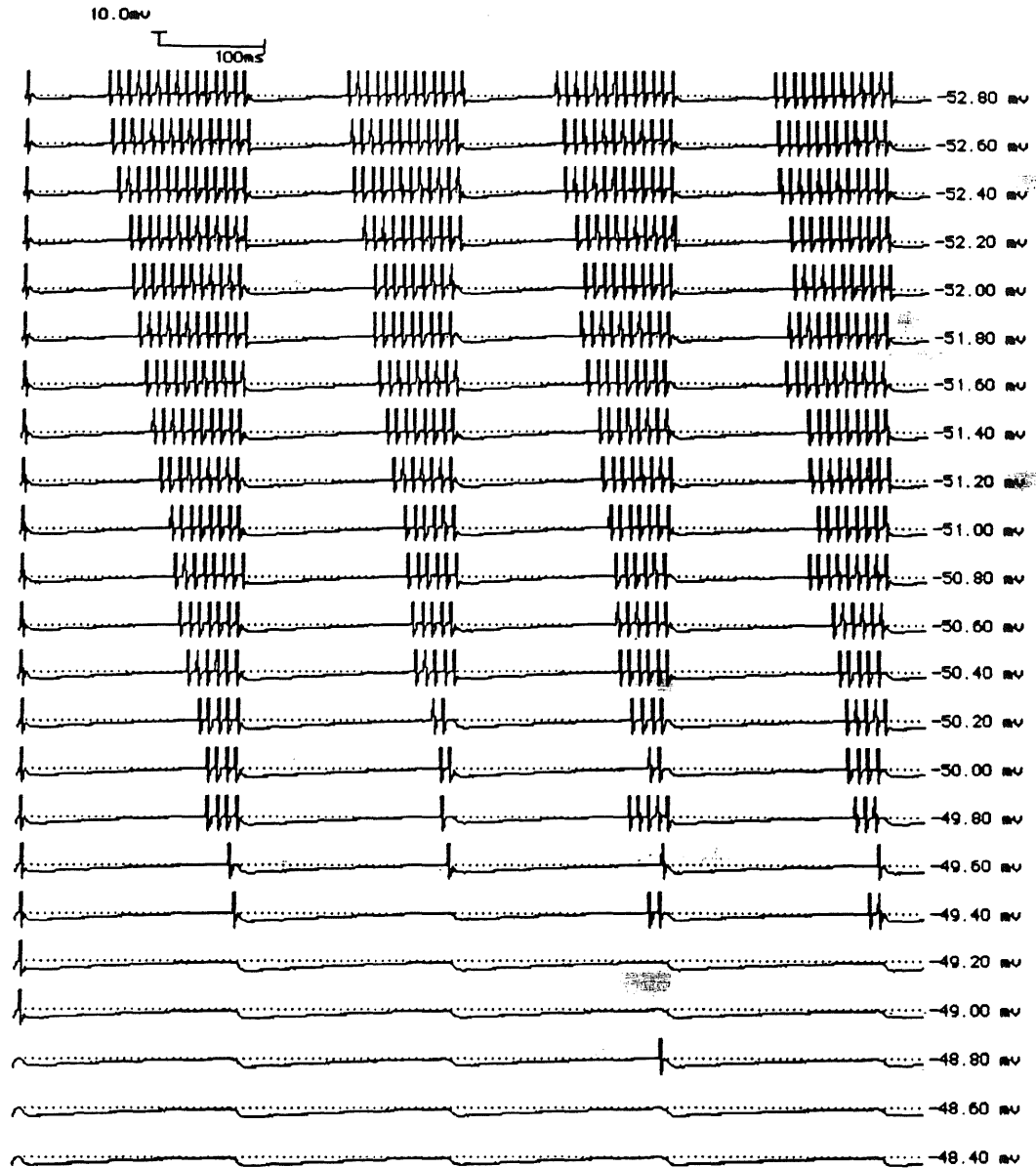
Figure 3.3: Cell potentials for 23 external tufted to deep mitral cells (upper to lower) demonstrating rhythmic firing behavior in response to a constant 50 impulses/sec olfactory nerve input. For this simulation, granule and periglomerular cells were given a refractory period of 200ms. The dashed lines show the normal (non-refractory) firing thresholds: -52.8mV + 0.2imV for the ith cell, where i increased with depth from the most external tufted cell (eT: $i = 0$) to the deepest mitral cell (M: $i = 22$). There was no gradation in M/T to GR connections for thus run.

connections resulted in a deviation in the number of inputs to each cell and thus a deviation in excitatory and inhibitory strengths, resulting in membrane potentials and rhythmic behavior variations. As a result, the causes of such rhythmic behavior — refraction or IPSP length — have a strong effect on the regularity of the bursting patterns. Such regularities may be important if the structures receiving bulbar outputs have sensitive timing rules. Note also that the more rhythmic pattern also has a smoother response gradation by depth. Since the M/T main axons project farther with increasing depth (Mori, 1987), stronger odors could invoke more complicated processing since more distant structures would then receive bulbar outputs that they might not receive for weak odors. Strong odors, for example, might invoke identification in addition to detection. Also, centrifugal inputs to the granule cells (Mori, 1987) might be used to increase bulbar sensitivity by reducing bulbar inhibition (Antón, 1991b) if only weak, short-reaching odors were detected. Inhibition of inhibitory granule cells, for example, could reduce the inhibitory response of granule cells from mitral/tufted excitation.

3.4   Frequency-to-spatial transform

To test the frequency-to-spatial transform hypotheses, simulation runs were conducted in which the constant input olfactory nerve (ON) frequencies were varied from spontaneous noise levels (1 impulse/sec) up to the highest level of activation reported (60 impulses/sec) in 10 impulses/sec increments. The initial firing latencies for the impulses on each receptor axon were randomly distributed, spreading the input over the 1ms simulation time steps. The stability of the transformation was tested by making series of these runs using differing inhibitory strengths (peak synaptic conductances) on the primary cells or varying ranges of threshold gradations. Further tests were made in which the number of dendrodendritic GR connections were made non-uniform based on the reported lengths of the M/T secondary dendrites by depth (see Methods section).

Figure 3.5 plots the number of simulated mitral/tufted cells responding to ON stimulation, as a function of the frequency of the ON activity, for these series of simulation runs.   Note that the number of responding cells increases monotonically with ON stimulation frequency in a sigmoidal fashion with an off range, a near-linear response range, and a saturation range. Simulation parameters such as the M/T inhibitory conductances (Figure 3.5a) and the range of mitral/tufted firing thresholds (Figure 3.5b) influence the frequencies at which response begins and saturates by shifting the response curve. Weaker IPSPs allowed the M/T potentials to rise higher before the next wave of inhibition was activated, resulting in a narrower but more sensitive response range (solid line, Figure 3.5a). Also, smaller threshold increments and a lower minimum threshold made each M/T cell more responsive since they were then easier to fire; as a result, the glomerulus saturates at a lower input ON frequency and has a steeper, more sensitive transformation.
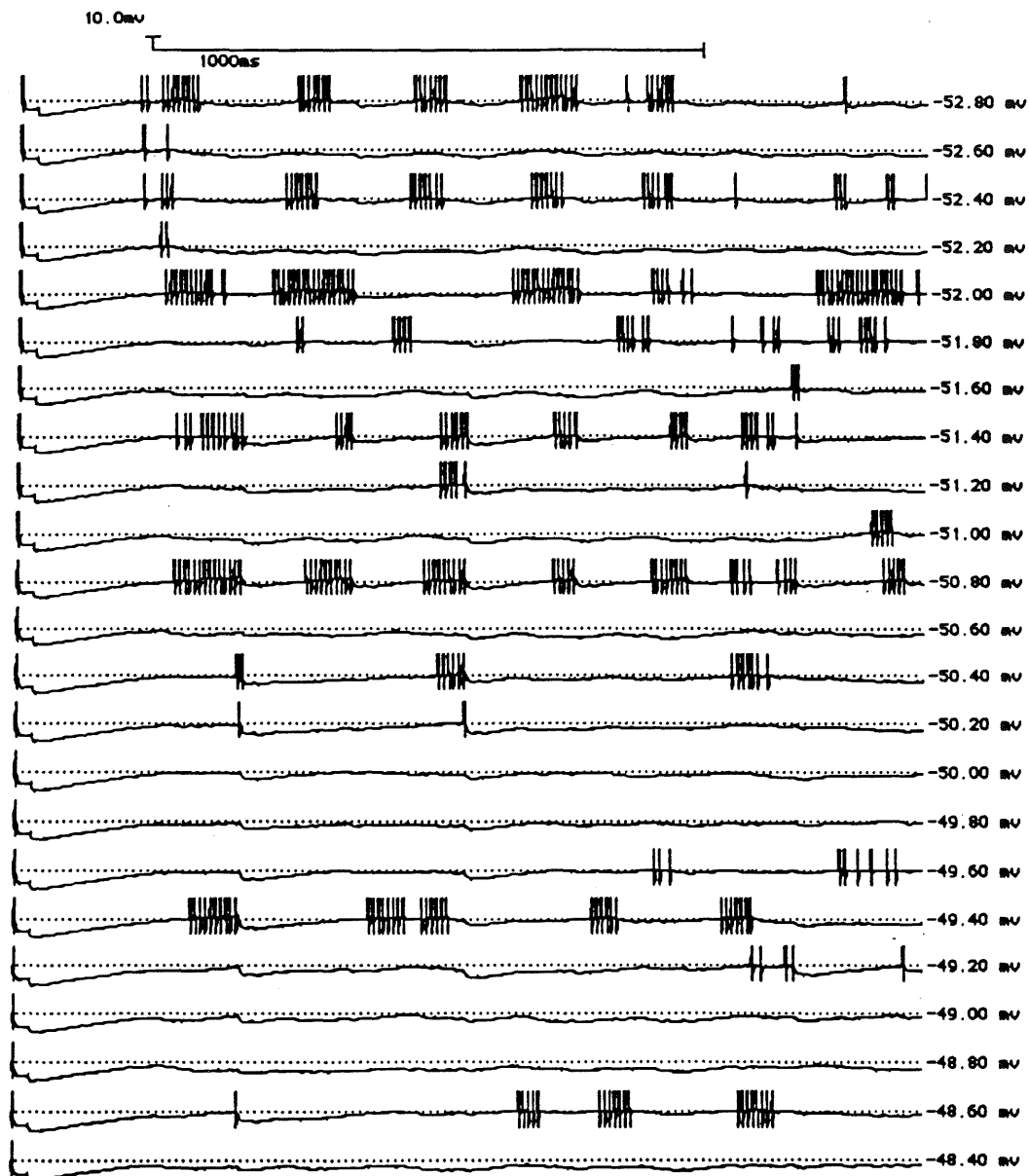
Figure 3.4: Similar test of rhythmic firing behavior as for Figure 3.3 except for a shorter 25ms GR refractory period and a stronger 60 impulses/sec olfactory nerve input.

The transformation effect was also present when setting the number of M/T secondary dendrodendritic connections with GR cells relative to the reported total lengths of the secondary dendrites by depth (Figure 3.5c). This reduction in inhibitory connections for the more superficial M/T cells allowed them to respond more robustly to excitation. This reduced inhibition was often enough to allow a few of the more superficial cells to cross threshold and fire (compared to the uniform connectivity shown in Figure 3.5b). Note that in a few cases the number of M/T respondents was reduced; in these cases the more robust tufted bursting increased the excitation of the inhibitory cells which was sufficient to increase the graded inhibition to the few deep mitral cells that had barely reached firing threshold before. As a result, there was no general trend towards an increase or decrease in the total number of cells with the reduced inhibitory synapses. This reduction did, however, reduce slightly the effect that changes in the threshold gradation had on the transformation since the solid and dashed transformation curves moved closer to one another slightly (compared to Figure 3.5b). The reduction in inhibition also strengthened the rhythmic output of the glomerulus by allowing the tufted cells to respond more strongly under weak input conditions which in turn kept the interneuronal responses stronger. Since only a subset of external tufted cells project outside of the bulb (Schoenfeld and Macrides, 1984; Mori, 1987), such highly-responsive external cells could be used to strengthen rhythmicity without impacting extrabulbar information processing.

Figure 3.5: The number of mitral/tufted (M/T) cells responding within a single simulated glomerulus versus the input firing frequency of the receptor axons stepped to a constant test value. The interneuronal refractory period was 200ms. (a) Effects of varying inhibition strength on the spatial response curve. M/T inhibitory synaptic conductances G_{syn0_j} were 0.5nS (solid line), 1nS (long dashes), and 2nS (short dashes). M/T firing thresholds were -52.8mV + 0.2imV for the ith cell, where i increased with depth from the most external tufted cell (eT: $i = 0$) to the deepest mitral cell (M: $i = 22$). The number of dendrodendritic connections with GR cells was equal for each M/T cell. (b) Effects of varying the threshold gradations on the spatial response curve. M/T firing thresholds were -54.0mV + 0.10imV (solid line), -53.4mV + 0.15imV (long dashes), and -52.8mV + 0.20imV (short dashes). G_{syn0_j} = 2nS while the number of dendrodendritic connections with GR cells was equal for each M/T cell. (c) Effect on spatial response curves from (b) when changing the number of dendrodendritic connections with GR cells for each M/T cell to be relative to the reported total lengths of the M/T secondary dendrites by cell depth (see Methods). The M/T firing thresholds were -54.0mV + 0.10i mV (solid line) and -52.8mV + 0.20i mV (short dashes).

(a)

(b)

(c)
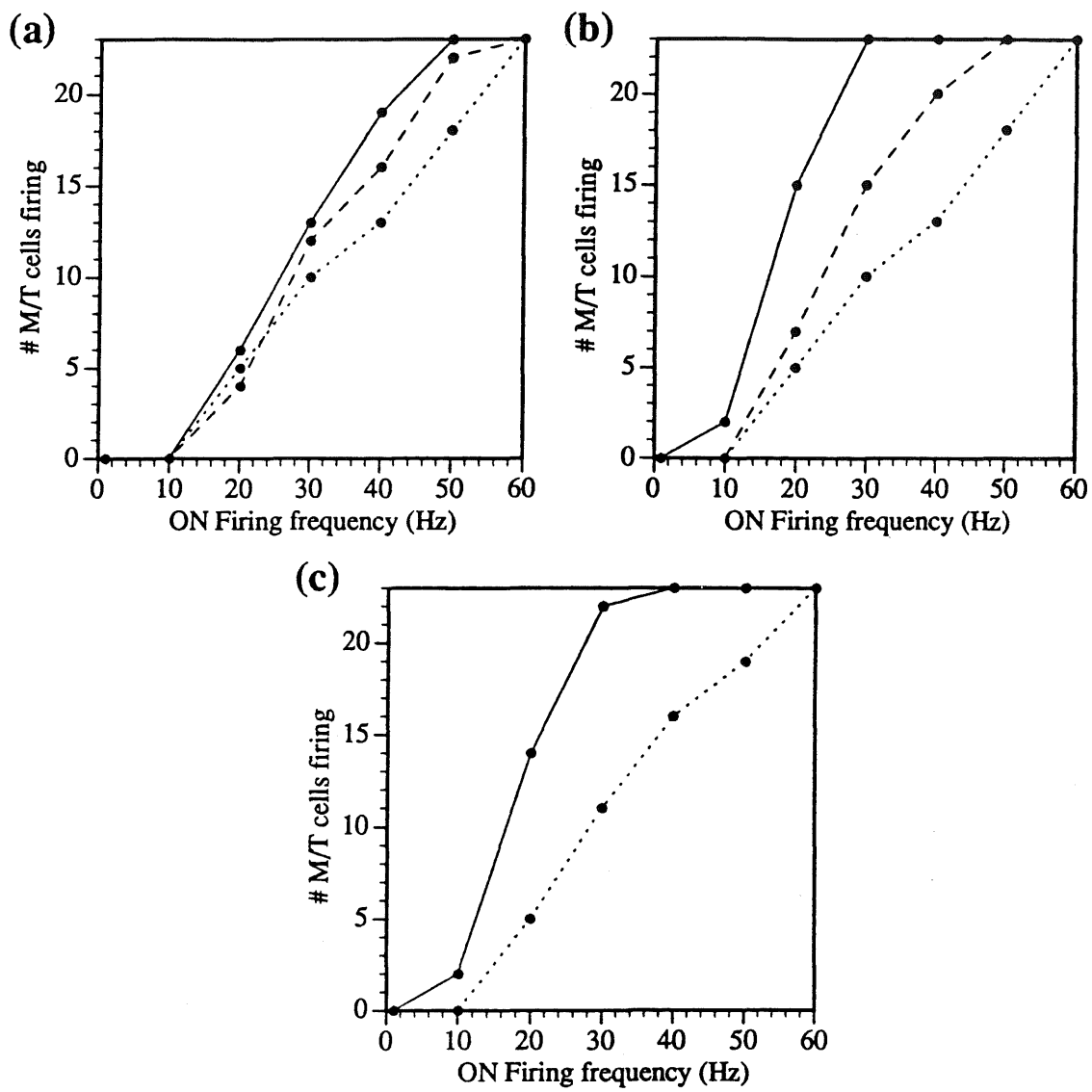
3.5 Discussion

The data presented above, then, indicates that one of the functions of the olfactory bulb may be to transform frequency-related concentration inputs into a spatial representation in the number of primary bulbar cells responding. This transformation has been shown to contribute to the interesting computational capabilities exhibited by higher-level computer simulations of interacting olfactory structures (see Ambros-Ingerson, 1990; Ambros-Ingerson et al., 1990; Granger et al., 1990a). These higher-level simulations demonstrated that the transformation of concentration data into a spatial representation can cause efferent cortical cells to respond in a pattern representative of the dominant odor passed by the bulb due to the domination of the response space by the higher-concentration odors. The combination of this property with feedback masking cycles resulted in a hierarchical clustering algorithm for input cues to the olfactory system.

Since the response range of the frequency-to-spatial transformation curve can be shifted over the range of input frequencies, it is reasonable to infer that the 'gain' of the bulb system should be controllable via centrifugal modulation of granule or periglomerular cell excitability; indeed, these cells receive relatively large centrifugal projections from septal regions and the horizontal limb of the diagonal band of Broca (Mori, 1987). For example, centrifugal inputs onto GR cells could modulate the background GR activation levels and thus modulate the strengths of reciprocal inhibitory responses from subsequent M/T activations since the dendrodendritic synapses are believed to be graded by pre-synaptic potential levels; this effect would be similar to the changes in M/T IPSP strengths shown in Figure 3.5a.

Also, volleys in the anterior commissure or centrifugal fibers from the olfactory cortex cause large mitral cell IPSPs via the activations of GR cells (Mori and Takagi, 1978b; Mori, 1987). This should have an effect on M/T cells similar to raising the firing thresholds by lowering the background (resting) membrane potential in M/T cells, making them harder to fire by increasing the amount of excitation needed for firing. The simulations shown in Figure 3.5b demonstrate that such threshold changes can also shift the response curve of the glomerulus slice.

Such shifts in the response curve of the frequency-to-spatial transformation would then allow for higher-function control of the sensitivity of the M/T cell response to ON frequencies and thus to the odor concentration at the receptor sheet. If the curve is moved to the left via efferent inhibition of (inhibitory) GR cells, then the bulb will become more sensitive to lower frequency inputs. On the other hand, efferent excitation of GR cells would move the transformation curve to the right, thus requiring higher-frequency ON inputs for bulb response.

Such a control approach would permit the olfactory system to operate in different modes. High-concentration odors would be detected at the expense of hidden odors by shifting the response to the higher frequencies. Low-concentration odors would be detected at the possible expense of noise problems by shifting the re-

sponse to the lower frequencies. Hidden odors could be detected by using a simple masking operation (Granger et al., 1990a, b; Ambros-Ingerson et al., 1990). High-concentration odors could first be detected with the response curve set for high frequencies; the odors hidden due to lower concentrations could subsequently be uncovered by masking the glomeruli that respond to the high-concentration odor and shifting the response curve to the lower frequencies.

As a result of the shifting of response curves, low-concentration odors can be detected while maintaining a transformation curve that can measure small concentration differences in the response range. Thus, the total odor concentration could be determined grossly by the strengths of the centrifugal controls on the bulb and precisely within the gross range by the number of M/T cells responding.

We are currently extending the simulation to include multiple glomeruli and their interactions via the long mitral/tufted secondary dendrites and through granule and periglomerular lateral contacts. Extensions to multiple glomeruli will allow the investigation of competition between odor components by testing the interactions between glomeruli for different spatial ON inputs. It is possible that the larger system will behave in ways much more complex than those hypothesized here for individual glomeruli.

Smaller scale extensions may include the range of synaptic types involving the periglomerular interneurons beyond the reciprocal dendrodendritic connections included in this work. Additional depth differences between the mitral and tufted cells could also be included by reflecting the differences in PSP lengths recorded by Schneider and Scott (1983). Deeper primary cells have shorter EPSPs and IPSPs. Despite these complexities, deeper cells remain harder in general to excite orthodromically (Schneider and Scott, 1983), so we expect the frequency-to-spatial transformation to remain.

Further extensions could include a test for rhythmic behavior given a very short (5ms, say) period between repeated dendrodendritic activations rather than the present 200ms length. On the other hand, a 180ms GR IPSP could be implemented to follow ON stimulation (Wellis and Scott, 1990) rather than relying on the more abstract refractory periods. Also, the dendrodendritic connectivity restrictions by depth between the M/T and GR cells could be extended to the axodendritic connections. This would provide a greater inhibitory isolation by depth between M/T cells than the current GR peripheral dendritic extents provide and might yield an avenue for easier activations of the deeper mitral cells given early activation (followed by inhibition) of the superficial tufted cells.

In summary, the temporal EPSP summation in mitral/tufted cells can cause higher membrane potentials corresponding to higher input frequencies. Threshold gradations by depth for the primary M/T cells thus cause the number of cells responding to reflect the input frequency and give the bulb the capability of transforming odor-concentration information expressed in the input receptor firing frequency into a spatial representation via the number of M/T primary cells firing.

Chapter 4

Strength and Plasticity of Graded Dendrodendritic Synapses and Lateral Inhibition in the Olfactory Bulb

4.1 Introduction

Many ideas have been advanced concerning the utility of dendritic spines in neuronal processing (Wilson, 1984, 1988; Coss and Perkel, 1985; Rall and Segev, 1987; Koch and Poggio, 1987; Segev and Rall, 1988). These include control and modulation of information transfer from the input site to the rest of the cell by changes in input resistance (Rall, 1970; Rall and Rinzel, 1971; Koch and Poggio, 1983) to devices for concentrating calcium (Coss and Perkel, 1985; Gambel and Koch, 1987; Holmes, 1990) to sites for active membrane amplification (Diamond and Yasargil, 1969; Jack et al., 1975; Shepherd et al., 1985; Miller et al., 1985; Perkel and Perkel, 1985; Segev and Rall, 1988) and control of inputs (Koch and Poggio, 1987; Shepherd and Brayton, 1987; Shepherd et al., 1989). These effects are generally concerned with axodendritic synaptic connections where the dendritic spine is postsynaptic and the effects are studies for the postsynaptic cell only. More complicated synaptic arrangements, however, are found in neuronal structures that contain dendritic spines. Dendrodendritic connections in the olfactory bulb, for example, involve synaptic spines on the interneurons (Shepherd, 1979; Mori, 1987). Since the strengths of these synapses are believed to be graded based on the presynaptic voltage (Shepherd, 1979; Mori, 1987), a number of complications arise in the dendrodendritic spine case.

  First, presynaptic depolarizations may remain below the cellular firing threshold but above the activation threshold for the dendrodendritic synapse. As a result, spines may concentrate local charge in the spine head in order to increase the local potential beyond what would be achieved in a dendritic shaft (Rall, 1974; Koch and Poggio, 1983; Kawato et al., 1984; Wilson, 1984); this increase in local response would facilitate larger graded reciprocal responses (Jack et al., 1975) at the expense of reducing the overall potential contribution at the base of the spine neck. Even if the presynaptic depolarizations were above the firing threshold, an action potential may not significantly propagate back through the dendritic tree from the axon hillock to the dendrodendritic sites. Thus, spines could function to permit large reciprocal responses at low levels of local input without having to modify the synaptic gradation to amplify the synaptic response at these low levels. As a result, the synaptic response curve could be broad in order to allow the grading of lateral

inhibition based on global depolarization levels while simultaneously permitting strong reciprocal responses to small local inputs; such inhibition in stages could help control bulbar excitation over a wider range of input levels.

Furthermore, changes in the spine neck axial resistance could influence the strengths of the reciprocal response by increasing the input resistance at the spine head, thereby increasing the local response and thus the reciprocal response. Such changes in spine neck resistance — once a candidate for axodendritic potentiation and LTP (Rall, 1970, 1974, 1978; Rall and Rinzel, 1971; Wilson, 1984; Coss and Perkel, 1985; Jung et al., 1991) — might function to effect memory traces by (presynaptically) modifying the inhibitory response of the granule cell for dendrodendritic synapses. Brennan et al. have reported that changes in synaptic efficacy at these dendrodendritic synapses in the accessory olfactory bulb create a behaviorally-relevant olfactory recognition memory in mice (Brennan et al., 1990). Also, activation history has been shown to affect spine neck geometries in axodendritic synapses (Fifková and van Harrenveld, 1977; Lee et al., 1980; Desmond and Levy, 1983; Chang and Greenough, 1984; Wilson, 1984; Coss and Perkel, 1985; Koch and Poggio, 1987), thus opening the possibility of such changes in dendrodendritic synapses on spines. As a result, spine neck resistance changes — either by changes in the cytoplasmic resistance or through changes in the spine geometry — could express relevant memories through modification of bulb performance in the recognition process.

4.2 Methods

To test the impact of spine geometries on dendrodendritic inhibition, biophysical computer simulations were constructed to model the anatomical and biophysical properties of olfactory bulb mitral (M) and granule (GR) cells as well as graded reciprocal synapses between the cell types. The simulations — based on the multi-compartmental approach of Rall (1964) and written in SABER (Carnevale et al., 1990) — directly modeled the electrical properties of the passive membranes of cell sections and the interactions between these sections.

The simulations used the cylindrical geometries and passive membrane properties of Shepherd and Brayton in their study of lateral inhibition in the olfactory bulb (Shepherd and Brayton, 1978, 1979) (see Figure 4.1). Like these studies, the simulations described below included cylindrical representations of dendritic components from two mitral cells synapsing on a single granule interneuron. The M, GR shaft, GR spine head, and GR spine neck cylindrical-compartment diameters were $4\mu m$, $1\mu m$, $1\mu m$, and $0.2\mu m$, respectively. The M, GR shaft, GR spine head, and GR spine neck compartment lengths were $100\mu m$, $50\mu m$, $3\mu m$, and $3\mu m$, respectively. Mitral and granule specific membrane resistances were $2K\Omega\text{-}cm^2$ and $4K\Omega\text{-}cm^2$, respectively. All compartments had a capacitance of $80\Omega\text{-}cm$ and cytoplasmic resistance of $1\mu F/cm^2$ (Shepherd and Brayton, 1978). Compartment axial

(a)

(b)

5

5
10
4
4 9
3
8
3 7
2
6
2 5 1
1
GR

M2

1
M1

GR$_4$ GR$_3$

GR$_8$

M2$_3$

(c)

GR$_1$ GR$_2$

M1$_3$

GR$_7$
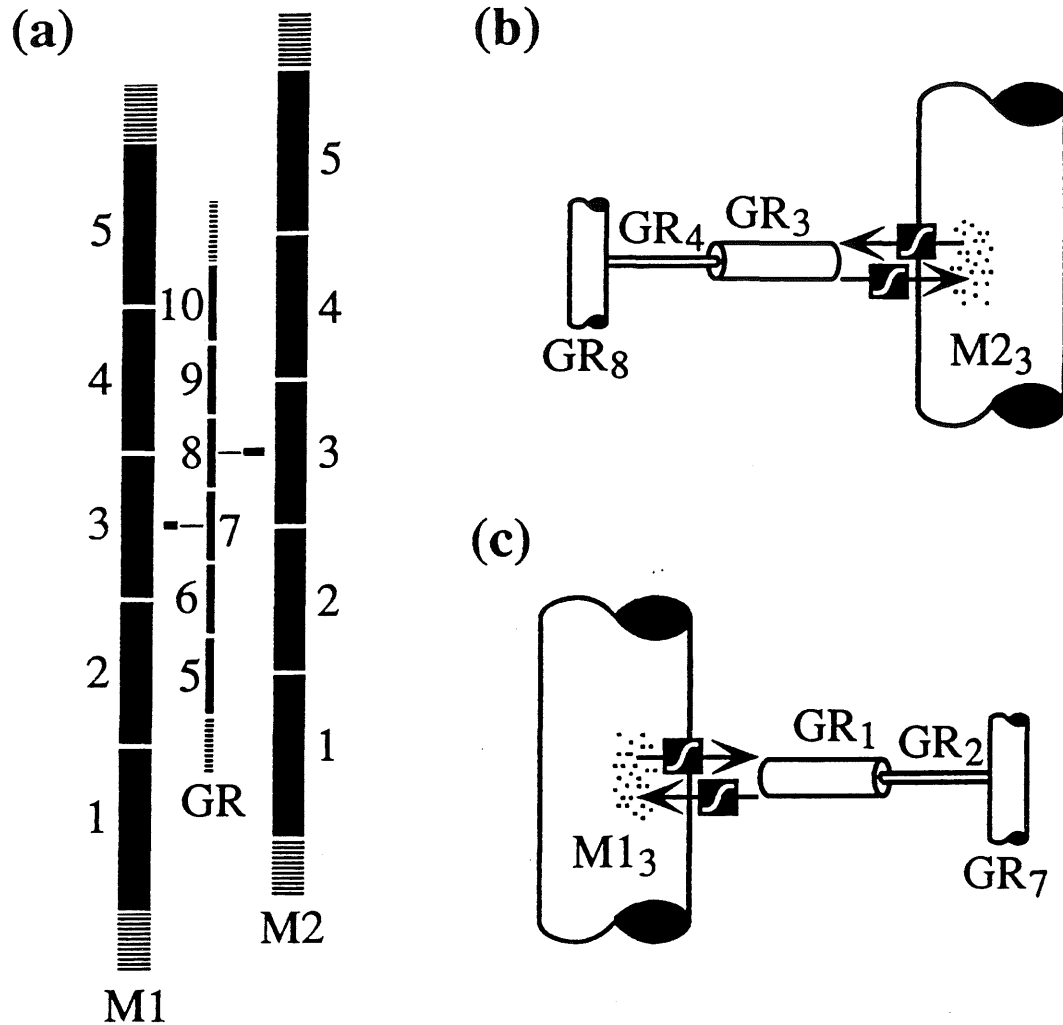
Figure 4.1: (a) Compartmental representation of the cylindrical sections of the cells in the model. The simulation included two mitral cells (M1 and M2) and a single granule cell (GR) dendrodendritically that connected to both M1 and M2. Enlargements (b) and (c) show the bulbar dendrodendritic connections as found in the bulb. The simulation test cases were activated with a voltage clamp spike in M1$_1$ with peak amplitude of 110mv (relative to the resting potential), linear rise and fall times of 0.5msec, and 0.01msec peak plateau.

resistances, membrane resistances, and membrane capacitances were computed using the cylindrical transformations of Rall (Rall, 1977; Segev et al., 1985).

Additional tests were also performed using the dimensions reported from serial reconstructions of granule dendritic spines recently reported by Woolf et al. (1991). Here the mean major axis (1.36μm) was used for the head cylinder length with an effective radius of 0.51μm. Also, the mean spine necks were found to be shorter and a bit fatter (1.73μm mean length and 0.23μm mean diameter) than those modeled by Shepherd and Brayton.

Graded synapses were added to all simulations using a simple model of transmitter release and receptor bonding (see Figure 4.2a). Presynaptic voltage was measured through an ideal time delay (0.5ms) representing calcium channel activation and/or other biochemical reactions necessary for transmitter release (Shepherd, 1979). Delayed voltages above the activation threshold (5mv) were graded by a sigmoidal function to produce the transmitter current $i_t(v) = 1/(1 + e^{a(v_b - v)})$ with peak slope $a/4$ at $v = v_b$. This current was then injected into a simple RC filter $(v = iR + C^{-1} \int i \; dt)$ that smoothed the current rise and fall times, representing the transmitter diffusion across the synaptic cleft, receptor binding dynamics, and the probabilistic nature of channel closings (Colquhoun, 1981). The voltage in this RC circuit was then used to control the graded postsynaptic conductance $g_{sym} = g_{peak}v_c$. This synapse model exhibits the overall sigmoidal relationship between presynaptic potential and peak postsynaptic response seen in both spiking (Shepherd, 1979; Graubard et al., 1983; Koch and Poggio, 1987) and non-spiking neurons (Katz and Miledi, 1967; Graubard, 1978; Shepherd, 1979; Koch and Poggio, 1987) (see Figure 4.2b). For all except the narrow gradation tests (Figure 4.6), the grading sigmoid saturated at approximately 100mV above resting potential, had a midpoint $v_b = $ 50mV, and time constant $a = 100$.

4.3 Results

Location of granule dendrodendritic synapses on spine heads rather than dendritic shafts increased the reciprocal granule response while reducing the granule response through lateral synapses. This effect was shown in simulations using cylinder sizes used by Shepherd and Brayton (1978, 1979) (Figure 4.3) and also those adding the spine sizes reported by Woolf et al. (1991) (Figure 4.4).
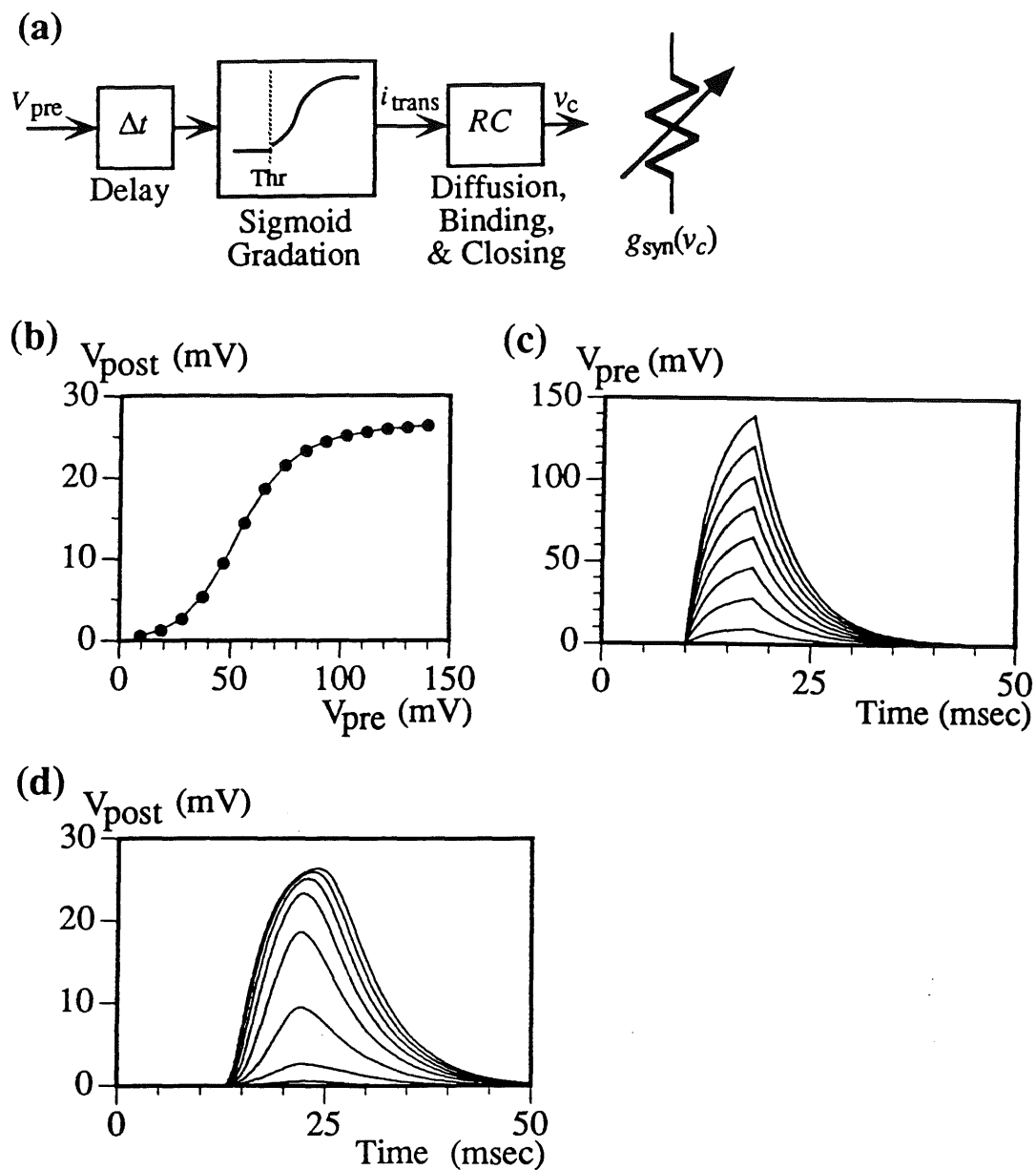
Figure 4.2: (a) Model of a graded synapse. Presynaptic voltage samplings were delayed, graded, and smooth to produce the controlling voltage for the post-synaptic conductance $g_{syn}(v_c)$. (b) Peak postsynaptic potentials given presynaptic spikes ranging from 10mv to 150mv in 10mv increments (relative to resting potential) with $a = 100$ and $v_b = 50$mv. Sample presynaptic (c) and postsynaptic (d) potentials from the graded synapse model.

Figure 4.3: Comparison of synaptic effects when locating dendrodendritic synapses on granule spine heads GR_1 and GR_3 (dashed lines) or on dendritic shaft compartments GR_7 and GR_8 at base of spine necks (solid lines). Cylindrical size parameters were from Shepherd and Brayton (1978, 1979). (a) IPSPs in $M1_3$ (reciprocal inhibition: heavy lines) and $M2_3$ (lateral inhibition: thin lines) following the excitatory spike in $M1_1$. The excitatory mitral spikes went off the plotting scale due to the close-up of the IPSPs. (b) Inhibitory synaptic conductances on $M1_3$ (heavy lines) and $M2_3$ (thin lines). (c) Granule synaptic site potentials. (d) Dendrodendritic synaptic currents into GR_1 (dashed line) and GR_7 (solid line).
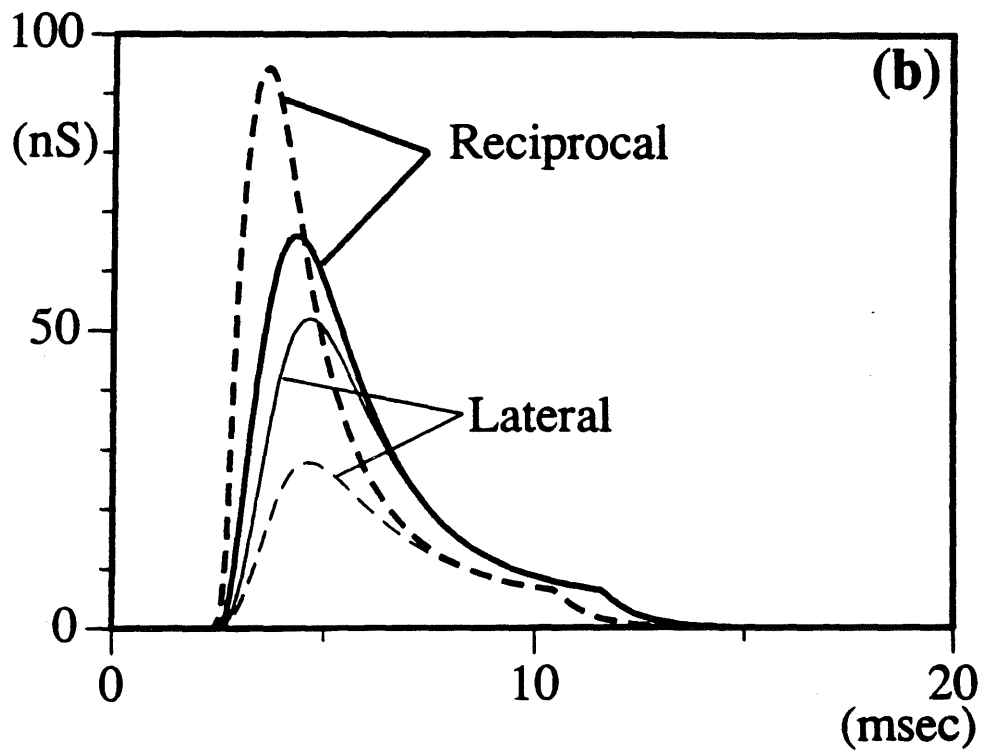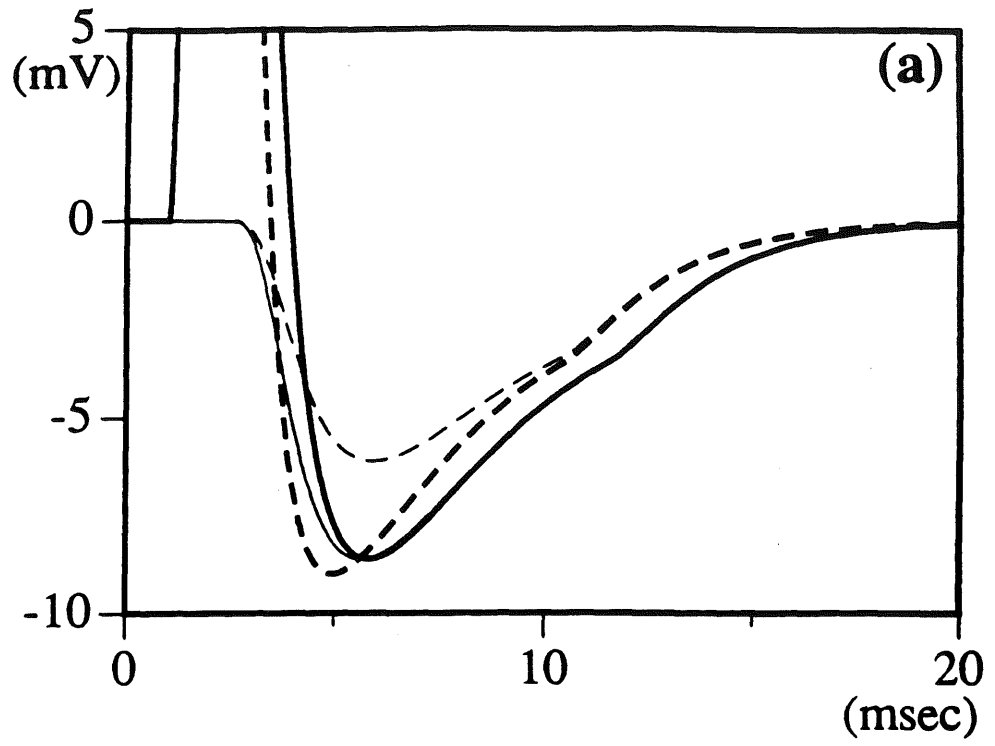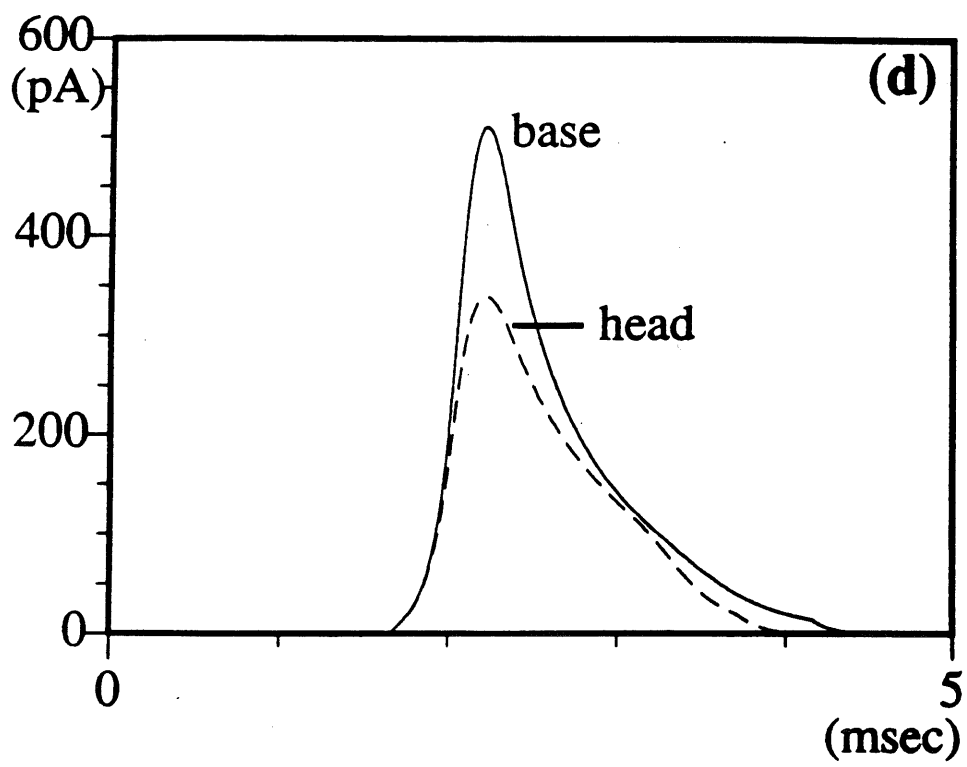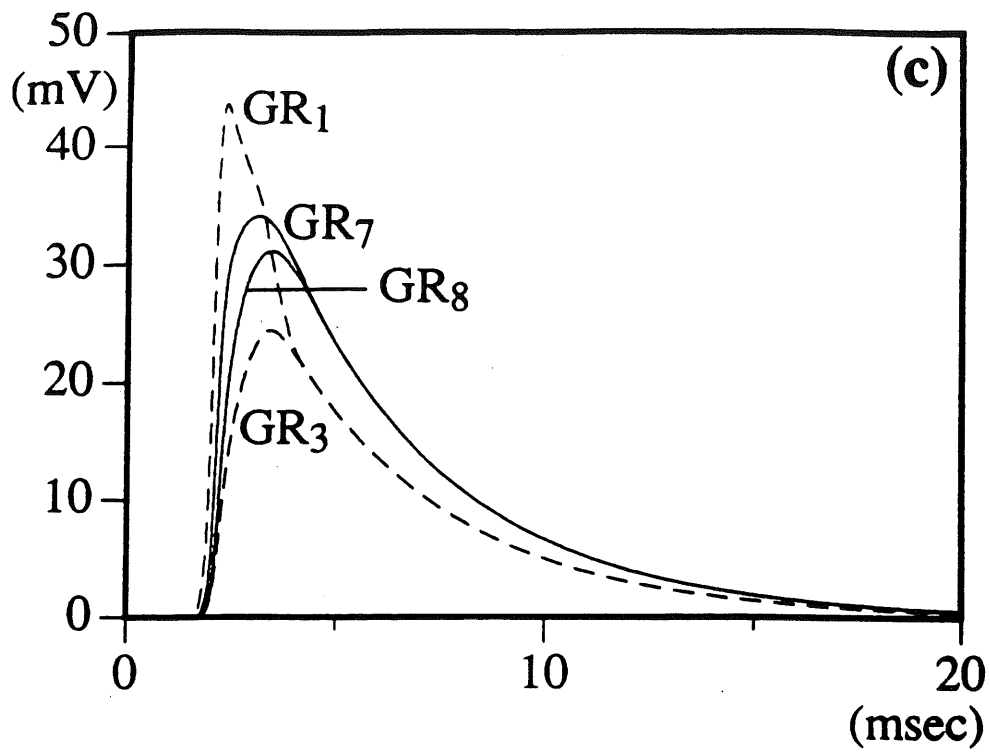
In both cases the reciprocal and lateral responses were measured following an excitatory spike in $M1_1$ when the granule dendrodendritic synapses were all located on the dendritic shaft (GR_7 and GR_8). The responses were also measured when the granule dendrodendritic synapses were moved to the spine heads (GR_1 and GR_3) adjacent to the previous shaft locations. As expected, locating the excited synapse on the spine head GR_1 caused larger local potentials despite making smaller synaptic currents (Chang, 1952; Rall and Rinzel, 1971; Rall, 1974; Jack et al., 1975; Koch and Poggio, 1983; Wilson, 1984; Rall and Segev, 1987; Segev and Rall, 1988). These larger local potentials in turn facilitated the dendrodendritic reciprocal response back on to $M1_3$ since the synapse was graded by the presynaptic potential. Thus, moving the synapse from the granule dendritic shaft (GR_7) to the spine head (GR_1) facilitated the reciprocal response. In addition, synapsing on the head reduced the lateral inhibitory response due to the smaller synaptic current in GR_1, resulting in a smaller EPSP propagating throughout the granule interneuron. The movement of the lateral synapse from the dendritic shaft GR_8 to the spine head GR_3 had a negligible effect on the reciprocal and lateral responses due to the small size of the spine when compared to the granule dendritic shaft. This lateral synapse received no excitatory input from $M2_3$ in either case. The resulting mitral cell IPSPs for the exclusive Shepherd and Brayton case are also shown in Figure 4.3a. The IPSPs obtained using the spine dimensions reported by Woolf et al. (1991) were smaller since the necks were shorter and since the IPSPs overlapped more with the excitatory spine in M1; the reciprocal and lateral effects were evident, however, in the synaptic conductance plots using the Woolf et al. data (Figure 4.4a).

In addition, the effects due to changes in input spine neck axial resistance on reciprocal and lateral inhibitions were also tested. These changes were simulated in two ways: by changing the cytoplasmic resistance R_i of GR_2 directly and by changing the neck cylinder diameter of the input spine neck GR_2. The effects due to changes in R_i directly are shown in Figure 4.5 while narrowing the neck diameter produced nearly identical results. In both cases an increase in the axial resistance increased the reciprocal response (due to higher local potentials in the spine heads) while decreasing the lateral response (due to smaller global potentials in the granule dendritic tree). Other tests adding changes in the resistance of the lateral spine neck GR_4 showed a negligible effect on the inhibitions since spines being depolarized by the dendritic tree closely mirror the tree potential due to the very small spine capacitance compared to the rest of the dendritic tree.

All of these tests were performed with dendrodendritic synapses graded over a broad range of presynaptic values. The grading sigmoid saturated at about 100mV above resting potential, had a midpoint (v_b) of 50mV, and time constant $a = 100$. This broad range enabled the synapse to remain sensitive to the peak voltages attained in the spine head and thus to the changes in spine neck resistance. If, however, the gradation range was much shorter (i.e., having a high dynamic gain), then the synapses mostly emphasized the behavior of the presynaptic potential in the

sensitive range. For example, Figure 4.6 shows the result of repeating the cytoplasmic resistance experiment of Figure 4.5 using a sigmoidal gradation more sensitive to the presynaptic potentials in the range 5–35mV. Here the increase in neck resistance did not result in an increase in the reciprocal response since the potentials fell faster with the higher neck resistance (Figure 4.6b). The small synaptic gain still recognized, however, that the response in GR_1 peaked higher than the response in GR_3; as a result, the reciprocal response was still stronger than the lateral response but the difference was not as pronounced (Figure 4.6a). The overall granule cell potential was much lower in the high neck resistance case since much less synaptic current was generated (Figure 4.6c) due to the higher input impedance (Rall and Rinzel, 1971; Koch and Poggio, 1983; Wilson, 1984). In general, then, increases in the spine neck resistance favor the reciprocal response over the lateral response, even if the synaptic gradation is limited.

4.4   Discussion

As a result of reciprocally synapsing on dendritic spines rather than dendritic shafts, high levels of granule excitation are not required to initiate a strong reciprocal response back onto a mitral cell. Such spine synapsing, however, does reduce the synaptic current injected into the granule cell and thus reduces the overall granule dendritic tree excitation. As a result, larger levels of granule excitation (and thus mitral excitation) are needed to obtain strong lateral inhibition. Thus, granule-mediated inhibition in the olfactory bulb may take on a two-level approach: reciprocal inhibition dominating at low levels of activity with lateral inhibition requiring higher levels. This two-level approach is compatible with the observation that lateral inhibition tends to be stronger than reciprocal inhibition in experimental conditions (where the levels of activation are high) (Wilson and Leon, 1987a; Woolf et al., 1991). This two-level approach is also compatible with the conjecture that low levels of activity promote detection while high levels promote competition and identification (Wilson and Leon, 1987a). Spine structures add the capability for control of excitation and memory implementation even at low levels by facilitating

---

Figure 4.4:   Repeat of spine location test of Figure 4.3 but using the spine sizes reported by Woolf et al. (1991). Dendrodendritic synapses located on granule spine heads GR_1 and GR_3 (dashed lines) or on dendritic shaft compartments GR_7 and GR_8 at base of spine necks (solid lines). (a) Inhibitory synaptic conductances on $M1_3$ (heavy lines) and $M2_3$ (thin lines). (b) Granule synaptic site potentials. (c) Dendrodendritic synaptic currents into GR_1 (dashed line) and GR_7 (solid line).
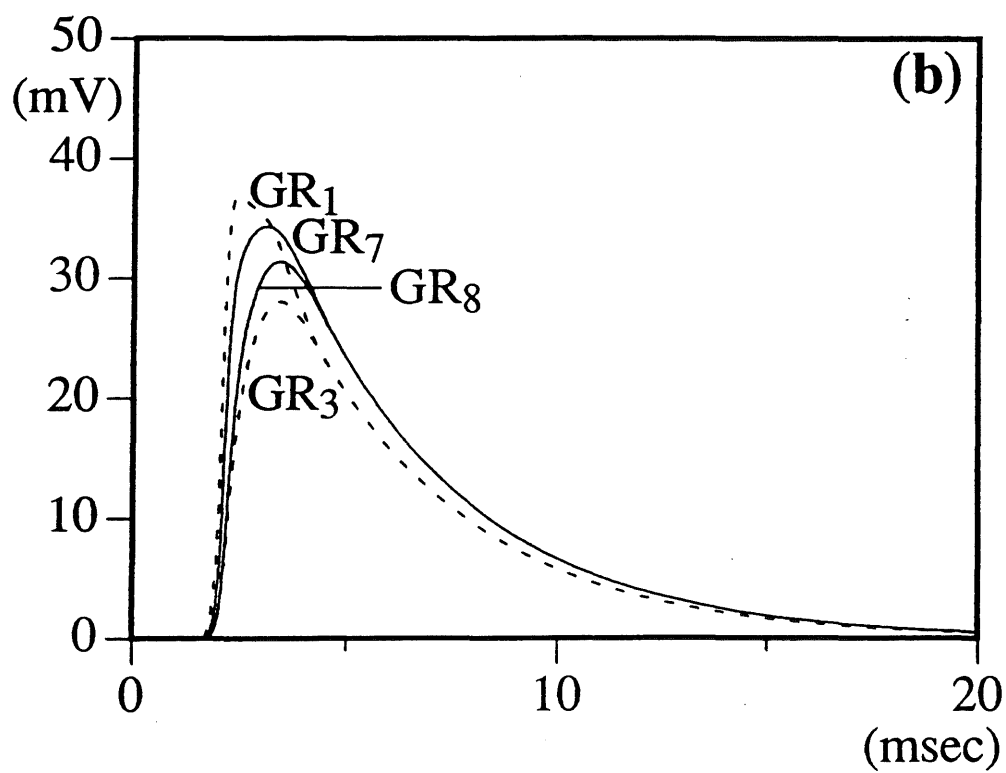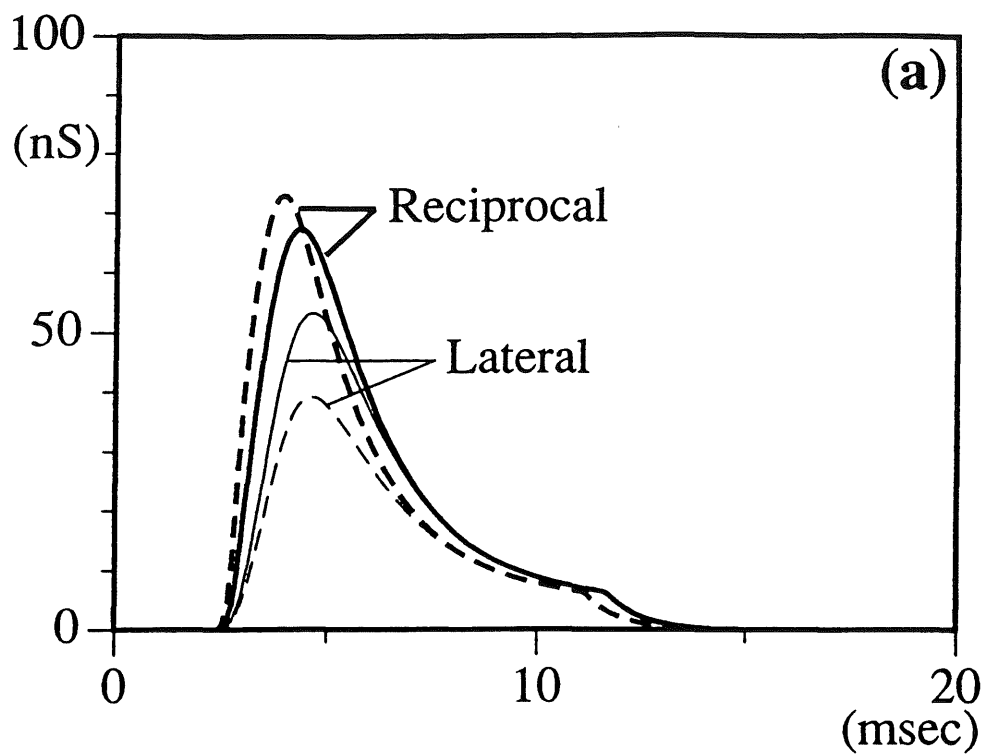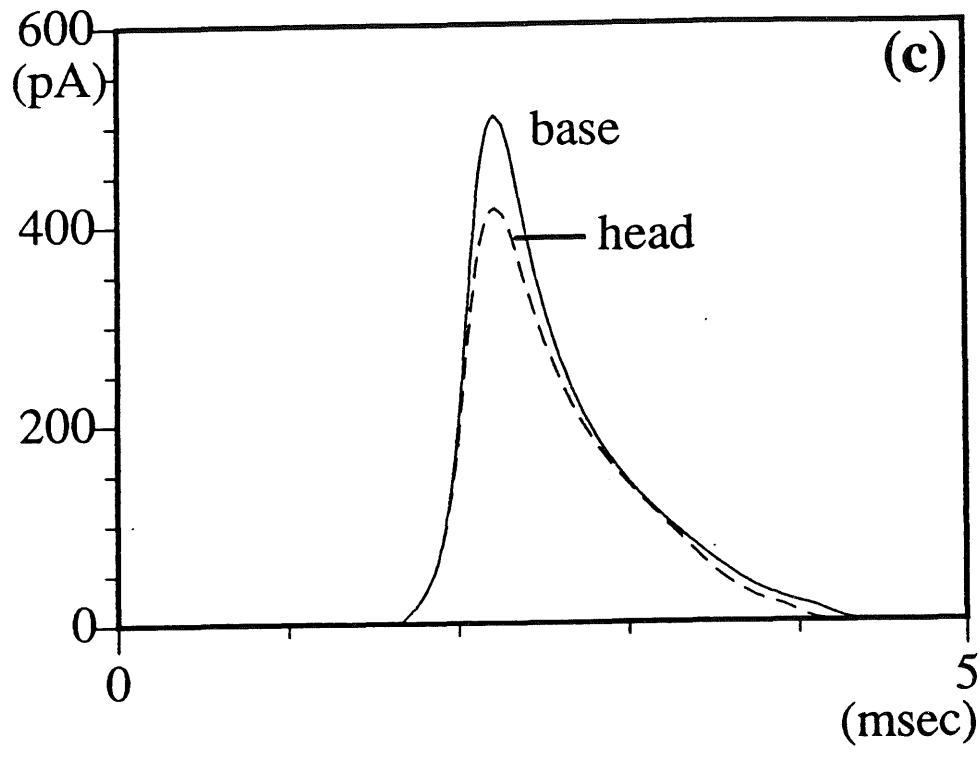
the reciprocal response. At high levels, sufficient granule excitation would allow strong lateral inhibitions in addition to the reciprocal inhibitions and would help mediate competition between odors for identification of the strongest odor (Granger et al., 1990b).

Dendrodendritic synaptic plasticity in the olfactory bulb could be implemented by changes in spine neck resistance. Increases in spine neck resistances strengthen the reciprocal response from the spine while reducing the activated spine's contribution to the overall granule depolarization and thus to the lateral response. Decreases in neck resistance have the opposite effect: reduced reciprocal inhibition and greater lateral inhibition.

Various methods could be used to change spine neck resistances. Many types of organelles are commonly found in and near granule spine necks and heads (Woolf et al., 1991). Movement of these organelles in or out of the spines could produce quick and reversible changes in the effective axial resistance of the spine neck. Neck varicosity volumes in cat retinal amacrine cells, for example, contain volumes beyond those of the organelles that cause the varicosities (Sasaki-Sherrington, 1984); such excess volumes could translate into higher effective neck diameters and thus lower axial resistances. Since these varicosities can move at 0.17–0.47μm/sec (Sasaki-Sherrington, 1984), organelle movement could provide a fairly quick, reversible, and synapse-specific modulation of the reciprocal and lateral inhibition in the bulb.

In addition, longer-term changes in neck resistance are possible by cytoskeletal changes enlarging the neck diameter adjacent to the head (Wilson, 1984; Coss and Perkel, 1985). This type of change — originally proposed as a means for expressing potentiation in axodendritic synapses (Rall, 1970, 1974, 1978; Rall and Rinzel, 1971) — could influence dendrodendritic synaptic efficacy by lowering the effective spine resistance and thus reducing the reciprocal response and increasing the lateral response. Even after such shape changes, further fine-tuning of neck resistance could still be possible by way of organelle movement as mentioned above.

The flexibility of concentrating inhibition either reciprocally or laterally as needed through spine neck resistance changes provides an elegant and flexible solution to the connectivity issue raised by Woolf et al. (1991). In the boundary views they presented, multiple connections from a granule cell to the same mitral cell would provide strong reciprocal inhibition while limiting the available connections

Figure 4.5: Effect of quadrupling the spine neck GR_2 cytoplasmic resistance R_i from 80Ω-cm (solid lines) to 320Ω-cm (dashed lines). Spine sizes were those reported by Woolf et al. (1991). (a) Inhibitory synaptic conductances on Ml_3 (heavy lines) and $M2_3$ (thin lines). (b) Dendrodendritic synaptic current into spine head GR_1. (c) Spine head potentials.
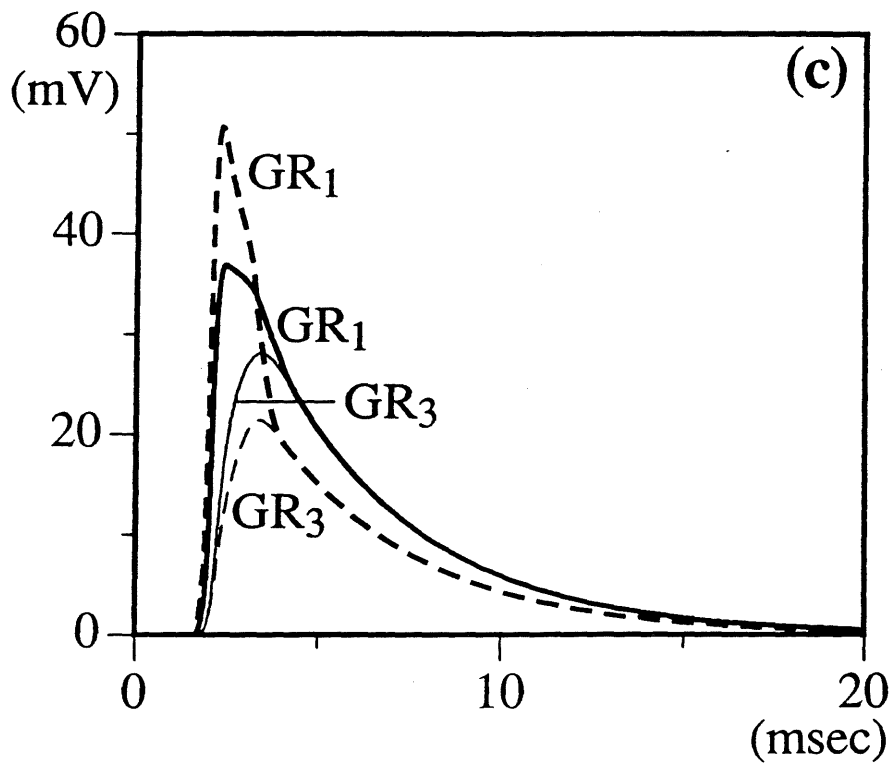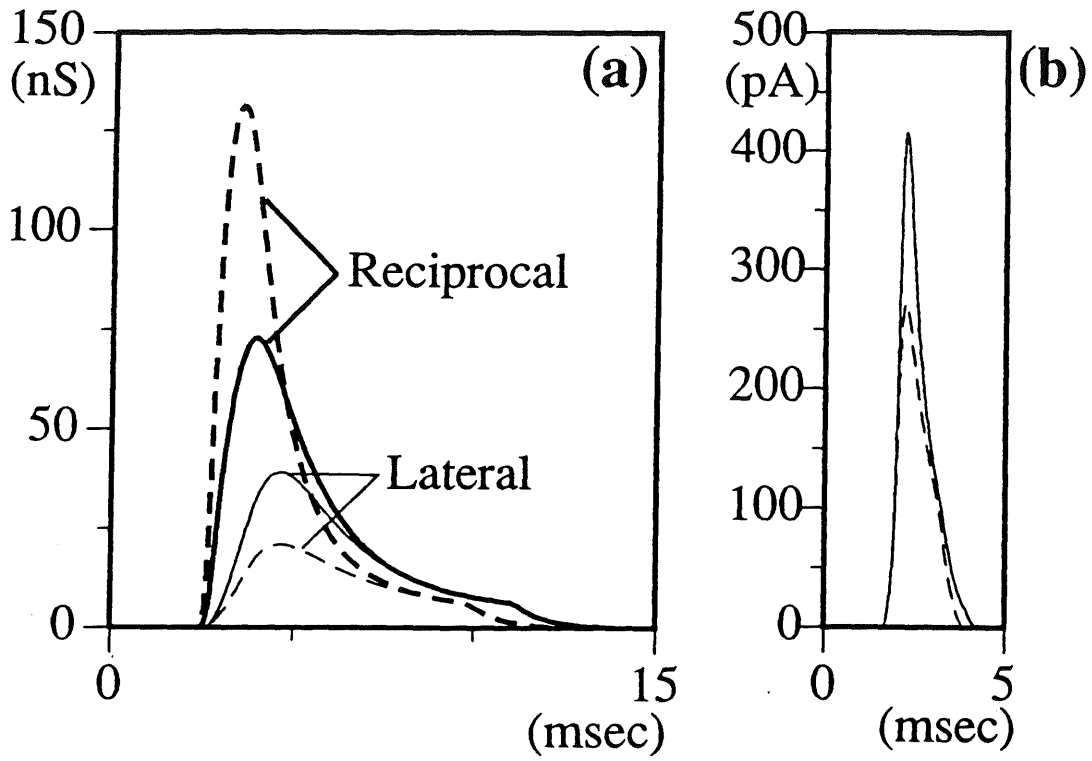
for lateral inhibition; conversely, limitation to single connections between granule and mitral cells would minimize reciprocal inhibition and spread lateral inhibition to more mitral cells. Thus, the granule-to-mitral connectivity can be seen as a reciprocal versus lateral inhibition issue. By changing spine neck resistances, however, a granule cell can dynamically (and possibly reversibly) increase or decrease the competing reciprocal and lateral inhibitions as needed without resorting to duplicate contacts. Thus, the apparent absence of duplicate connections (Woolf et al., 1991) does not necessarily preclude strong reciprocal responses.

As for the impact of plasticity on memorial functions, the olfactory bulb has been implicated as a site for memory storage. Brennan et al. have associated pregnancy-block memories in mice with changes in mitral-granule dendrodendritic efficacy in the accessory olfactory bulb (AOB) (Brennan et al., 1990). These behaviorally-relevant memories are reportedly formed when norepinephrine centrifugal inputs to granule cells (Shepherd, 1979; Mori, 1987) partially block granule inhibition to permit sustained mitral excitation during learning. Such sustained excitation would then indicate which synapses need modification to remember the present odor. While the type of memory trace (increased or decreased reciprocal inhibition) was not determined, the study does implicate dendrodendritic synaptic weights in the AOB in a behaviorally-relevant memory.

Computationally, the use of dendrodendritic plasticity in structures like the olfactory bulb may provide the capability of a *recognition memory* together with either a *block* or *pass* function. The learning of odors could entail either increases or decreases in the reciprocal inhibition on the associated mitral/tufted cells via spine neck resistances or other types of plasticities. Increases in inhibition of the learned odor would *block* (or withhold) the learned odors from continued transmission to efferent structures; decreases in inhibition would strengthen and *pass* the learned odors preferentially over unlearned or novel odors. Such a recognition memory could be used to implement behavioral functions depending on the actions taken for the cues passed or blocked. For example, pregnancy-block memories (Brennan et al., 1990) could be implemented by such a recognition memory if pregnancy blocking was initiated based on the presence or absence of odors received from the AOB.

Figure 4.6:   Effect of narrow synapse gradation on changes in spine neck GR_2 cytoplasmic resistance. Sigmoid parameters are now $v_b = 20$mV, $a = 400$ while R_i ranges from 80Ω-cm (solid lines) to 320Ω-cm (dashed lines). Spine sizes were those reported by Woolf et al. (1991). (a) Inhibitory conductances on $M1_3$ (reciprocal response: heavy lines) and $M2_3$ (lateral response: thin lines). (b) Dendrodendritic synaptic current into spine head GR_1. (c) Spine head potentials. Dashed line indicates approximate potential where synaptic gradation saturates.
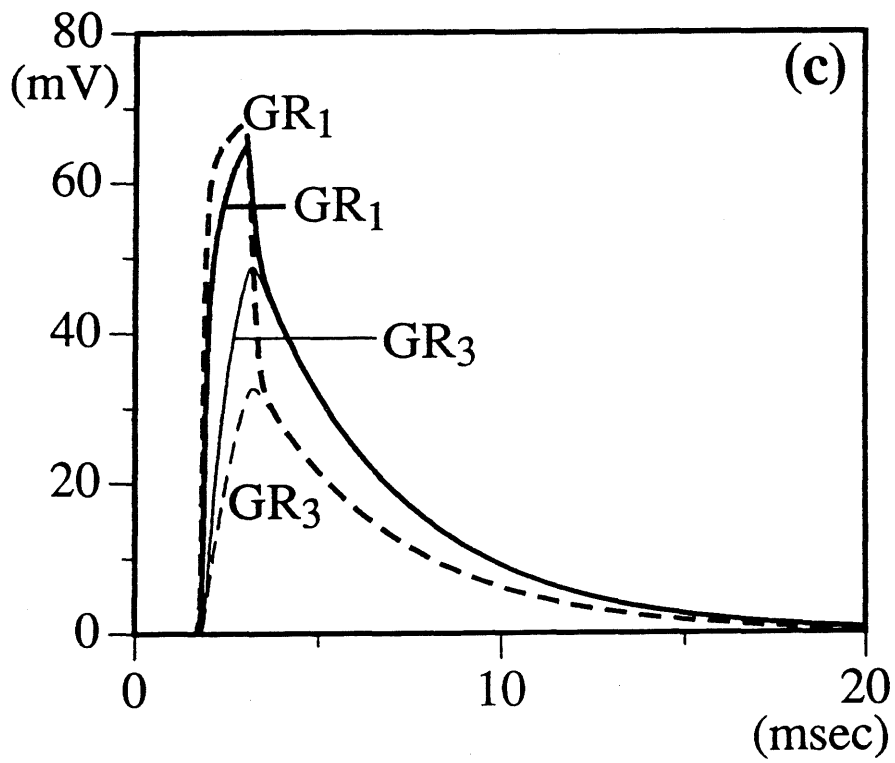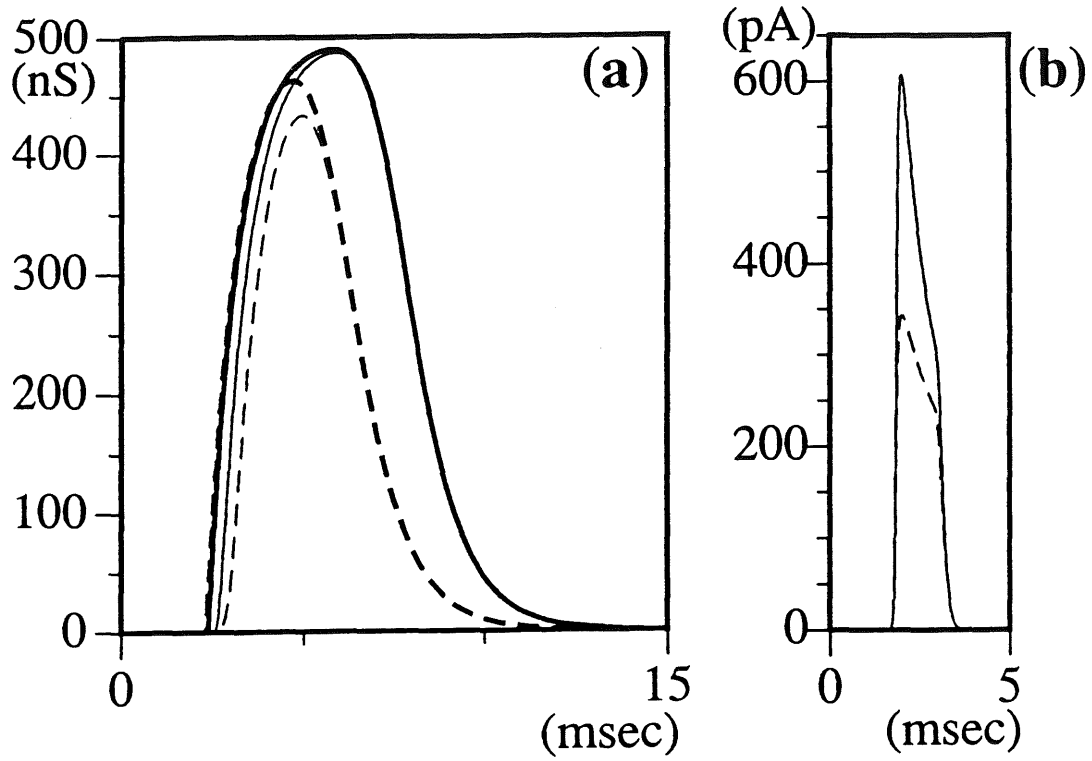
In the case of a recognition memory blocking familiar stud odors, pregnancy block could be initiated if any odor is passed by the AOB. In the case of a recognition memory passing familiar stud odors, receipt of the odors from the AOB would indicate permission for pregnancy to continue.

Centrifugal inputs to granule cells could control learning in a manner similar to AOB learning (Brennan et al., 1990) outlined above by controlling granule inhibition. These centrifugal inputs could also allow the association of learning with any desired behavioral or sensory contributions via higher brain centers (Wilson and Leon, 1988; Brennan et al., 1990).

Furthermore, reductions in overall inhibition levels in the main olfactory bulb (MOB) have been associated with early olfactory exposure in the rat (Wilson and Leon, 1987b). Rats that have been deprived of early olfactory inputs develop more responsive cells (both excited and suppressed) as well as increased paired-pulse inhibition compared to control rats (Guthrie et al., 1990; Wilson et al., 1990). This reduction may be caused by early concentration of inhibition onto common odors in the rat's environment while lowering the overall levels of inhibition. While this early learning is associated with cell growth and specific increases in glomerular regions associated with the control odors (Woo et al., 1987), this paradigm of increasing inhibition onto specific odors while lowering the background inhibition levels is compatible with spine neck resistance plasticity. An increased resistance would lower lateral inhibition, allowing more excitatory responses in lateral mitral/tufted cells and a stronger conditioning inhibition. Also, an increased resistance would simultaneously increase reciprocal inhibition, causing the reciprocal mitral/tufted cell to respond in a suppressive manner. Thus, growth in neck resistance during deprived development (via neck lengthening and/or narrowing) could contribute to the reactivity and inhibitions effects observed while olfactory experience in control rats could reduce these resistance effects by head enlargement or rounding.

Many examples of spines with higher neck resistance in young or deprived animals are presented by Coss and Perkel (1985). In one example, jewel fish deprived of environmental or social experience had more narrow heads and longer stems (resulting in higher neck resistance) than the fish with extensive social experience (Coss and Globus, 1978; Coss, 1979; Coss and Globus, 1979; Coss and Perkel, 1985). In another example, ten-week-old mynah birds had shorter necks with larger diameters than the older one-year-old mynah birds aged in a normal environmental (Rausch and Scheich, 1982; Coss and Perkel, 1985). In normal, non-deprived animals, a reduction in effective spine neck resistance (either directly or through spine neck bulging that enlarges the head) could negate these growths effects. Reductions due to head enlargement (Fifková and van Harrenveld, 1977 ; Desmond and Levy, 1983) or rounding (Lee et al., 1980; Chang and Greenough, 1984) could accompany developmental growth in non-deprived (control) rats. Such spine head changes have been observed after receipt of brief trains of high-frequency electrical stimulation (Coss and Perkel, 1985) that would be available during receipt of natural odors present

in the control rats and counteract the growth effects of deprived animals.

In addition to memorial operations, small changes in granule-mediated inhibition could be used to prevent strong or prevalent odors received from the environment from dominating the identification and detection process by selectively dampening (i.e., slightly inhibiting) the mitral/tufted cells that respond to that odor. Such a partial habituation would not prevent passage or blocking of the dominant odor but would aid in the detection of other odors hidden in the olfactory inputs. As a result, weak inhibitions could help control odor inputs from an environment with prevalent or dominant odors while strong inhibitions (or facilitations) of memorable odors could provide a detection/gating function.

The changes in reciprocal and lateral responses associated with altered spine neck resistances rely in general on synaptic gradation over the operating range of granule potentials. If the synapses were not graded then they would not be able to reflect in their weights the modulations in peak potential due to spine neck changes. Note that even in the event of narrow gradations (high dynamic gains), the dendritic spines would still influence the dendrodendritic synapses. Once the peak gain was reached, changes in spine neck resistance would reduce the lateral inhibition much more strongly that the reciprocal inhibition (see Figure 4.6). Thus, changes in spines would still favor reciprocal responses over lateral responses but to a lesser degree.

There are other reasons why a broad synaptic gradation would be useful in the bulb beyond expression of neck resistance alterations through changed reciprocal and lateral inhibitions. For example, if the granule-to-mitral synaptic gradations were broad then overall bulbar activity could be modulated over a large range of input levels; centrifugal input onto granule cells could then smoothly control global or regional bulbar activity by medium-term changes in granule-cell resting potentials. Strong inputs, for example, might be dampened if the granule cell resting potentials were centrifugally raised to increase the inhibition strength of the bulb. Such higher starting potentials would result in proportionately higher inhibitions if the synapses were still graded at the higher potential levels. Likewise, weak inputs — either by themselves or uncovered by refraction or masking of stronger inputs (Granger et al., 1990b) — might become detectable if the granule cell resting potentials were centrifugally lowered to reduce the inhibition strength of the bulb. These lower starting potentials would result in proportionately lower inhibitions if the gradations were broad.

This type of control over bulbar inhibition could also help to maximize concentration determination by higher brain centers. A physiological model of the olfactory bulb has revealed that the olfactory bulb may transform concentration data from frequency input to spatial output coding (see Chapters 2 and 3; also Antón et al., 1991a, c, d). This transformation depends on the gradation of mitral/tufted firing thresholds by depth (Schneider and Scott, 1983; Mori, 1987). A wide threshold gradation would allow transformation of the full range of input odor concentrations at

the expense of resolution. Conversely, a narrow threshold gradation would increase resolution at the graded concentration while obstructing the gradation at higher and lower concentration levels. A supervisory system could then use centrifugal control of granule inhibition levels to elevate or lower different odor responses into a high resolution (narrow gradation) range. The resulting spatially-coded concentration data from bulbar outputs could then be combined with the centrifugal control levels (scale levels) obtain a better view of the input.

If, on the other hand, the dendrodendritic synaptic gradations were narrow then resting-potential changes and thus spine neck changes would become ineffective once the saturation limits were reached. Factors other than peak potential would then be expressed by the graded synapses. In Figure 4.6, for example, the fall time of the potentials greatly influenced the postsynaptic potential on the mitral side. Furthermore, narrow gradations might cause the inhibitions to switch abruptly on and off and be much more sensitive to minor noise and other fluctuations. Thus, broad synaptic gradations over the operating range of granule membrane potentials might be expected due to afforded computational features.

While the simulations above do not include active spine membranes, such membranes would also influence dendrodendritic inhibitions. We would expect that increased spine neck potentials from membrane activation (Jack et al., 1975; Miller et al., 1985; Shepherd et al., 1985; Perkel and Perkel, 1985; Rall and Segev, 1987; Shepherd and Brayton, 1987; Segev and Rall, 1988) would strongly reinforce the reciprocal response while also contributing to the lateral response. Such active properties would introduce another layer of inhibitory activity in the bulb. If the spine activation threshold was above the dendrodendritic threshold, then reciprocal inhibition could operate as before until the spiking threshold was reached. Above the spiking threshold, both reciprocal and lateral responses would be strengthened by the active membrane. In addition, increased spine neck resistance would make it easier for the spine potential to reach the active spine spiking threshold. Spike propagation would then spread the resistance-based memory effects through the granule dendritic tree.

These results, therefore, demonstrate that dendritic spines can influence dendrodendritic potentials in both a presynaptic and postsynaptic manner. Not only can dendrodendritic inputs into a spine head facilitate the reciprocal response at the expense of reduced lateral inhibition, but the spine neck is a possible site for presynaptic and postsynaptic plasticity in these dendrodendritic connections. Changes in the spine neck diameter or cytoplasmic resistance further emphasize or increase the reciprocal response over the reduced lateral response. Such changes in spine neck resistance provide a possible candidate for memory traces in the olfactory bulb by modulating granule-to-mitral inhibition.

Chapter 5

Summary and Conclusions

The olfactory system has a number of interesting and useful sensory processing capabilities: rapid odor detection (often within 200ms) over a very broad range of input strengths as well as excellent classification, recognition, and memory capabilities. As a result, the study of the neuronal structures involved should provide functional, distributed, and flexible approaches to solving data processing problems that have similar requirements.

The olfactory bulb is the first neuronal structure receiving olfactory data directly from the receptor epithelium. Since much is known about this input data, the olfactory bulb provides a good starting place for studying olfactory sensory processing.

The combination of frequency-coded concentration inputs and primary-cell firing threshold gradations have been shown to result in the possibility of a frequency-to-spatial encoder function by the bulb (Chapter 3). This encoder function was demonstrated using a novel physiological modeling paradigm (Chapter 2) in which the interactive effects between synaptic inputs are modeled using a lumped-circuit representation.

Additional simulations tested the function of dendritic spines in reciprocal dendrodendritic processing (Chapter 4). These biophysical simulations demonstrated that synapsing on the spine heads rather than dendritic shafts of granule inhibitory interneurons facilitate the reciprocal inhibition at all levels of granule excitation while reducing the lateral inhibitory effect. Also, changes in spine neck resistance were shown to affect these inhibitions; increased resistance increased the reciprocal inhibition and decreased the lateral inhibition while the reverse effect held for resistance decreases.

5.1 Implications of Bulb Results for Olfactory Processing

Global field potential data (EEGs) suggest that the number of primary bulb cells responding to an odor is normalized to about 20% (Freeman, 1978a, 1978b; Freeman and Schneider, 1982). Since the simulation presented in Chapter 3 only included one glomerular section, it was not possible to investigate whether, under what conditions, and to what precision such a normalization may take place. While inhibitory competition between glomerular regions for the right to respond seems

a reasonable method for such normalization, it might appear at first that such a normalization would run contrary to a spatial output. One possible explanation might be a normalized approach in which the glomeruli receiving the strongest inputs (highest concentration) would respond, causing sufficient lateral inhibition to block the response of cells from glomeruli receiving weaker inputs (Ambros-Ingerson, 1990; Granger et al., 1990b). The frequency-to-spatial transformation could actually cooperate with the normalization process since more cellular responses to an odor implies stronger lateral inhibition of other glomeruli. Also, if no dominant odors were present then large numbers of glomeruli would respond but each glomeruli would only have a few cells firing, yeilding a small but roughly normalized response.

Another important question is what bulbar interneurons may participate in such a normalization. Periglomerular axons extend across 4–6 glomerular widths (Land, 1973); thus, if the axonal outputs of these interneurons were inhibitory then a limited but strong inhibition of neighboring cells could lead to an on-center/off-surround effect and a low percentage of responding glomeruli.

On the other hand, granule cells are believed to be inhibitory and receive inputs from mitral/tufted cells from as far as half-way across the bulb (Mori, 1987). Thus, a simple lateral inhibition may allow the most strongly excited glomeruli to suppress the other bulbar glomeruli. Interestingly, the facilitation of reciprocal inhibition by dendritic spines at low levels of granule excitation would also strengthen the repression of low excitation mitral/tufted cells without significant influence on lateral inhibition to other glomeruli. Thus, only the strongly excited glomeruli would impose lateral inhibition on its neighbors via granule cells while weak glomeruli would receive lateral inhibition from the strong glomeruli as well as reciprocal inhibition due to its own low excitations.

In any event, frequency-to-spatial transformation together with normalization and granule masking has been shown to yield useful computational properties when combined in large abstract models of bulbar-cortical processing (Ambros-Ingerson, 1990; Ambros-Ingerson et al., 1990; Granger et al., 1990a, b). In these models, the normalization process with the spatial response allowed only the strongest odors to respond first; subsequent masking of the strong odors allowed for detection of hidden odors and/or odor categorization.

5.2 Utility and Applicability of Physiological Modeling

The simulation of the olfactory bulb testing the frequency-to-spatial transformation hypothesis (Chapter 3) illustrated the usefulness of physiological modeling given the neural properties deemed relevant to the function under study (Antón et al., 1991d). First, representation of the temporal aspects of the PSPs provided testing of the transformation hypothesis. Second, the efficiency of the method allowed large

numbers of cells to be simulated. Extensions of the simulation to include large numbers of cells, centrifugal inputs, or more interacting structures (e.g., multiple glomeruli) could be included without a large impact on the simulation time since the computational complexity scales linearly with the number of synapses simulated. Third, the interactive PSP functions reduced concerns that possible saturation and other non-linear effects would be relevant to the transformation and yet excluded from the simulation. Fourth, the efficiency allowed for rapid testing of simulation parameters when compared to simulation methods that consume large amounts of time. Fifth, the model produced realistic data (somatic potential combined with linear approximations of action potential spikes) that permitted the use of one's experience with physiological data in understanding the results. More abstract methods that do not provide temporal PSP data would not permit the use of these visual intuitions.

While the physiological approach had many benefits, there were properties that could not be considered due to the nature of the physiological model. The lumped-circuit approach eliminated effects on the PSPs due to local rather than global effects unless abstract approximations are made to compensate for them. For example, inputs to the granule cells from the mitral cells are made on spine heads rather than dendritic shafts (Shepherd, 1979; Mori, 1987). These spines tend to facilitate the reciprocal response back on to the same mitral cell (Chapter 4). This effect was modeled by lowering the granule-to-mitral dendrodendritic activation threshold to ensure a proper reciprocal response. Of course, this approximation would also facilitate lateral inhibitions to other mitral cells due to the lumped nature of the granule membrane potential. This problem might be corrected at the programming level by activating the lower granule-to-mitral threshold only if the same synapse received mitral-to-granule activation. Consideration of such abstract programming fixes must be weighed together with the increased effort and complexity the fixes impose, and the need to consider such problems at all must be weighed given the task presented to the simulation work.

Compartmental simulations excel at simulating spatial influences in varied dendritic trees (Rall, 1964, 1967, 1989; Jack et al., 1975; Segev et al., 1989). While their computational overhead is much higher than that for physiological models, they can provide accurate simulation of complex structures. In addition, the availability of existing simulation environments such as SPICE (Segev et al., 1985; Bunow et al., 1985), SABER (Carnevale et al., 1990), and GENESIS (Wilson and Bower, 1989) permit a tradeoff of reduced programming time for increased computer time.

One approach to studying a neuronal structure is to use more detailed models (e.g., compartmental simulations, mathematical models) to answer questions of relevance to the computation under study and to follow with more abstract modeling (e.g., fewer-compartment simulations, physiological models) to study the relevant complexities while reducing the computational overhead in order to allow simulations of larger structures with greater extent (Wilson and Bower, 1989). This

approach will also help in the often formidable task of teasing apart the relevant parameters from the irrelevant, the relevant parameter ranges from the irrelevant, and the relevant anatomical details from the irrelevant. The multi-level approach was utilized, for example, to test the spine effects on the mitral/granule cell interaction in greater detail using SABER while keeping the larger olfactory bulb simulation at the more abstract physiological level (Antón et al., 1991b,d; Chapter 4). Furthermore, the frequency-to-spatial transformation itself, tested at the physiological level, was subsequently employed in a more abstract simulation involving cortico-bulbar interactions in the olfactory system (Ambros-Ingerson, 1990; Ambros-Ingerson et al., 1990; Granger et al., 1990b). In this study, a sigmoid function matching the physiological simulation data was used to relate each abstract glomeruli input level to the fraction of primary M/T cells activated in each respective glomerular slice. This sigmoid reflects, therefore, the frequency-to-spatial transformation effect on a population of cells without direct simulation of the individual M/T cell potentials and the firing threshold gradation.

Like the more traditional neurobiological disciplines, then, computational studies at various levels of resolution and accuracy often prove useful in understanding the larger behavior of a neuronal system. Interestingly, the rich variety of biological complexities such as spine structures should be viewed positively given the possible impact they may have on the computations performed. If one is trying to reverse engineer a brain structure or trying to hypothesize an architectural solution to a processing problem, then these complexities provide a large array of tools from which to conjecture solutions to the immense computational problems handled by the brain. Blinding ourselves to these interesting complexities may limit our ability to use neural networks to solve practical problems or limit our understanding of how the brain functions.

References

Adrian, E. D. (1950) The electrical activity of the mammalian olfactory bulb. *Electroenceph. Clin. Neurophysiol.*, **2**:377–388.

Allison, A. C. (1953) The morphology of the olfactory system in the vertebrates. *Biol. Rev.*, **28**:195–244.

Ambros-Ingerson, J. (1990) Computational properties and behavioral expression of cortical-peripheral interactions suggested by a model of olfactory bulb and piriform cortex. Ph.D. Thesis, University of California, Irvine.

Ambros-Ingerson, J., Granger R., and Lynch, G. (1990) Simulation of paleocortex performs hierarchical clustering. *Science*, **247**:1344–1348.

Antón, P. S., Granger, R., and Lynch, G. (1991a) A physiological model of cellular potentials with membrane time-constant and driving-force effects. (Submitted).

Antón, P. S., Granger, R., and Lynch, G. (1991b) Simulated dendritic spines influence reciprocal synaptic strengths and lateral inhibition in the olfactory bulb. (Submitted).

Antón, P. S., Granger, R., and Lynch, G. (1991c). Temporal information processing in synapses, cells, and circuits. To appear in: T. McKenna, J. Davis, and S. Zornetzer (Eds.) *Single Neuron Computation*. New York: Academic Press.

Antón, P. S., Lynch, G., and Granger, R. (1991d) Computation of frequency-to-spatial transform by olfactory bulb glomeruli. To appear in *Biol. Cybern.*

Brennan, P., Kaba, H., and Keverne, E. B. (1990) Olfactory recognition: a simple memory system. *Science*, **250**:1223–1226.

Bunow, B., Segev, I., and Fleshman, W. (1985) Modeling the electrical behavior of anatomically complex neurons using a network analysis program: excitable membrane. *Biol. Cybern.*, **53**:41–56.

Carnevale, N. T., Woolf, T. B., and Shepherd, G. M. (1990) Neuron simulations with SABER. *J. Neurosci. Meth.*, **33**:135–148.

Carpenter, G. A. (1989) Neural network models for pattern recognition and associative memory. *Neural Networks*, **2**:243-257.

84

Castellucci, V. F. (1985) The chemical senses: taste and smell. In: Kandel, E. R. and Schwartz, J. H. (Eds.) *Principles of Neural Science*, 2nd edition. Elsevier, New York Amsterdam Oxford, pp. 409–425.

Chang, F. -L. and Greenough, W. T. (1984) Transient and enduring morphological correlates of synaptic activity and efficacy change in the rat hyppocampal slice. *Brain Res.*, **309**:35–46.

Chang, H. -T. (1952) Cortical neurons with particular reference to the apical dendrites. *Cold Spring Harbor Symp. Quant. Biol.*, **17**:189–202.

Colquhoun, D. (1981) How fast do drugs work? *Trends Pharmacol. Sci.*, **2**:212–217.

Coss, R. G. (1979) Delayed plasticity of an instinct: Recognition and avoidance of 2 facing eyes by the jewel fish. *Devel. Psychobiol.*, **12**:335–345.

Coss, R. G. and Globus, A. (1978) Spine stems on tectal interneurons in jewel fish are shortened by social stimulation. *Science*, **200**:787–789.

Coss, R. G. and Globus, A. (1979) Social experience affects the development of dendritic spines and branches on tectal interneurons in the jewel fish. *Devel. Psychobiol.*, **12**:347–358.

Coss, R. G. and Perkel, D. H. (1985) The function of dendritic spines: a review of theoretical issues. *Behav. Neural Biol.*, **44**:151–185.

deVries, H. and Stuiver, M. (1961) The absolute sensitivity of the human sense of smell. In: Rosenblith, W. A. (Ed.) *Sensory Communication*. MIT Press, Cambridge.

Desmond, N. L. and Levy, W. B. (1983) Synaptic correlates of associative potentiation/depression: An ultrastructural study in the hippocampus. *Brain Res.*, **265**:21–30.

Desoer, C. A. and Kuh, E. S. (1969) *Basic Circuit Theory*. McGraw-Hill, New York.

Diamond, J. and Yasargil, G. M. (1969) Synaptic function in fish spinal cord: dendritic integration. *Prog. Brain Res.*, **31**:201–209.

Eisenberg, J., Freeman, W. J., and Burke, B. (1989) Hardware architecture of a neural network model simulating pattern recognition by the olfactory bulb. *Neural Networks*, **2**(4): 315–325.

Fifková, E. and van Harreveld, A. (1977) Long-lasting morphological changes in dendritic spines of dentate granular cells following stimulation of the entorhinal area. *J. Neurocytol.*, **6**:211–230.

Freeman, W. J. (1978a) Spatial properties of an EEG event in the olfactory bulb and cortex. *Electroencephalography & Clin. Neurophysiol.*, **44**: 586–605.

Freeman, W. J. (1978b) Spatial frequency analysis of an EEG event in the olfactory bulb. In D. A. Otto (Ed.), *Multidisciplinary perspectives in event-related brain potential research.* Washington, D. C.: U.S. Government Printing Office EPA Q 600/9-77-043, pp. 533–542.

Freeman, W. J. (1982) Changes in spatial patterns of rabbit olfactory EEG with conditioning odors. *Physiology.*, **19**(1): 44–56.

Freeman, W. J. (1987) Simulation of chaotic EEG patterns with a dynamic model of the olfactory system. *Biol. Cybern.*, **56**:139–150.

Freeman, W. J. and Schneider, W. (1982) Changes in spatial patterns of rabbit olfactory EEG with conditioning to odors. *Psychophysiol.*, **19**:44–56.

Gambel, E. and Koch, C. (1987) The dynamics of free calcium in dendritic spines in response to repetitive synaptic input. *Science*, **236**:1311–1315.

Getchell, T. V. (1986) Functional properties of vertebrate olfactory receptor neurons. *Physiol. Rev.*, **66**:772–818.

Getchell, T. V. and Shepherd, G. M. (1978) Responses of olfactory receptor cells to step pulses of odour at different concentrations in the salamander. *J. Physiol.*, **282**:521–540.

Getting, P. A. (1989) Reconstruction of small neural networks. In: C. Koch and I. Segev (Eds.) *Methods in Neuronal Modeling.* MIT Press, Cambridge, pp. 171–194.

Granger, R., Ambros-Ingerson, J., and Lynch, G. (1989) Derivation of encoding characteristics of layer II cerebral cortex. *J. Cog. Neurosci.*, **1**:64–91.

Granger, R., Ambros-Ingerson, J., Antón, P., and Lynch, G. (1990a) Unsupervised perceptual learning: a paleocortical model. In: Hanson, S. J. and Olson, C. R. (Eds.) *Connectionist Modeling and Brain Function: The Developing Interface.* MIT Press, Cambridge, pp. 105–131.

Granger, R., Ambros-Ingerson, J., Staubli, U., and Lynch, G. (1990b) Memorial operation of multiple, interacting simulated brain structures. In: Gluck, M. and Rumelhart, D. (Eds.) *Neuroscience and Connectionist Theory.* Lawrence Erlbaum Associates, Hillsdale, pp. 95–129.

86

Graubard, K. (1978) Synaptic transmission without action potentials: input-output properties of a nonspiking presynaptic neuron. *J. Neurophys.*, **41**(4):1014–1025.

Graubard, K., Raper, J. A., and Hartline, D. K. (1983) Graded synaptic transmission between identified spiking neurons. *J. Neurophys.*, **50**(2):508–521.

Guthrie, K. M., Wilson, D. A., and Leon, M. (1990) Early unilateral deprivation modifies olfactory bulb function. *J. Neurosci.*, **10**(10):3402–3412.

Holmes, W. R., Is the function of dendritic spines to concentrate calcium? *Brain Research*, 519 (1990) 338–342.

Hinton, G. E. (1987) Connectionist learning procedures. Technical Report CMU-CS-87-115 (version 2), C.S. Dept., Carnegie-Mellon University, Pittsburgh, PA 15213.

Hodgkin, A.L. and Huxley, A.F. (1952) A quantitative description of membrane current and its application to conduction and excitation in nerve. *J. Physiol. (London)*, **117**:500–544.

Jack, J. (1979) An introduction to linear cable theory. In: F. O. Schmitt and F. G. Worden (Eds.) *The Neurosciences: Fourth Study Program.* MIT Press, Cambridge.

Jack, J. J. B., Noble, D., and Tsien, R. W. (1975, 1983) *Electric Current Flow in Excitable Cells.* Clarendon Press, Oxford.

Jung, M. W., Larson., J., and Lynch, G. (1991) Evidence that changes in spine neck resistance are not responsible for expression of LTP. *Synapse*, **7**:216–220.

Kandel, E. R. (1985) Chemically gated ion channels at central synapses. In: E. R. Kandel and J. H. Schwartz (Eds.) *Principles of Neural Science*, 2nd ed. Elsevier/North-Holland, New York, pp. 108–119.

Kandel, E. R. and Siegelbaum, S. (1985) Principles underlying electrical and chemical synaptic transmission. In: E. R. Kandel and J. H. Schwartz (Eds.) *Principles of Neural Science*, 2nd ed. Elsevier/North-Holland, New York, pp. 87–107.

Katz, B. and Miledi, R. (1967) A study of synaptic transmission in the absence of nerve impulses. *J. Physiol.*, **192**:407–436.

Kawato, M., Hamaguchi, T., Murakami, F., and Tsukahara, N. (1984) Quantitative analysis of electrical properties of dendritic spines. *Biol. Cybern.*, **50**:447–454.

Kleinfeld, D. and Sompolinsky, H. (1989) Associative network models for central pattern generators. In: C. Koch and I. Segev (Eds.) *Methods in Neuronal Modeling*. MIT Press, Cambridge, pp. 195–246.

Koch, C. and Poggio, T. (1983) A theoretical analysis of electrical properties of spines. *Proc. R. Soc. Lond.* B, **218**:455–477.

Koch, C. and Poggio, T. (1987) Biophysics of computation: neurons, synapses, and membranes. In: Edelman, G. M., Gall, W. E., and Cowan, W. M. (Eds.) *Synaptic Function*. John Wiley & Sons, New York, pp. 63–697.

Koch, C., Poggio, T., and Torre, V. (1982) Retinal gangleon cells: a functional interpretation of dendritic morphology. *Phil. Trans. R. Soc. Lond.* B, **298**:227–264.

Koester, J. (1985a) Resting membrane potential and action potential. In: E. R. Kandel and J. H. Schwartz (Eds.) *Principles of Neural Science*, 2nd ed. Elsevier/North-Holland, New York, pp. 49–57.

Koester, J. (1985b) Nongated channels and the passive membrane properties of the neuron. In: E. R. Kandel and J. H. Schwartz (Eds.) *Principles of Neural Science*, 2nd ed. Elsevier/North-Holland, New York, pp. 58–65.

Koester, J. (1985c) Functional consequences of passive membrane properties of the neuron. In: E. R. Kandel and J. H. Schwartz (Eds.) *Principles of Neural Science*, 2nd ed. Elsevier/North-Holland, New York, pp. 66–74.

Koester, J. (1985d) Voltage-gated channels and the generation of the action potential. In: E. R. Kandel and J. H. Schwartz (Eds.) *Principles of Neural Science*, 2nd ed. Elsevier/North-Holland, New York, pp. 75–86.

Kuffler, S. W., Nicholls, J. G., and Martin, A. R. (1984) *From Neuron to Brain*. Sinauer Associates, Sunderland.

Land, L. J. (1973) Localized projection of olfactory nerves to rabbit olfactory bulb. *Brain Res.*, **63**:153–166.

Lee, K. S., Schottler, F., Oliver, M., and Lynch, G. (1980) Brief bursts of high-frequency stimulation produce two types of structural change in rat hippocampus. *J. Neurophysiol.*, **44**:247–258.

Li, Z. and Hopfield, J. J. (1989a) Modeling the olfactory bulb and its neural oscillatory processings. *Biol. Cybern.*, **61**(5):379–392.

Li, Z. and Hopfield, J. J. (1989b) Modeling the olfactory bulb — coupled nonlinear oscillators. In: Touretzky, D. S. (Ed.) *Advances in Neural Information Processing Systems I*. Morgan Kaufmann, San Mateo, pp. 402–409.

88

MacGregor, R. J. (1987) *Neural and Brain Modeling.* Academic Press, San Diego.

Macrides, F., Eichenbaum, H. B., and Forbes, W. B. (1982) Temporal relationship between sniffing and the limbic (theta) rhythm during odor discrimination reversal learning. *J. Neurosci.*, **2**:1705–1717.

Macrides, F. and Schneider, S. P. (1982) Laminar organization of mitral and tufted cells in the main olfactory bulb of the adult hamster. *J. Compar. Neurol.*, **208**:419–430.

Mead, C. (1989) *Analog VLSI and Neural Systems.* Addison-Wesley, Reading.

Miller, J. P., Rall, W., and Rinzel, J., (1985) Synatic amplification by active membrane in dendritic spines. *Brain Research*, **325**:325–330.

Mori, K. (1987) Membrane and synaptic properties of identified neurons in the olfactory bulb. *Prog. Neurobiol.*, **29**:275–320.

Mori, K., Kishi, K., and Ojima, H. (1983) Distribution of dendrites of mitral, displaced mitral, tufted, and granule cells in the rabbit olfactory bulb. *J. Compar. Neurol.*, **219**:339–355.

Mori, K. and Takagi, S. F. (1978a) An intracellular study of dendrodendritic inhibitory synapses on mitral cells in the rabbit olfactory bulb. *J. Physiol.*, **279**:569–588.

Mori, K. and Takagi, S. F. (1978b) Activation and inhibition of olfactory bulb neurons by anterior commissure volleys in the rabbit. *J. Physiol.*, **279**:589–604.

Nowycky, M. C., Mori, K., and Shepherd, G. M. (1981) Blockage of synaptic inhibition reveals long-lasting synaptic excitation in isolated turtle olfactory bulb. *J. Neurophysiol.*, **46**(3):649–658.

Onoda, N. and Mori, K. (1980) Depth distribution of temporal firing patterns in olfactory bulb related to air-intake cycles. *J. Neurophysiol.*, **44**(1):29–39.

Orona, E., Rainer, E. C., and Scott, J. W. (1984) Dendritic and axonal organization of mitral and tufted cells in the rat olfactory bulb. *J. Comp. Neurol.*, **226**:346–356.

Perkel, D. H. (1964) A digital-computer model of nerve cell functioning. The Rand Corporation, Memorandum RM-4132-NIH.

Perkel, D. H. and Perkel, D. J. (1985) Dendritic spines: role of active membrane in modulating synaptic efficacy. *Brain Research*, **325**:331–335.

Rall, W. (1962) Theory of physiological properties of dendrites. *Ann. N. Y. Acad. Sci.*, **96**(4):1071–1092.

Rall, W. (1964) Theoretical significance of dendritic trees for neuronal input-output relations. In: R. F. Reiss (Ed.) *Neural Theory and Modeling*. Stanford Univ. Press, Stanford.

Rall, W. (1967) Distinguishing theoretical synaptic potentials computed for different soma-dendritic distributions of synaptic inputs. *J. Neurophysiol.*, **30**:1138–1168.

Rall, W. (1969) Time constant and electrotonic length of membrane cylinders and neurons. *Biophy. J.*, **9**:1483–1508.

Rall, W. (1970) Cable properties of dendrites and effects of synaptic location. In: P. Anderson and J. K. S. Jansen (Eds.), *Excitatory Synaptic Mechanisms*. Scandinavian Univ. Books, Oslo pp. 175–187.

Rall, W. (1974) Dendritic spines, synaptic potency and neuronal plasticity. In: C. D. Woody, K. A. Brown, T. J. Crow, and J. D. Knispel (Eds.), *Cellular Mechanisms Subserving Changes in Neuronal Activity*. Brain Inform. Service Res. Report, Vol. 3, Los Angeles, pp. 13–21.

Rall, W. (1977) Core conductor theory and cable properties of neurons. In: E. R. Kandel (Ed.), *Handbook of Physiology. The Nervous System*, Sect. 1, Vol. 1., pt. 1. Am. Physiol. Soc., Bethesda, pp. 39–97.

Rall, W. (1978) Dendritic spines and synaptic potency. In: R. Porter (Ed.), *Studies in Neurophysiology*. Cambridge Univ. Press, Cambridge, pp. 203–209.

Rall, W. (1989) Cable theory for dendritic neurons. In: C. Koch and I. Segev (Eds.) *Methods in Neuronal Modeling*. MIT Press, Cambridge, MA.

Rall, W. and Rinzel, J. (1971) Dendritic spine function and synaptic attenuation calculations. *Soc. Neurosci. Abstracts*, **1**:64.

Rall, W. and Segev, I. (1987) Functional possibilities for synapses on dendrites and dendritic spines. In: G. M. Edelman, W. E. Gall, and W. M. Cowan (Eds.) *Synaptic Function*. Wiley, New York.

Rall, W. and Shepherd, G. M. (1968) Theoretical reconstruction of field potentials and dendrodendritic synaptic interactions in olfactory bulb. *J. of Neurophysiology*, **31**:884–915.

Rall, W., Shepherd, G. M., Reese, T. S., and Brightman, M. W. (1966) Dendrodendritic synaptic pathway for inhibition in the olfactory bulb. *Exp. Neurol.*, **14**:44–56.

90

Rausch, G. and Scheich, H. (1982) Dendritic spine loss and enlargement during maturation of the speech control system in the mymah bird (*Gracula religiosa*). *Neurosci. Let.*, **29**:129–133.

Rinzel, J. and Ermentrout, G. B. (1989) Analysis of neural excitability and oscillations. In C. Koch and I. Segev, (Eds.), *Methods in Neuronal Modeling*. MIT Press, Cambridge, MA.

Roman, F. U., Staubli, U., and Lynch, G. (1987) Evidence for synaptic potentiation in a cortical network during learning. *Brain Res.*, **418**:221–226.

Sasaki-Sherrington, Sharon E., Jacobs, J. R., and Stevens, J. K. (1984) Intracellular control of axial shape in non-uniform neurites: a serial electron microscopic analysis of organelles and microtubules in AI and AII retinal amacrine neurites. *J. Cell Biol.*, **98**:1279–1290.

Schild, D. (1986) System analysis of the goldfish olfactory bulb: spatio-temporal transfer properties of the mitral cell granule cell complex. *Biol. Cybern.*, **54**:9–19.

Schneider, S. P. and Scott, J. W. (1983) Orthodromic response properties of rat olfactory bulb mitral and tufted cells correlate with their projection patterns. *J. Neurophysiol.*, **50**(2):358–378.

Schoenfeld, T. A. and Macrides, F. (1984) Topographical organization of connections between the main olfactory bulb and pars externa of the anterior olfactory nucleus in the hamster. *J. Comp. Neurol.*, **227**:121–135.

Segev, I., Fleshman, J. W., and Burke, R. E. (1989) Compartmental Models of Complex Neurons. In: C. Koch and I. Segev (Eds.) *Methods in Neuronal Modeling*. MIT Press, Cambridge, MA.

Segev, I., Fleshman, J. W., Miller, J. P., and Bunow, B. (1985) Modeling the electrical behavior of anatomically complex neurons using a network analysis program: passive membrane. *Biol. Cybern.*, **53**:27–40.

Segev, I. and Parnas, I. (1983) Synaptic integration mechanisms. Theoretical and experimental investigation of temporal postsynaptic interactions between excitatory and inhibitory inputs. *Biophy. J.*, **41**:41–50.

Segev, I. and Rall, W. (1988) Computational study of an excitable dendritic spine. *J. Neurophysiol.*, **60**(2):499–523.

Shamma, S. (1989) Spatial and temporal processing in central auditory networks. In: C. Koch and I. Segev (Eds.) *Methods in Neuronal Modeling*. MIT Press, Cambridge, MA.

Shepherd, G. M. (1972) Synaptic organization of the mammalian olfactory bulb. *Physiol. Rev.*, **52**(4):864–917.

Shepherd, G. M. (1979) *The Synaptic Organization of the Brain*, 2nd Edition. Oxford Univ Press, New York, Oxford.

Shepherd, G. M. and Brayton, R. K. (1978) Analysis of a dendrodendritic synaptic circuit by computer simulation. IBM Research Report RC7344 (#31192), Yorktown Heights.

Shepherd, G. M. and Brayton, R. K. (1979) Computer simulation of a dendrodendritic synaptic circuit for self- and lateral-inhibition in the olfactory bulb. *Brain Research*, **175**:377-382.

Shepherd, G. M. and Brayton, R. K. (1987) Logic operations are properties of computer-simulated interactions between excitable dendritic spines. *Neuroscience*, **21**(1):151–165.

Shepherd, G. M., Brayton, R. K., Miller, J. P., Segev, I., Rinzel, J., and Rall, W. (1985) Signal enhancement in distal cortical dendrites by means of interactions between active dendritic spines. *Proc. Nat'l Acad. Sci. USA*, **82**:2192–2195.

Shepherd, G. M., Woolf, T. B., and Carnevale, N. T. (1989) Comparisons between active properties of distal dendritic branches and spines: Implications for neuronal computations. *J. Cog. Neurosci.*, **1**(3):273–286.

Tuckwell, H. C. (1988) *Introduction to Theoretical Neurobiology, Vol. 1.* Cambridge University Press, Cambridge.

Vodyanoy, V. (1988) Molecular sensor based on olfactory transduction. In: Hong, F. T. (Ed.) *Molecular Electronics: Biosensors and Biocomputers.* Plenum, New York London, pp. 317–328.

Walløe, L., Jansen, J. K. S., and Nygaard, K. (1969) A computer simulated model of a second order sensory neuron. *Kybernetik*, **6**:130–140.

Wehmeier, U., Dong, D., Koch, C., and Van Essen, D. (1989) Modeling the mammalian visual system. In: C. Koch and I. Segev (Eds.) *Methods in Neuronal Modeling.* MIT Press, Cambridge, pp. 335–360.

Wellis, D. P. and Scott, J. W. (1990) Intracellular responses of identified rat olfactory bulb interneurons to electrical and odor stimulation. *J. Neurophysiol.*, **64**(3):932–947.

Wilson, C. J., (1984) Passive cable properties of dendritic spines and spiny neurons. *J. Neurosci.*, **4**(1):281–297.

Wilson, C. J. (1988) Cellular mechanisms controlling the strength of synapses. *J. Elec. Micro. Tech.*, **10**:293–313.

Wilson, D. A., Guthrie, K. M., and Leon, M. (1990) Modification of olfactory bulb synaptic inhibition by early unilateral olfactory deprivation. *Neurosci. Lett.*, **116**:250–256.

Wilson, D. A. and Leon, M. (1987a) Evidence of lateral synaptic interactions in olfactory bulb output cell responses to odors. *Brain Res.*, **417**:175–180.

Wilson, D. A. and Leon, M. (1987b) Abrupt decrease in synaptic inhibition in the postnatal rat olfactory bulb. *Dev. Brain Res.*, **33**:134–138.

Wilson, D. A. and Leon, M. (1988) Spatial patterns of olfactory bulb single-unit responses to learned olfactory cues in young rats. *J. Neurophysiol.*, **59**(6):1770–1782.

Wilson, M. A. and Bower, J. M. (1989) The simulation of large-scale neural networks. In C. Koch and I. Segev, (Eds.), *Methods in Neuronal Modeling*. MIT Press, Cambridge, MA.

Woo, C. C., Coopersmith, R., and Leon, M. (1987) Localized changes in olfactory bulb morphology associated with early olfactory learning. *J. Comp. Neurol.*, **263**:113–125.

Woolf, T. B., Shepherd, G. M., and Greer, C. A. (1991) Serial reconstruction of granule cell spines in the mammalian olfactory bulb. *Synapse*, **7**:181–192.

Appendix A: Graded Synapse Code

Here are the simple SABER templates used to build the graded synapse model.

```
\# ********************************************************************
\# Template Function:  Graded Synapse
\# ********************************************************************

template grsyn  pre_p pre_m post_p post_m =
                latency, vb, siga, thr, Gsyn, Esyn, trtau

electrical pre_p, pre_m, post_p, post_m  \# post-synaptic nodes:
                                         \#      plus & minus

                                \#... Declarations w/ defaults
number Esyn,                    \# post-synaptic driving force
       trtau,                   \# transmitter time constant
       latency   = 2m,          \# synaptic time delay
       vb        = 50m,         \# sigmoid bias voltage
       siga      = 50,          \# sigmoid time constant
       thr       = 5m,          \# threshold = 5mv
       Gsyn      = 40n          \# synaptic conductance

\{
   \#...Synaptic Cleft Delay
   delay.syn     pre_p pre_m postDelay 0   = td=latency, a=1

   \#...Transform sigmoid of presynaptic voltage into a current
   vccs_sigmoid.syn postDelay 0 0 transm   =
                   ipeak=1, vb=vb, a=siga, threshold=thr

   \#...transmitter time-constant parameters: rc=trtau
   r.transmitter transm 0   = 1
   c.transmitter transm 0   = trtau

   \#...Synaptic branch of membrane
   lvcg.syn  transm 0  post_p synBranch =
             cond=Gsyn, vc_low=-1000m, vc_hi=2000m,
             vg_low=-1000m, vg_hi=1000m, i_err=1p
   v.syn  synBranch post_m  = Esyn
\}
```

```
\###############################################################
\# Language:    SABER MAST
\# Template Function:  Sigmoidal voltage controlled current source
\#
\#     i=ipeak/2 at Vin = vb      (if vb>threshold)
\#
\#     width of the "linear" range
\#         increases when increasing time const a
\#         narrows   when decreasing time const a
\#     Note: we assume that the response curve should be above 0mV!
\###############################################################

element template vccs_sigmoid  ip im op om =
                               ipeak, vb, a, threshold


                            \#...Connections:
electrical ip, im,          \# in  nodes: plus & minus
           op, om           \# out nodes: plus & minus
                            \#...Arguments:
number  ipeak,              \# Peak output current
        vb,                 \# bias voltage
        a,                  \# exp time const
        threshold           \# activation threshold
\{
   val v    vin, vout       \# Quantities useful for output:
   val i    i_out
   number   low_lin, hi_lin \# ends of the approx. linear ranges
   number   nonlin_width    \# approx. width of nonlinear range
   struc \{number bp, inc;\} svin[*], nvin[*]
                            \# Sample points & Newton steps


   parameters \{
      \#..assume linear above&below
      \# vb+-3*(deltaV max slope line reaches peak)
      low_lin = vb - 3*2/a
      hi_lin  = vb + 3*2/a
      nonlin_width = hi_lin - low_lin
      message("%:low_lin=%, Vb=%, hi_lin=%",
              instance(),low_lin,vb,hi_lin)
      if (hi_lin<0) \{
         message("Note: hi_lin=% less than 0mV in %",
                 hi_lin, instance())
```

```
        \#...relative y-axis error of 0.1% in non-linear range
        svin = [(-200m,1m), (low_lin,0.001*4/a),
                (hi_lin,1m), (0,1m), (200m,0)]
    \}
    else if (low_lin<0) \{
        message("Note: low_lin=% less than 0mV in %",
                low_lin, instance())
        \#...relative y-axis error of 0.1% in nonlinear range
        svin = [(-200m,1m), (low_lin,0.001*4/a), (0,0.001*4/a),
                (hi_lin,1m), (200m,0)]
    \}
    else \{
        svin = [(-200m,1m), (0,1m), (low_lin,0.001*4/a),
                (hi_lin,1m), (200m,0)]
    \}
    nvin = [(-200m,1.9*nonlin_width), (200m,0)]
\}
values \{
    vin  = v(ip) - v(im)
    vout = v(op) - v(om)
    if (vin < threshold) \{
        i_out = 0
    \}
    else \{
        i_out = ipeak * exp(a*vin) / (exp(a*vin) + exp(a*vb))
    \}
\}
control_section \{
    sample_points (vin, svin)
    newton_step   (vin, nvin)
\}
equations \{
    i(op->om) += i_out
\}
\}
```

```
\#  ***************************************************************
\# Language:    SABER MAST
\# Template Function:  Linear voltage controlled conductance
\#  ***************************************************************

element template lvcg  cp cm gp gm =
                       cond, vc_low, vc_hi, vg_low, vg_hi, i_err


                          \#..Connections:
electrical  cp, cm, gp, gm   \# conductance nodes: plus and minus


                          \#..Arguments:
number  cond,             \# conductance
        vc_low, vc_hi,    \# control voltage operating range
        vg_low, vg_hi,    \# conductance voltage operating range
        i_err             \# max current error through conductor
\{
    val i   ig            \# Current through G
    val v   vc            \# Input controlling voltage
    val v   vg            \# conductance voltage
    val g   g_now         \# calculate g(t) for extraction

    number  vc_absmax,        \# max( abs(vc_low), abs(vc_hi) )
            vg_absmax         \# max( abs(vg_low), abs(vg_hi) )

    struc \{number bp, inc;\} sp_vc[*]  \# control sample points
    struc \{number bp, inc;\} sp_vg[*]  \# conductance sample point

    parameters \{
        if (vc_hi<vc_low) error("%: vc_hi=%<vc_low=%",
                            instance(),vc_hi,vc_low)
        if (vg_hi<vg_low) error("%: vg_hi=%<vg_low=%",
                            instance(),vg_hi,vg_low)
        if (abs(vc_low)>abs(vc_hi)) vc_absmax = abs(vc_low)
        else                        vc_absmax = abs(vc_hi)
        if (abs(vg_low)>abs(vg_hi)) vg_absmax = abs(vg_low)
        else                        vg_absmax = abs(vg_hi)

        \#\#\# Set sample point intervals:
        \#\#\#... y = slope * x, so x_interval = y_i_err / slope
        \#.. if vc_low<vc_hi<0
        if (vc_hi<0) \{
```

```
        sp_vc = [(vc_low,i_err/(cond*vg_absmax)),
                 (vc_hi,0), (0,0)]
    \}
    \#..else if vc_low<0<vc_hi
    else if (vc_low<0) \{
        sp_vc = [(vc_low,i_err/(cond*vg_absmax)),
                 (0,      i_err/(cond*vg_absmax)), (vc_hi,0)]
    \}
    \#..else 0<vc_low<vc_hi
    else \{
          sp_vc = [(0,0), (vc_low,i_err/(cond*vg_absmax)),
                   (vc_hi,0)]
    \}


    \#\#\# Set sample points for vg
    \#.. if vg_low<vg_hi<0
    if (vg_hi<0) \{
        sp_vg = [(vg_low,i_err/(cond*vc_absmax)),
                 (vg_hi,0), (0,0)]
    \}
    \#..else if vg_low<0<vg_hi
    else if (vg_low<0) \{
        sp_vg = [(vg_low,i_err/(cond*vc_absmax)),
                 (0,      i_err/(cond*vc_absmax)), (vg_hi,0)]
    \}
    \#..else 0<vg_low<vg_hi
    else \{
          sp_vg = [(0,0), (vg_low,i_err/(cond*vc_absmax)),
                   (vg_hi,0)]
    \}
\}
values \{
    vc  = v(cp) - v(cm)
    vg  = v(gp) - v(gm)
    g_now = vc*cond          \# for extraction
    ig  = vc*cond * vg
\}
control_section \{
    sample_points (vc, sp_vc)
    sample_points (vg, sp_vg)
    pl_set(ig,(vc,vg))
\}
```

```
    equations \{
        i(gp->gm) += ig
    \}
\}
```